The Evolution of Early-Type Galaxies

by

Joannah Louise Hinz

A Dissertation Submitted to the Faculty of the

DEPARTMENT OF ASTRONOMY

In Partial Fulfillment of the Requirements
For the Degree of

Doctor of Philosophy

In the Graduate College

The University of Arizona

2003

ProQuest Information and Learning Company
300 North Zeeb Road
P.O. Box 1346
Ann Arbor, MI 48106-1346

THE UNIVERSITY OF ARIZONA ®
GRADUATE COLLEGE

As members of the Final Examination Committee, we certify that we have read the dissertation prepared by Joannah Louise Hinz

entitled The Evolution of Early-Type Galaxies

and recommend that it be accepted as fulfilling the dissertation requirement for the Degree of Doctor of Philosophy

George Rieke	4/10/03 Date
Donald W. McCarthy, Jr.	4/10/03 Date
Dennis Zaritsky	4/10/03 Date
	Date
	Date

Final approval and acceptance of this dissertation is contingent upon the candidate's submission of the final copy of the dissertation to the Graduate College.

I hereby certify that I have read this dissertation prepared under my direction and recommend that it be accepted as fulfilling the dissertation requirement.

Dissertation Director George Rieke — 4/10/03 Date

Statement by Author

This dissertation has been submitted in partial fulfillment of requirements for an advanced degree at The University of Arizona and is deposited in the University Library to be made available to borrowers under rules of the Library.

Brief quotations from this dissertation are allowable without special permission, provided that accurate acknowledgment of source is made. Requests for permission for extended quotation from or reproduction of this manuscript in whole or in part may be granted by the head of the major department or the Dean of the Graduate College when in his or her judgment the proposed use of the material is in the interests of scholarship. In all other instances, however, permission must be obtained from the author.

Signed: 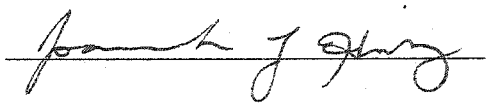

Acknowledgements

The Virgo S0 research made use of the GOLD Mine Database, operated by the Universita' degli Studi di Milano-Bicocca. This research also has made use of the NASA/IPAC Extragalactic Database (NED) which is operated by the Jet Propulsion Laboratory, California Institute of Technology, under contract with the National Aeronautics and Space Administration.

The staff at all of the telescopes used for obtaining my thesis data have been wonderful. This includes the MMT staff and operators, the 90-inch staff, and the 61-inch staff (particularly for switching cages at the last minute, responding to my pleas for TBS time, and answering late night phone calls).

George Rieke has been a fantastic science advisor and a wonderful mentor. My co-advisor, Nelson Caldwell, has been a great teacher and has had a huge influence on the way I think about galaxy evolution.

Many thanks to Don McCarthy and the advanced teenage astronomy campers of 2002 for understanding how important it was to me to get the Coma imaging data. You were all very patient and supportive, and I couldn't have done it without you.

Huge thanks are due to the people who have been there to answer questions about data reduction and analysis: Chad Engelbracht, Rose Finn, John Moustakas, Jane Rigby, and Chien Peng.

Thanks to Andy Marble, Kris Eriksen, and Lei Bai, who took some of the MMT Blue Channel spectra of Coma S0s during conditions not acceptable for their own project, and to Craig Foltz who agreed to put my project first on the bright backup list. Thanks to Rose Finn for taking last minute H and K_s images of two of the ULIRGs.

Thanks also to my husband, Phil Hinz, for both his technical and emotional support. He has been there for me constantly for scientific discussion, helpful hints, computer support, and encouragement. He's been the best friend, colleague, and husband that I could ever have asked for.

Thanks also to others who have extended moral support during grad school. There are many women, in particular, who have been inspirations and guides for balancing work and family, and who have supported my interest in women-in-science issues. They are Audra Baleisis, Valorie Burkholder, Rose Finn, Melanie Freed, Elizabeth Holmes, Aimee Hungerford, Janice Lee, Cathy Petry, Shoko Sakai, Jennifer Scott, Ann Zabludoff and my mother, Penny Smith.

Dedication

This work is dedicated to the memory of my step-mother and friend, Cydneh Barnes-Smith.

Table of Contents

List of Tables 7

List of Figures 9

Abstract 10

Chapter 1. INTRODUCTION 12
1.1. S0 Galaxies 12
1.2. Ultraluminous Infrared Galaxies 15

Chapter 2. OBSERVATIONS AND DATA REDUCTION 20
2.1. Infrared Imaging and Spectra of the ULIRGs 20
2.1.1. Sample Selection 20
2.1.2. ULIRG Observations 20
2.1.3. Velocity Dispersions 25
2.2. Optical Imaging and Spectra of Cluster S0 Galaxies 31
2.2.1. Sample Selection 31
2.2.2. Coma Cluster Observations 32
2.2.3. Virgo Cluster Observations 37

Chapter 3. TULLY-FISHER RELATION FOR CLUSTER S0'S . 53
3.1. Determination of Rotation Curves 53
3.2. Rotation-Luminosity Relations 66

Chapter 4. DYNAMICAL MASSES OF ULIRGS 82
4.1. Calculation of Dynamical Masses 82
4.1.1. Light Profiles 82
4.1.2. Mass Models 82
4.2. Comparing Molecular Masses to Dynamical Masses 86

Chapter 5. SUMMARY AND CONCLUSIONS 92

References 95

List of Tables

TABLE 2.1. Near-infrared imaging of the ULIRG sample. Column header explanations. Col. (1): Galaxy name. Col. (2): Near-infrared imaging band. Col. (3): Exposure time in minutes. Col. (4): Date of imaging observation. Col. (5): Instrument and telescope used for the near-infrared imaging. 23

TABLE 2.2. Near-infrared spectroscopy of the ULIRG sample. Column header explanations. Col. (1): Galaxy name. Col. (2): Morphological type from the NASA Extragalactic Database or Scoville et al. (2000). Col. (3): Redshift. Col. (4): Spectroscopy exposure time in minutes. Col. (5): Date of observation. 25

TABLE 2.3. Calculated velocity dispersions of the ULIRG sample. Column header explanations. Col. (1): Galaxy name. Col. (2): Velocity dispersion in km s^{-1} from this work. Col. (3): Velocity dispersion in km s^{-1} from other works: a.) Shier et al. (1996), b.) Tacconi et al. (2002). . . . 31

TABLE 2.4. Coma S0 Sample. Column header explanations. Col. (1): Galaxy name. Col. (2): Morphological type. Col. (3): Epoch J2000 right ascension. Col. (4): Epoch J2000 declination. Col. (5): Apparent B-band magnitude. Col. (6): Position angle of major axis (degrees). Col. (7): Date of spectroscopic observation. Col. (8): Spectroscopy exposure time (minutes). Those galaxies marked with asterisks are not included in the final analysis; rotation curves for these four S0s were not of high enough quality at the scalelengths necessary to extract a maximum circular velocity for the TFR. 50

TABLE 2.5. Virgo S0 Sample. Column header explanations. Col. (1): Galaxy name. Col. (2): Morphological type. Col. (3): Epoch J2000 right ascension. Col. (4): Epoch J2000 declination. Col. (5): Apparent B-band magnitude. Col. (6): Position angle of major axis (degrees). Col. (7): Date of spectroscopic observation. Col. (8): Spectroscopy exposure time (minutes). Those galaxies marked with asterisks are not included in the final analysis; rotation curves for those two S0s were not of high enough quality at the scalelengths necessary to extract a maximum circular velocity for the TFR. All galaxies have H-band FITS images from the GOLD Mine database except for VCC 1030 which has K-band data only. 52

TABLE 3.1. The S0 galaxy sample magnitudes and derived maximum velocities. Column header explanations. Col. (1): Galaxy name. Col (2): I-band absolute magnitude. Col. (3): H-band absolute magnitude. Col. (4): Maximum circular velocity (km s^{-1}). 67

LIST OF TABLES—*Continued*

TABLE 4.1. Scale radii for the ULIRG sample. Column header explanations. Col. (1): Galaxy name. Col. (2): H-band exponential disk scale-length in parsecs. Col. (3): H-band effective radius of the bulge in parsecs. . . 83

TABLE 4.2. Masses for the ULIRG sample. Column header explanations. Col. (1): Galaxy name. Col. (2): Log of the molecular hydrogen mass from Scoville et al. (2000) in solar masses. Col. (3): Log of the dynamical mass in solar masses from a.) Alonso-Herrero et al. (2001), b.) Shier et al. (1996), c.) Tacconi et al. (2002). Col. (4): Log of the calculated dynamical mass in solar masses from this work for a disk model. Col. (5): Log of the calculated dynamical mass in solar masses from this work for a spherical, $\eta = 2$ model. Col. (6): Log of the calculated dynamical mass is solar masses from this work for a spherical, $\eta = 3$ model. 89

List of Figures

FIGURE 2.1. DSS Optical Images of ULIRGs 21
FIGURE 2.2. H-band Images of ULIRGs 24
FIGURE 2.3. CO Absorption Band ULIRG Spectra 30
FIGURE 2.4. Coma S0 Sky Positions 33
FIGURE 2.5. Virgo S0 Sky Positions 34
FIGURE 2.6. Template Star and S0 Spectra 36
FIGURE 2.7. Intensity Profiles for Coma S0s 49

FIGURE 3.1. Rotation curve for CGCG 160-109 55
FIGURE 3.2. Rotation curve for CGCG 160-119 56
FIGURE 3.3. Rotation curve for CGCG 160-214 57
FIGURE 3.4. Rotation curve for IC 3946 58
FIGURE 3.5. Rotation curve for IC 3955 59
FIGURE 3.6. Rotation curves for IC 3976 60
FIGURE 3.7. Rotation curve for IC 3990 61
FIGURE 3.8. Rotation curves for IC 4088 62
FIGURE 3.9. Rotation curve for IC 4111 63
FIGURE 3.10. Rotation curves for NGC 4873 64
FIGURE 3.11. Rotation curve for UGC 8122 65
FIGURE 3.12. I-band TFR 68
FIGURE 3.13. ΔM_I versus R_{BULGE}/R_{DISK} 72
FIGURE 3.14. H versus I Magnitudes 75
FIGURE 3.15. I versus $I-H$ 76
FIGURE 3.16. Coma Cluster H-band TFR 79
FIGURE 3.17. Virgo and Coma Cluster H-band TFR 80
FIGURE 3.18. Virgo, Coma and Field S0 H-band TFR 81

Abstract

We use the Tully-Fisher relation (TFR) to compare the behavior of S0 and late-type spiral galaxies. We determine circular velocities based on stellar kinematics derived from stellar absorption line spectroscopy for ten S0s in the Coma Cluster and eight S0s in the Virgo Cluster. We combine these results with similar measurements of thirteen Coma S0 galaxies obtained previously. We find that there is only a small offset, $\Delta m_H \sim 0.2$, in the H-band luminosity at a given circular velocity, $v_c \sim 200$ km s^{-1}, between late-type spirals and the S0 data presented here. This result implies a similar total H-band mass-to-light ratio (within an effective radius) among disk galaxies of different Hubble type. As the older stellar population in S0s is dimmer, this suggests a somewhat larger fraction of stellar mass in these S0s than in late-type spirals. These results do not seem to agree with the proposal that star formation in S0s was switched off suddenly a few Gigayears ago due to outside mechanisms and that a large ~ 2 mag offset is expected.

We also find that the relation between (I- and H-band) luminosity and v_c for the S0 galaxies is at best poorly defined and has a scatter of ~ 1 mag, significantly larger than the Tully-Fisher relation (TFR) for late-type spirals in clusters, where the observed I- and H-band scatter is $\sigma \sim 0.3$ mag. This substantial scatter is similar to that found in a study of 18 nearby S0 galaxies in the field (Neistein et al. 1999) where $\sigma_I \sim 0.7$ mag, implying that no tight TFR holds for field S0 galaxies. Our scatter is also much larger than that found by Mathieu et al. (2002) ($\sigma_I \sim 0.3$ mag) for six nearby S0s.

Our results suggest that differing formation histories can lead to S0s with diverse properties and that S0s are more likely to be the outcomes of minor mergers or some "pre-processing" in groups of galaxies falling into clusters, rather than simply late-type spirals that have been stripped of their gas but are kinematically preserved.

We suggest that it is likely that many mechanisms, such as slow encounters, tidal interactions, and gas stripping, may have occurred in the lifetimes of the galaxies and produced the heterogeneous class of S0s that we observe today.

We also present a study of the dynamics and content of a sample of ten nearby ultraluminous infrared galaxies (ULIRGs) based on 2.3 μm CO absorption line spectroscopy and near-infrared H- and K_s-band imaging. Using velocity dispersions derived from the spectroscopy, disk scale-lengths obtained from the imaging, and a set of likely model density profiles, dynamical masses for each ULIRG are calculated and compared to molecular gas mass estimates derived from millimeter interferometric observations and from a standard conversion between ^{12}CO emission and H_2 mass.

For a majority of the ULIRGs in the sample, we cannot reconcile the large amounts of nuclear molecular gas mass predicted by the standard conversion with our estimates of dynamical masses for the galaxies. Indeed, for several of the galaxies, the calculated molecular gas mass exceeds or completely fills the total dynamical mass budget for the system. Molecular gas masses are found to be up to ten times the dynamical masses.

Our results imply that ULIRGs, as the likely products of equal-mass mergers of disk galaxies, do not have huge amounts of molecular gas ($10^{10} - 10^{11}$ $M_\odot$) at their centers, and that the standard conversion of ^{12}CO to H_2 in all likelihood overestimates gas masses and cannot be used in these environments. This in turn suggests much more modest levels of extinction in the near-infrared for ULIRGs than originally predicted ($A_V \sim$ 10-20 versus $A_V \sim$ 100-1000). The lower gas mass estimates forced by our observations imply that the star formation efficiency in these systems is very high and triggered by cloud-cloud collisions, shocks, and winds rather than by gravitational instabilities in circumnuclear gas disks.

Chapter 1
INTRODUCTION

The formation and evolution of galaxies is a topic that has long been studied in astronomy. In this work, the detailed kinematic properties of two specific types of galaxies, lenticular, or S0, galaxies and ultraluminous infrared galaxies, are investigated in order to better understand their origin and evolution. Both these classes are generally recognized as possible transitions or links between the two main galaxy types, spiral and elliptical. Exploring these links is essential for creating a complete picture of galaxy formation in the universe.

1.1 S0 Galaxies

S0 galaxies show a diversity of structural, kinematic, photometric, and spectroscopic properties. Recent analytic arguments and numerical simulations from Bekki, Shioya, & Couch (2002) suggest two formation scenarios that may explain this behavior. The first, in which the spirals maintain their thin-disk component, is a gradual transformation, with efficient stripping of the halo gas and, therefore, dramatically suppressed star formation. The second scenario is the rapid transformation of a spiral through a merger with another, less massive disk galaxy. In contrast to the first case, this latter development would produce a red S0 with a thicker disk and a bigger bulge because of the triggered central starbursts and dynamical heating of both disks.

We can test the two scenarios by exploring the two-parameter Tully-Fisher relation (TFR) for S0s. The TFR is an empirical correlation between stellar luminosity and the observed rotation velocity for late-type spiral galaxies. Since the seminal work of Tully & Fisher (1977), based on global H I profile widths and absolute photographic magnitudes, various forms of the TFR have been used to determine the distances

and to probe the dynamics and evolution of spiral galaxies. Although H I is the most popular kinematic probe, measurements also have been obtained from H II emission optical rotation curves (Dressler & Faber 1990; Mathewson et al. 1992; Schommer et al. 1993; Courteau et al. 1993; Giovanelli et al. 1997) and optical stellar absorption rotation curves (e.g., Neistein et al. 1999). Various photometric bands have been utilized, including B and R bands (Pierce & Tully 1988), I-band (Bernstein et al. 1994; Giovanelli et al. 1997), H-band (Aaronson and Mould 1978; Aaronson et al. 1979), and J, K, and L bands (Malhotra et al. 1996).

By using the TFR as a dynamical probe (rather than the more common use as a distance indicator) we can see if flat, rotationally supported exponential disks of S0s are akin to those of spirals. If S0 galaxies were normal spirals in their youth, now modified by outside mechanisms such as cluster infall or galaxy harassment that stripped the gas from them and truncated star formation (e.g., Moss & Whittle 2000), we would expect S0 galaxies to hew closely to the TFR (i.e., a two-parameter L-v_c relation), defined by late-type spirals. We should find only a magnitude shift due to the subsequent stellar fading and an asymmetric drift correction to compensate for subsequent heating of the stellar disk. If, on the contrary, their luminosities bear little resemblance to those of spiral disks with similar rotation speeds, it would indicate that the evolution of S0 galaxies has been regulated by processes more characteristic of elliptical formation (e.g., mergers). A poor rotation-luminosity correlation might also suggest that even S0 galaxies within a given cluster environment are a mixed morphological class containing galaxies with diverse formation histories and multiple outside influences such as slow encounters, collisional heating and ram pressure stripping (Moore et al. 1999), and strangulation (Larson, Tinsley & Caldwell 1980), as suggested by Bekki, Shioya & Couch (2002).

The TFR has been studied primarily in late-type spirals (Sb-Sd) with some work on Sa's. Recently, the TFR has been explored for a sample of polar ring galaxies based on optical, near-infrared and H I data (Iodice et al. 2003). An analogous

general relation for S0 galaxies cannot be derived from H I line profiles due to the gas-poor nature of the galaxies. For the S0s in which H I emission has been detected (e.g., Roberts et al. 1991), the gas has been observed in many cases to have counter-rotating components, inner and outer rings (van Driel & van Woerden 1991), or other unusual structures that would make for extremely complex rotation curves.

There have been four attempts in the past to study the TFR in field S0 galaxies. All have used optical spectra to measure the dynamics, given the complex behavior of H I in these galaxies. First, Dressler & Sandage (1983) observed 27 field S0 galaxies using B-band photographic plates and optical spectra of stellar absorption lines. They found considerable scatter in their v_{rot} versus M_B diagram and suggested three possibilities for this result: variation in mass-to-light ratios (M/L) between the S0s, contamination of the "disk rotation" by bulge light, and accidental inclusion of systems without true disks where velocity dispersion rather than rotation provides most of the kinetic energy. It is possible, however, that the inaccuracies inherent in photographic B magnitudes, the use of stellar rotation curves that were uncorrected for velocity dispersions, and the inaccurate distances could have obscured any true relation.

In the second effort, Neistein et al. (1999) observed 18 nearby field S0 galaxies (radial velocities < 200 km s^{-1}) in the I-band and extracted rotation curves from long-slit stellar absorption spectra. They found a large scatter in the TFR of approximately 0.7 magnitudes (or 0.15 in $\log_{10} v_c$) and concluded that perhaps S0 galaxies are a morphological mixed bag, produced by different formation and evolutionary scenarios. They suggested that a separate study of the S0 TFR in a cluster would provide a better measure of the scatter since the study would be insensitive to distance errors.

Hinz, Rix, & Bernstein (2001) then made very similar observations on a sample of thirteen S0 galaxies in the Coma cluster. The scatter in the TFR for these galaxies, ~ 0.5 mag, was still larger than that expected for late-type spirals. They also found that there was at most a small offset ($\Delta m_I \leq 0.2$) in the I-band luminosity at a given

circular velocity ($v_c \sim 200$ km s^{-1}) between late-type spirals and the S0 data. They suggested that a similar total I-band M/L, within an effective radius, existed among disk galaxies of differing Hubble type. As the older stellar population in S0 galaxies is dimmer, this suggested a somewhat larger fraction of stellar mass in these S0s than in late-type spirals. Again, it was implied that differing formation histories lead to S0s with diverse properties.

The last study, by Mathieu, Merrifield, & Kuijken (2002), investigated the detailed dynamical properties of six S0 galaxies. They found a fairly small scatter in an S0 TFR, equivalent to that known for late-types. They also found that their S0s were systematically offset from the late-type TFR by almost two magnitudes in the I-band relation, which is what would be expected if star formation in these galaxies had been truncated in the last few Gyrs.

This puzzling contradiction among studies on the dynamics of S0 galaxies may be due to several factors, including small sample sizes and poor velocity rotation curve data. Therefore, we present results on a new, larger sample of S0 galaxies from the Coma and Virgo clusters. The new Coma spectra were taken with the updated MMT, with the hope that the rotation curve data would be improved from Hinz, Rix & Bernstein (2001). We also probe a larger range of S0 luminosities than before, imperative for distinguishing between measurement biases or intrinsic scatter in the final TFR fit. The Coma and Virgo clusters are of quite different richness and population. Therefore, combined with previous work on field S0 galaxies, we can explore the TFR in these galaxies in three different environments: two cluster environments and the field environment.

1.2 Ultraluminous Infrared Galaxies

Ultraluminous infrared galaxies (ULIRGs) have extremely high bolometric luminosities and have spectral energy distributions that are dominated by infrared light (10-

1000μm luminosities above $10^{12}\,L_{\odot}$). Their morphologies are generally disturbed, sometimes with tidal tails or two discernable nuclei, serving as strong evidence that they are the products of mergers and interactions. Their infrared power is currently thought to be a combination of intense star formation triggered by advanced merger activity and different types of active galactic nucleus (AGN) activity. ULIRGs are very dusty and are observed to have both Seyfert 1 and Seyfert 2 type AGN. It has been suggested that such systems go through not only a luminous starburst phase, but later evolve into QSOs (Sanders et al. 1988).

That ULIRGs are probably the result of the collisions of two gas-rich disk galaxies suggests that they are precursors to elliptical galaxies (Toomre & Toomre 1972; Schweizer 1986; Herquist 1992, 1993). Studies in this area have used such tools as the fundamental plane, a three-parameter relation between effective radius, velocity dispersion and mean surface brightness for early-type galaxies (e.g., Djorgovski & Davis 1987; Dressler et al. 1987), in order to connect ULIRGs to ellipticals. Studies of this type (Genzel et al. 2001; Tacconi et al. 2002) have found that most ULIRGs are remarkably close to or on the fundamental plane of dynamically hot galaxies, particularly on the less "evolution-sensitive" effective radius-velocity dispersion projection. Only ULIRGs with the smallest effective radii are offset from the plane. The placement of ULIRGs within the fundamental plane matches the locations of intermediate-mass, disky (rotating) ellipticals. The closeness of ULIRGs to ellipticals on the fundamental plane is somewhat suprising, but is usually interpreted as a "conspiracy" of stellar evolution and extinction – the surface brightening of the new stellar population is obscured by heavy dust extinction, keeping the ULIRGs on the plane. However, the dynamical similarities of the ULIRGs and intermediate-mass ellipticals are robust and do not depend on the photometric properties. Therefore, ULIRGs are likely an important link to understanding the formation and evolution of early-type galaxies from gas-rich spirals.

In the conventional view of ULIRGs, one by-product of the merger of two gas-rich

disks is that huge masses of molecular gas have settled into their nuclei. Interferometric observations of ULIRGs at millimeter wavelengths seem to indicate that large concentrations of molecular gas exist at their centers. Calculations to derive gas masses using maps of the ^{12}CO J$=1 \rightarrow 0$ transition generally adopt a standard conversion factor between the ^{12}CO J$=1 \rightarrow 0$ luminosity and the molecular hydrogen (H_2) mass. The conversion was originally derived from observations of ^{12}CO to H_2 gas in giant molecular clouds in our own galaxy (Scoville & Good 1989) and takes the form

$$M_g = 1.2 \times 10^4 \; F_{CO} D^2_{Mpc} (1+z)^{-1} \; M_\odot$$

where M_g is the gas mass ($M(\mathrm{H_2 + He})$), F_{CO} is the measured interferometric spatial- and velocity-integrated CO flux in Jy km s^{-1}, D_{Mpc} is the distance to the galaxy in Mpc, and z is the redshift. The standard conversion factor that is adopted is equivalent to $N(H_2)/I_{CO} = 2.24 \times 10^{20}$ cm^{-2} (K km s^{-1})$^{-1}$. This standard conversion produces molecular gas masses in the range $10^{10} - 10^{11} M_\odot$ (Bryant & Scoville 1999), indicating extinctions as large as $A_v \sim 100 - 1000$ in the optical. If true, this would mean that even observations taken in the near-infrared would barely penetrate the surface of most ULIRGs and that much of their star formation activity would remain hidden from view.

However, some results have suggested that perhaps the standard conversion between CO flux and H_2 mass is not a valid method. Both theory and observations have intimated that the state of gas in the centers of ULIRGs is quite different from that in local giant molecular clouds. Maloney & Black (1988) argued that the high densities and temperatures of the molecular gas in dense starbursts would result in the standard ratio significantly overestimating the total mass. They stated that, while the conversion does seem to be constant over most of the Milky Way, the underlying reason for this is not well understood, and should not be assumed for other galaxies. The difference in estimated masses is important for understanding the way in which

stars are formed in these galaxies. For instance, if the large surface densities of gas in the circumnuclear disks predicted by the standard ratio are correct, then star formation occurs through instabilities in the disk (Taniguchi & Ohyama 1998). However, if lower mass estimates are valid, then star formation through cloud-cloud collision, shocks, and winds (Scoville, Sanders & Clemens 1986) are predicted. Additionally, using the standard conversion suggests a low star formation efficiency, whereas lower mass esimates yield high star formation efficiency.

Other works have challenged the molecular gas masses calculated from the standard conversion by comparing those values to measurements of the total dynamical masses. Shier, Rieke, & Rieke (1994) obtained dynamical masses for a sample of three ULIRGs based on velocity dispersions from near-infrared spectra and scalelengths derived from near-infrared light profiles. They found that in all three galaxies the total dynamical masses of the cores was less than the claimed H_2 masses. They concluded that, despite large errorbars of the dynamical masses, the standard conversion factor must be wrong for at least some luminous infrared galaxies.

Solomon et al. (1997) and Downes & Solomon (1998) concluded that the standard factor may be high by a factor of five based on a comparison of dynamical and gas masses derived from far-infrared observations. Lisenfeld, Isaak, & Hills (2000) also suggested, using submillimeter measurements of cold dust emission, that the molecular gas mass deduced from CO observations may be 2-3 times higher than would be deduced from thermal emission.

Alonso-Herrero et al. (2001) calculated a dynamical mass for NGC 1614 derived from Br γ spectroscopy (Puxley & Brand 1999) and their knowledge of the morphology and size of a ring of star formation revealed in HST/NICMOS Pa α images. They found that the total dynamical mass of the starburst region is nearly four times smaller than the mass of molecular gas estimated from the standard ratio of ^{12}CO $(1 \rightarrow 0)$ to H_2.

In order to more fully understand star formation and extinction in ULIRGs, which

are important links between the two more familiar galaxy morphologies, and to understand the formation of stars in extreme environments, we calculate dynamical masses for a sample of ten ULIRGs. Our observations improve on previous works not only by sample size but also by a significant increase in the signal-to-noise of the velocity dispersion spectra. This work should finally lay to rest the question of using the standard conversion in ULIRGs.

Chapter 2 describes our observational methods, as well as the basic data reduction steps. Chapter 3 discusses the detailed results of the S0 project. Chapter 4 contains the results of the ULIRG project, and Chapter 5 summarizes the projects and their main conclusions.

Chapter 2

OBSERVATIONS AND DATA REDUCTION

2.1 Infrared Imaging and Spectra of the ULIRGs

2.1.1 Sample Selection

Ten ultraluminous infrared galaxies were chosen for this study. These galaxies have K-band magnitudes in the range $\sim$12-13.5. All of the ULIRGs are nearby ($v <$ 17,000 km s^{-1}), and many have millimeter CO emission measurements (e.g., Sanders, Scoville, & Soifer 1991) as well as NICMOS-2 images of their inner regions (e.g., Scoville et al. 2000). Thus, we are able to choose galaxies with very compact nuclear CO with claimed high molecular gas mass and with simple nuclear structure (usually an $r^{1/4}$ or exponential profile).

The morphologies of the galaxies are varied, from late-type spirals to irregular mergers and interactions (see Table 2.1). Tidal tails and other features indicating recent merger activity can be seen in several of the ULIRGs (e.g., NGC 1614). Figure 2.1 shows 3' $\times$ 3' optical Digital Sky Survey (DSS) images for the sample.

2.1.2 ULIRG Observations

Near-infrared images (H and K_s) of the majority of galaxies in the ULIRG sample were obtained with the wide-field PISCES camera (McCarthy et al. 2001) at the 2.3-meter Bok and 6.5-meter MMT telescopes. Table 2.1 gives the dates and exposures times for each galaxy in both bands. All images were corrected for quadrant cross-talk effects known to be present in 1024 $\times$ 1024 HAWAII arrays with a custom C program written by Roelof de Jong. The images were then dark-subtracted with a combination of 11 dark frames of the appropriate exposure time. Each frame was

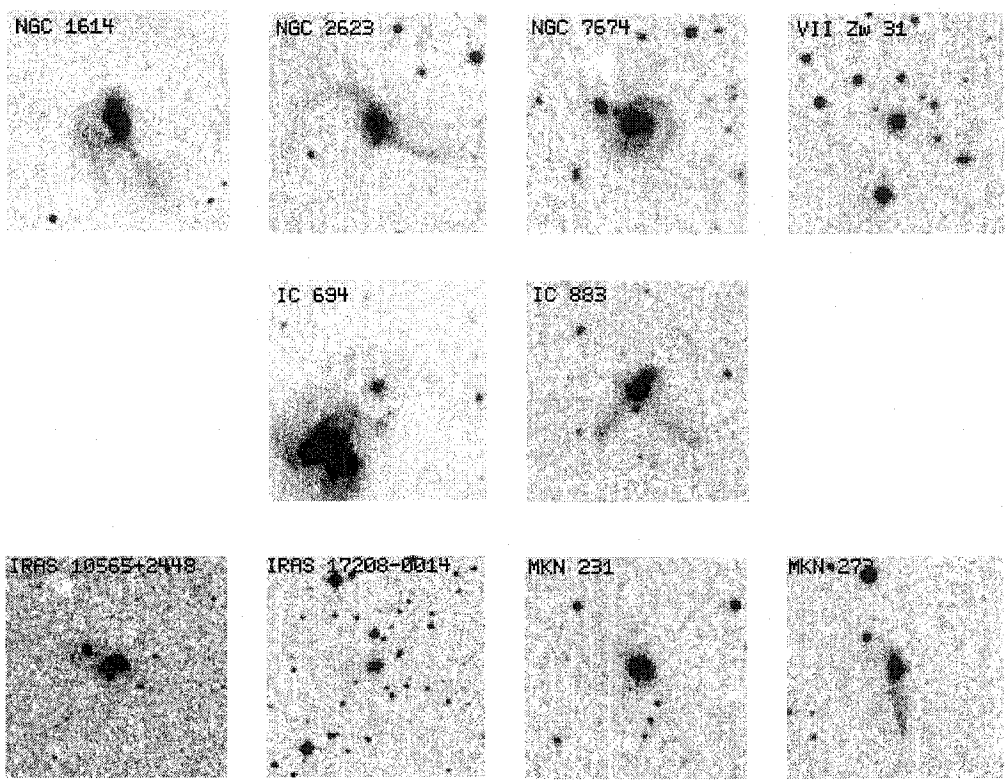

FIGURE 2.1. These DSS images of the ULIRG sample are 3' × 3', with north up and east to the left.

divided by a normalized flat-field created by a median combination and sigma-clip rejection of the dithered science frames. Bad pixels were masked out using a script that substitutes known hot or dead pixels with the value of the mode of the image. The PISCES field-of-view is an inscribed circle, so the outer edges of the images were also masked. Frames were corrected for geometric distortion using the IRAF tasks 'geomap' and 'geotran'. PISCES' distortion is known to be less than a 3% effect at the field edge so does not significantly contribute to poor image quality or errors in photometry. Images were then aligned and stacked using standard IRAF tasks. Seeing was $\sim$1.2-1.5" for the images taken at the 2.3-meter and $\sim$0.6" for images taken at the MMT. For two of the ULIRGs, NGC 1614 and IC 883, we rely solely on the NICMOS-2 observations and do not have wide-field images. Near-infrared images are shown in Figure 2.2. We note here that there has been some confusion in the literature regarding which galaxy is actually IC 694. As pointed out by Yamaoka et al. (1998), IC 694 is the small E/S0 galaxy, not the large merging pair of galaxies which is usually designated NGC 3690.

Near-infrared spectroscopy was taken at the MMT on December 5, 2000 and March 2-3, 2001 with the FSpec spectrograph (Williams et al. 1993). Table 2.2 shows the exposure times for each galaxy. The 600 lines mm^{-1} grating was used at $\sim$2.3 μm in order to observe the CO absorption bandheads, where one pixel corresponds to $\sim$3.3 Angstroms. The CO absorption features are one-sided, but sharp and strong. The bandheads have rest wavelengths of 2.2935 μm for ^{12}CO J = 2 $\rightarrow$ 0 and 2.3227 μm for ^{12}CO J = 3 $\rightarrow$ 1 (Kleinmann & Hall 1986). The exception to this procedure was Mkn 231, for which we attempted to measure the CO overtones at 1.67 μm. The terrestrial absorption spectrum was sampled by observing a star of type A V - G V between each separate galaxy observation. Cross-correlation template stars of K5 III - M2 III were also observed. All spectra were reduced as described by Engelbracht et al. (1998). Frames were dark-subtracted, trimmed, masked for bad pixels, sky-subtracted, and flat-fielded using IRAF tasks called by a custom 'fspecproc' script.

Name	Band	Exposure Time (min)	Date	Instrument/ Telescope
NGC 1614	H (F160W)	3	7 Feb 98	NICMOS-2/HST
NGC 2623	H	21	9 Dec 00	PISCES/2.3 m
	K_s	19	9 Dec 00	
NGC 7674	H	21	9 Dec 00	PISCES/2.3 m
	K_s	20	9 Dec 00	
IRAS 10565+2448	H	13	8 May 01	PISCES/2.3 m
	K_s	8	8 May 01	
IRAS 17208-0014	H	10	13 Mar 03	PISCES/6.5 m
	K_s	10	13 Mar 03	
IC 694	H	10	9 Apr 01	PISCES/6.5 m
	K_s	10	9 Apr 01	
IC 883	H (F160W)	6	21 Nov 97	NICMOS-2/HST
VII Zw31	H	7	8 May 01	PISCES/2.3 m
Mkn 231	H	10	8 May 01	PISCES/2.3 m
	K_s	7	8 May 01	
Mkn 273n	H	10	11 Mar 03	PISCES/6.5 m
	K_s	10	11 Mar 03	

TABLE 2.1. Near-infrared imaging of the ULIRG sample. Column header explanations. Col. (1): Galaxy name. Col. (2): Near-infrared imaging band. Col. (3): Exposure time in minutes. Col. (4): Date of imaging observation. Col. (5): Instrument and telescope used for the near-infrared imaging.

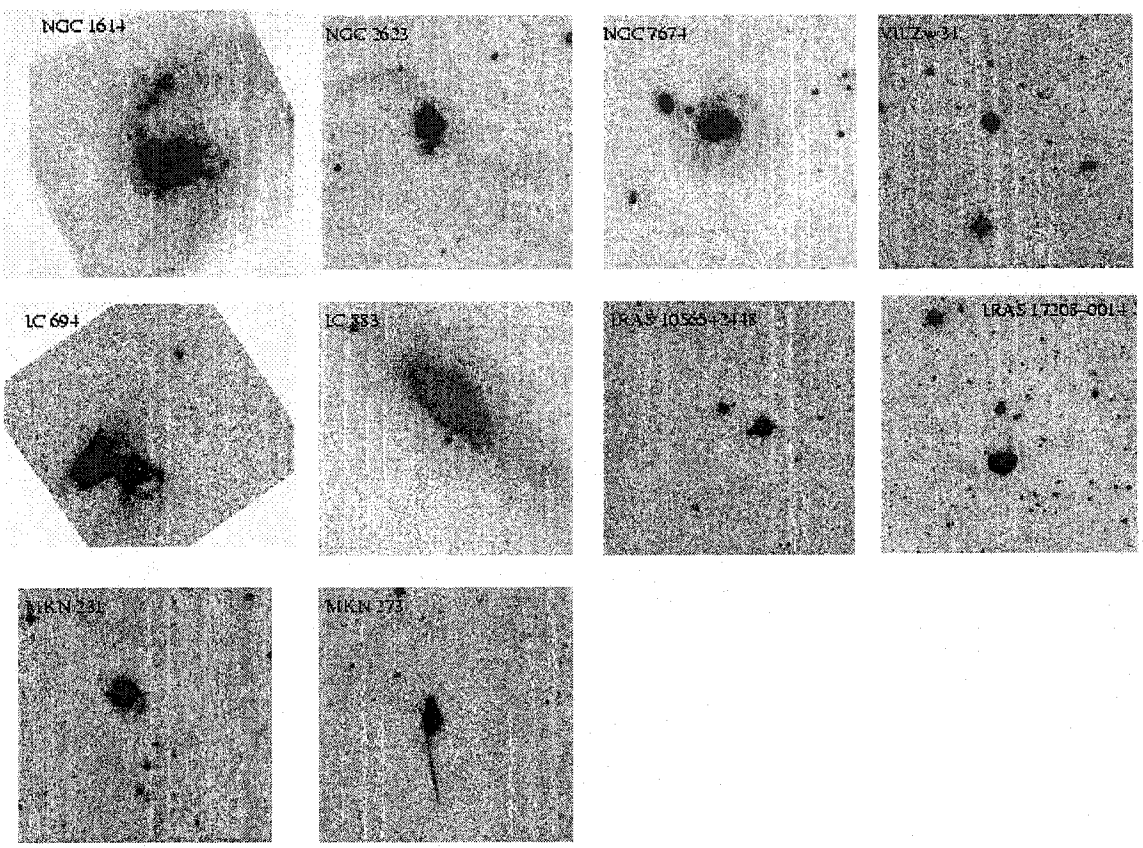

FIGURE 2.2. These H-band images of the ULIRG sample are approximately the same size as the DSS images, with north up and east to the left. The two NICMOS-2 images (NGC 1614 and IC 883) have fields of view of ~ 30".

Name	Type	z	Exposure Time (min)	Date
NGC 1614	SB(s)c pec; H II: Sy2	0.0156	60	5 Dec 00
NGC 2623	merger	0.019	108	5 Dec 00
NGC 7674	S(r)bc pec; H II: Sy2	0.0288	48	5 Dec 00
IRAS 10565+2448	H II	0.0431	36	5 Dec 00
			72	2 Mar 01
IRAS 17208-0014	Sbrst H II	0.0437	12	2 Mar 01
			36	3 Mar 01
IC 694	Sbrst AGN	0.012	84	3 Mar 01
IC 883	Im:pec; H II LINER	0.0245	60	3 Mar 01
VII Zw31	H II	0.0551	144	5 Dec 01
Mkn 231	SA(rs)c? pec; Syl	0.0435	48	2 Mar 01
Mkn 273n	Sy2	0.0385	84	3 Mar 01

TABLE 2.2. Near-infrared spectroscopy of the ULIRG sample. Column header explanations. Col. (1): Galaxy name. Col. (2): Morphological type from the NASA Extragalactic Database or Scoville et al. (2000). Col. (3): Redshift. Col. (4): Spectroscopy exposure time in minutes. Col. (5): Date of observation.

Multiple frames of objects were aligned and combined using 'nalign' and 'ircombine'. One-dimensional spectra of objects, standard stars, and sky frames were extracted. The one-dimensional galaxy and standard star spectra were wavelength calibrated using the wavelengths of OH airglow lines. Each galaxy spectrum was then divided by a template standard star spectrum of type K5 III - M2 III. The continuum in each star and galaxy spectrum was fitted with a low-order polynomial and subtracted with the 'splot' task.

2.1.3 Velocity Dispersions

In order to determine dynamical masses for each of the ULIRGs, the velocity dispersions must be calculated from the near-infrared spectra using template stars that also have CO absorption bands. There are three main techniques that can be used: the Fourier quotient method (Sargent et al. 1977), the cross-correlation method (Simkin 1974; Tonry & Davis 1979), and direct fitting (Franx, Illingworth, & Heckman 1989;

Rix & White 1992). In the Fourier quotient method, the galaxy is assumed to be the convolution of a single stellar template with a broadening function, B, which can be retrieved in the following way,

$$galaxy = template \otimes B$$
$$B = FFT^{-1}\left[\frac{FFT(galaxy)}{FFT(template)}\right].$$

The disadvantage of this method is the fact that the errors in the quotient are correlated, so that error analysis becomes difficult. Also, because the broadening function is fitted in Fourier space, absorption features from all parts of the spectrum interact with each other, making B very sensitive to template mismatches. In the cross-correlation method, the galaxy and template are correlated directly, and the location of the highest correlation peak is identified with the mean velocity. The dispersion is estimated by subtracting the width of the template autocorrelation peak in quadrature from the width of the cross-correlation peak. The drawback of this method is that the spectra must be padded with extra zeroes, possibly with some trimming of the spectral edges, resulting in lost information. The direct fitting method of Rix & White (1992) assumes that the galaxy differs from the template by the shape of the continuum and the kinematic broadening. The broadening is thought of as a superposition of multiple templates shifted in velocity space. The disadvantage for this method is that numerous templates of differing stellar types are almost certainly needed for a good fit to the galaxy spectrum, taking up more observing time. Also, this type of fitting program may get trapped in local minima if reasonable guesses for radial velocity and velocity dispersion are not passed. Of these choices, we use the cross-correlation method on our spectra. Although the spectra have to be carefully continuum-subtracted and padded with zeroes, we have trimmed very little information from either edge, and have tested that losing a few Angstroms of spectrum does not change the velocity dispersion results within the calculated error bars.

Velocity dispersions of the galaxies were calculated by comparing the width of their CO absorption bandheads to those of the template standard stars. This was achieved by first generating a series of broadened template star spectra with a range of Gaussians corresponding to velocity dispersions of 20-200 km s^{-1}. The broadened spectra were then cross-correlated with the original template star spectrum, and the width of the cross-correlation peak as a function of the Gaussian broadening was measured. Each galaxy spectrum was then cross-correlated with a template star. The width of the cross-correlation peak between the galaxy and template star revealed the velocity broadening, based on the broadened stellar template calibration. Velocity dispersions and uncertainties for each ULIRG are listed in Table 2.3. Uncertainties were estimated by simply looking at the range of dispersion values obtained from comparing multiple template stars with each galaxy.

Mkn 231 was observed at 1.67 μm in order to calculate the velocity dispersion from the CO bandheads there. However, due to difficulty in subtracting the continuum at this wavelength range, we used the Tacconi et al. (2002) value listed in Table 2.3 for the remainder of this work (see Shier 1995 for a discussion of continuum subtraction).

Spectra for all of the ULIRGs, showing the CO absorption bandheads, are shown in Figure 2.3. Three of our galaxies, NGC 1614, NGC 2623, and IC 694, overlap with a study of the power sources of luminous infrared galaxies by Shier, Rieke, & Rieke (1996). We find that the values for the velocity dispersions are higher for two of the ULIRGs than those found by Shier et al. (1996), while the value for IC 694 is in agreement. Table 2.3 shows a comparison to the Shier et al. (1996) values. The differences may arise from the fact that the Shier et al. (1996) data, while also obtained with FSpec, were taken at the 2.3-meter telescope rather than the 6.5-meter MMT, so the Shier et al. (1996) spectra have a lower signal-to-noise. Our dispersion value for Mkn 273N agrees with the value derived by Tacconi et al. (2002) within the errorbars.

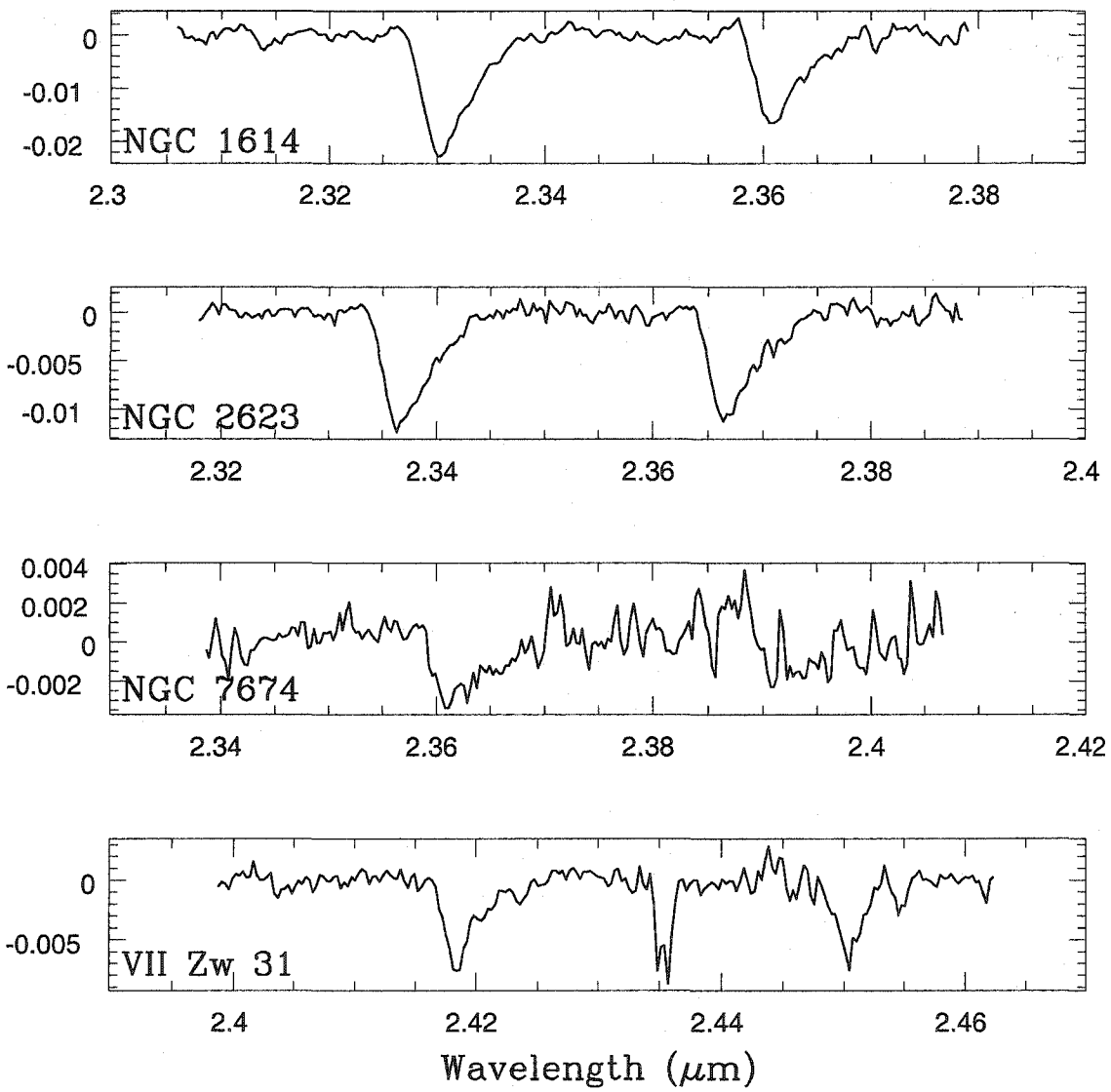
0
-0.01
-0.02
NGC 1614
2.3
2.32
2.34
2.36
2.38
0
-0.005
-0.01
NGC 2623
2.32
2.34
2.36
2.38
2.4
0.004
0.002
0
-0.002
NGC 7674
2.34
2.36
2.38
2.4
2.42
0
-0.005
VII Zw 31
2.4
2.42
2.44
2.46
Wavelength (μm)

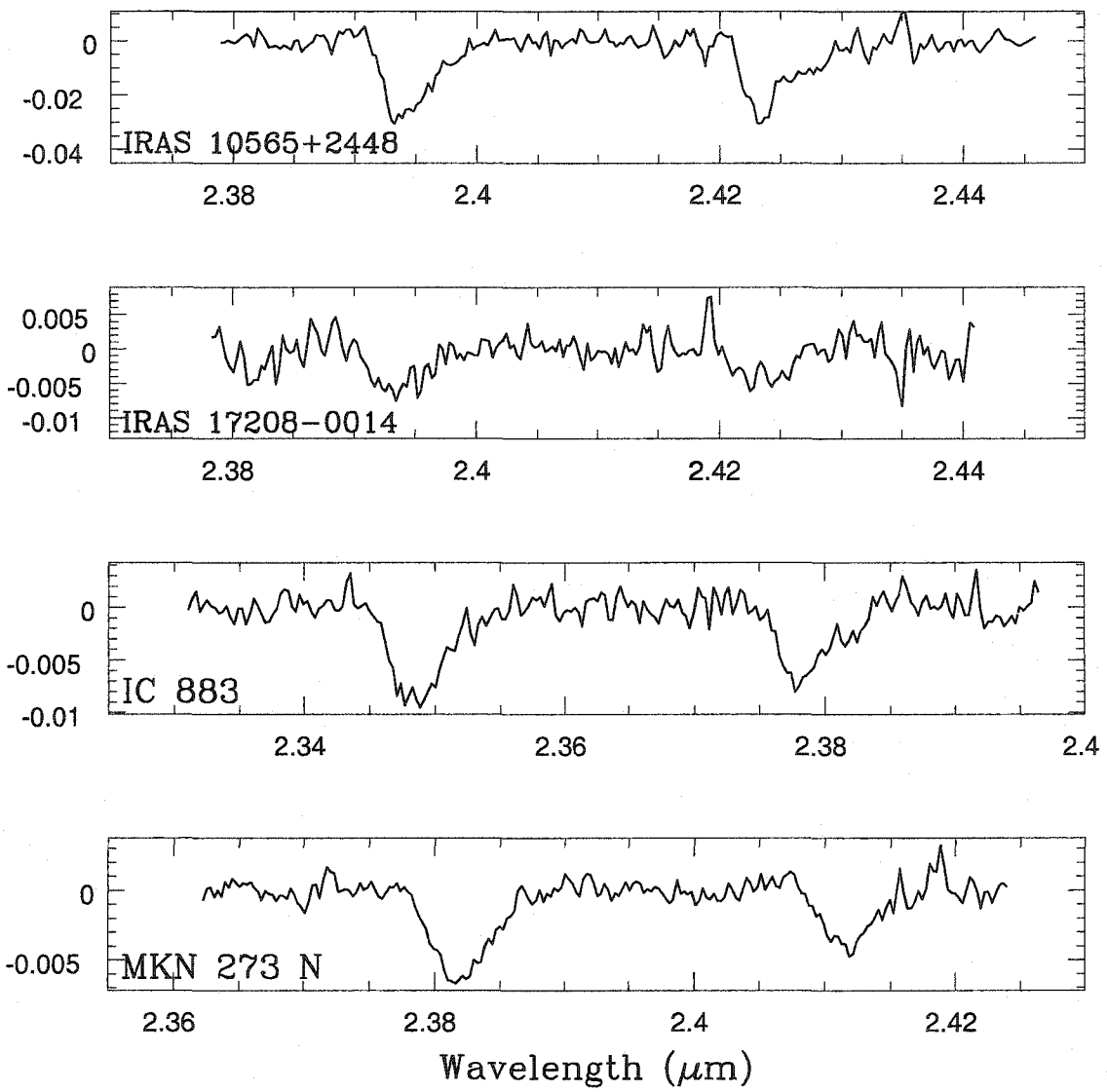
0
-0.02
-0.04
IRAS 10565+2448
2.38
2.4
2.42
2.44
0.005
0
-0.005
-0.01
IRAS 17208−0014
2.38
2.4
2.42
2.44
0
-0.005
-0.01
IC 883
2.34
2.36
2.38
2.4
0
-0.005
MKN 273 N
2.36
2.38
2.4
2.42
Wavelength (μm)

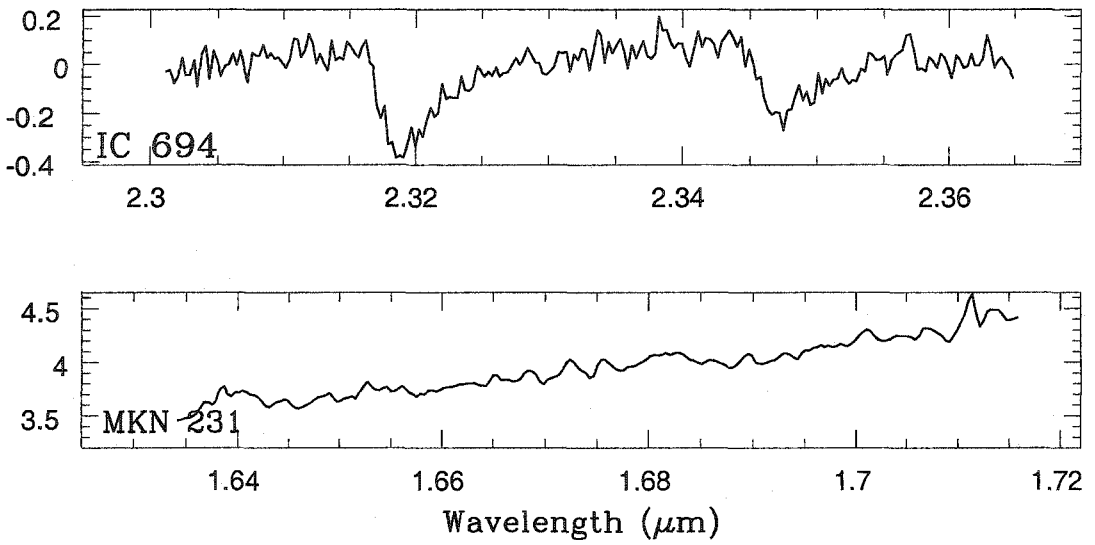

FIGURE 2.3. One-dimensional spectra of the ULIRG sample showing the CO absorption bandheads caused by the 2-0 and 3-1 molecular transitions. Mkn 231 was observed at 1.67 μm to measure the second overtone CO bands because of the dilution of the first overtone bands.

Name	σ (km s^{-1})	σ_{other} (km s^{-1})
NGC 1614	164 ± 8	75 ± 12 [a]
NGC 2623	153 ± 11	95 ± 13 [a]
NGC 7674	93 ± 26	—
IRAS 10565+2448	141 ± 4	—
IRAS 17208-0014	125 ± 28	—
IC 694	141 ± 17	135 ± 21 [a]
IC 883	151 ± 5	—
VII Zw31	98 ± 13	—
Mkn 231	—	115 ± 10 [b]
Mkn 273 N	232 ± 43	285 ± 30 [b]

TABLE 2.3. Calculated velocity dispersions of the ULIRG sample. Column header explanations. Col. (1): Galaxy name. Col. (2): Velocity dispersion in km s^{-1} from this work. Col. (3): Velocity dispersion in km s^{-1} from other works: a.) Shier et al. (1996), b.) Tacconi et al. (2002).

2.2 Optical Imaging and Spectra of Cluster S0 Galaxies

2.2.1 Sample Selection

In the original Coma sample of Hinz, Rix & Bernstein (2001), one Sab and thirteen S0 galaxies were selected from the catalog of Doi et al. (1995). Each galaxy was hand-picked based on symmetry and lack of interaction with other galaxies. Inclination angles also had to be sufficiently large ($> 50°$) to carry out absorption line spectroscopy. Cluster membership was assumed on the basis of the galaxy recessional velocity. Rotation curves for some of these galaxies did not extend far enough into their disks to be sure that the value of the velocity had stopped rising. Consequently, it is possible that the circular velocity and, therefore, the maximum velocity, was underestimated, leading to additional scatter in the TFR.

Our goals in this work are to increase the sample size of S0 galaxies in the Coma cluster and to extend the magnitude range of the sample on the faint end. Two of the galaxies in the original sample (IC 3990 and IC 4088) were re-observed to obtain

rotation curves farther into their disks. We picked targets using similar criteria as the first sample, although not specifically from the Doi et al. (1995) catalog: large inclination angle, lack of interaction with other galaxies in the cluster, and bright enough to be sure of obtaining a rotation curve with a reasonable exposure time. The locations of these galaxies within the cluster are shown in Figure 2.4.

The Virgo S0 galaxies were chosen in the same way as the Coma sample. In addition, we excluded S0s that were too large, i.e., those galaxies whose major axes exceeded the spectrograph slit length (70"). Cluster membership was assigned according to recessional velocity and based on the catalog of Binggeli, Sandage & Tammann (1985). The locations of the S0s within the Virgo cluster are shown in Figure 2.5.

2.2.2 Coma Cluster Observations

Long-slit optical spectra of 14 Coma Cluster S0 galaxies were obtained at the 6.5-meter MMT with the Blue Channel Spectrograph (Schmidt, Weymann & Foltz 1989). We used a 1200 lines mm^{-1} grating blazed at 4830 Angstroms in first order with a 1.5" $\times$ 180" slit. The wavelength coverage was 4530-6020 Angstroms. G- and K-giant standard stars were observed throughout the night to serve as kinematic templates for modeling the galaxy spectra. Table 2.4 gives the name, morphological type (from the NASA Extragalactic Database), RA, Dec, apparent B-band magnitude, position angle of the major axis, the date of observation, and the exposure time for each galaxy. He-Ne-Ar-Fe lamp exposures were taken between galaxy exposures for wavelength calibration purposes, as well as quartz lamp exposures for flat-fielding.

All spectra were bias-subtracted and trimmed. The quartz lamp spectra were used to remove small-scale response variations. They were normalized by a 4 - 10^{th} order cubic spline fit to the variation in response in the dispersion direction. Each star and galaxy spectrum was then divided by a normalized quartz lamp spectrum observed adjacent to it. The arc lamp spectra were used to correct star and galaxy

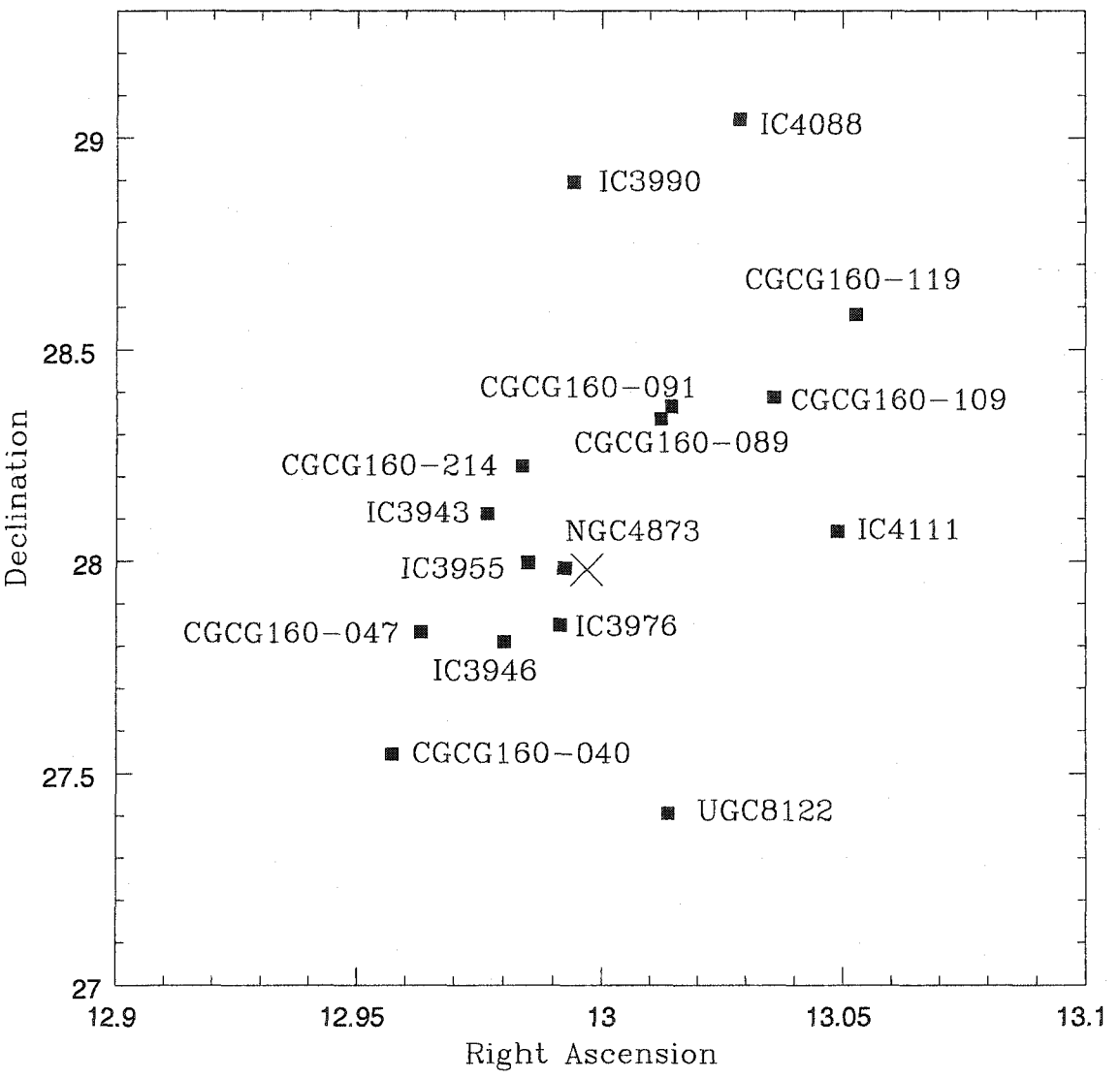

FIGURE 2.4. Coma S0 locations in the sky. An X marks the center of the cluster.

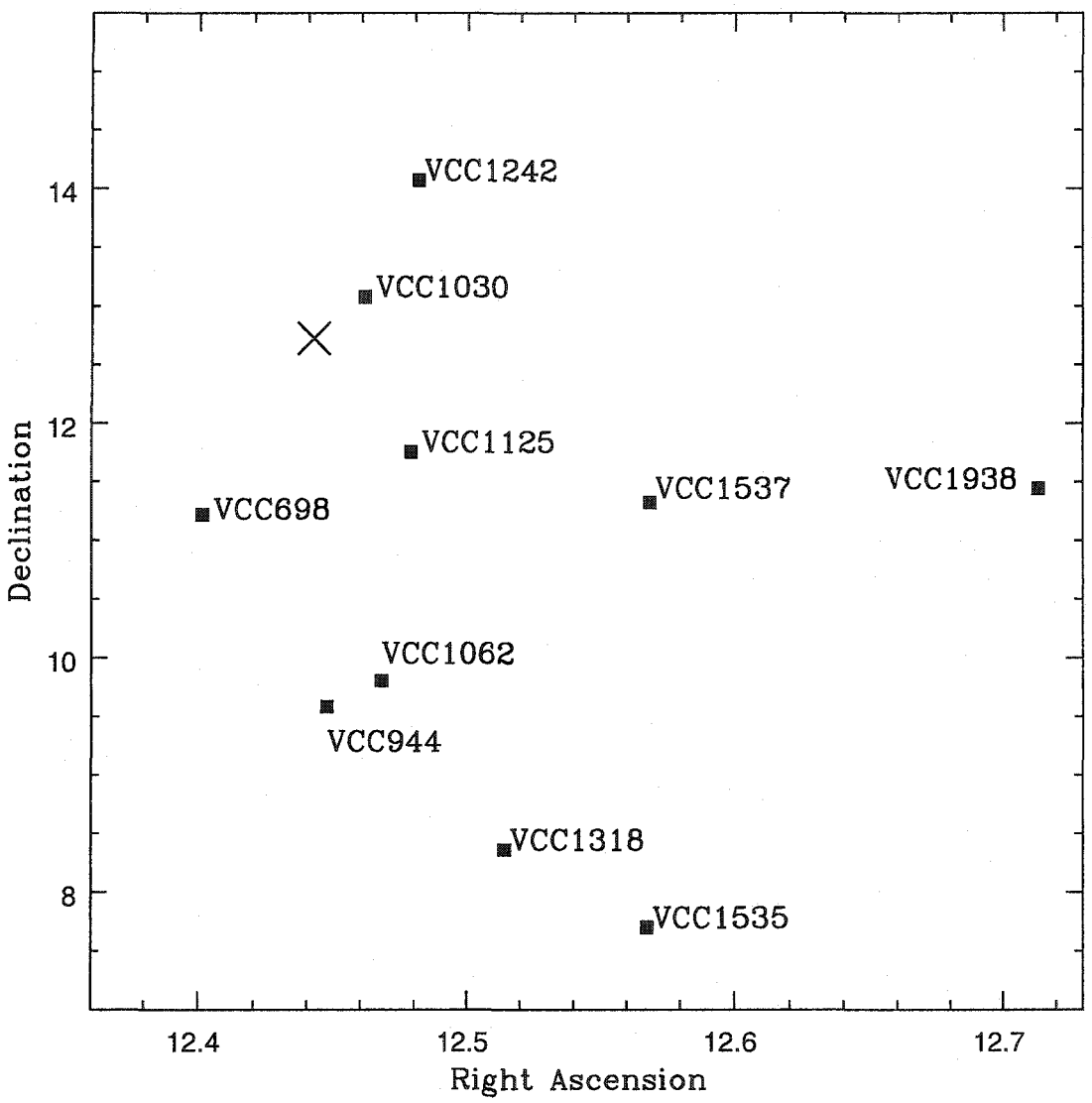

FIGURE 2.5. Virgo S0 locations in the sky. An X marks the center of the cluster.

spectra to uniform sampling in slit position and logarithmic wavelength space. These reduction techniques resulted in a wavelength solution accurate to $\sim$15 km s^{-1} at any pixel. Sky emission was removed from all science spectra by fitting the flux at the outer edges of the spectra and subtracting the result.

Kinematics for the galaxies are derived from the stellar absorption lines using the technique of Rix & White (1992). The two-dimensional galaxy spectra are binned into a series of one-dimensional spectra with comparable signal-to-noise and are then fit by a chi-squared minimization with a combination of shifted and broadened stellar templates. The kinematic data for the galaxies typically extend out to $\sim$2.5-3 kpc. Examples of standard star template and S0 galaxy spectra are shown in Figure 2.6. For four of the galaxies, CGCG 160-040, CGCG 160-047, CGCG 160-089, and CGCG 160-091, we could not extract rotation curves out to the regime where the rotational velocity is dominant. These were removed from the sample and are not discussed further, leaving us with 10 remaining Coma S0 galaxies in the new sample.

Kron-Cousins I-band images of the Coma S0s were obtained with a 2048×2048 CCD at the 1.55-meter Kuiper telescope on Mt. Bigelow over five nights in June 2002. The CCD was operated in a 3×3 binned mode for a scale of 0.45 arcsec pixel^{-1}. Typical exposure times were 6×300 seconds per galaxy with airmasses ranging from 1.1-1.8. Landolt (1992) photometric standard stars were observed throughout the night in both V- and I-bands at airmasses between 1.1 and 1.5.

All images were bias subtracted, trimmed, and flat-fielded with standard IRAF tasks. Flat-fields were created from a median combination of twilight flats and science images. Images of the same fields were aligned and combined. Foreground stars within $\sim$1.0 arcmin of each galaxy were removed using the IMEDIT task. Photometry on the Landolt standards was carried out using the PHOT package, and the transformation of instrumental magnitudes to standard magnitudes was handled by PHOTCAL. Elliptical isophotes were fitted to each galaxy using the ELLIPSE task, which calculates the mean intensity, ellipticity and position angle for each isophote.

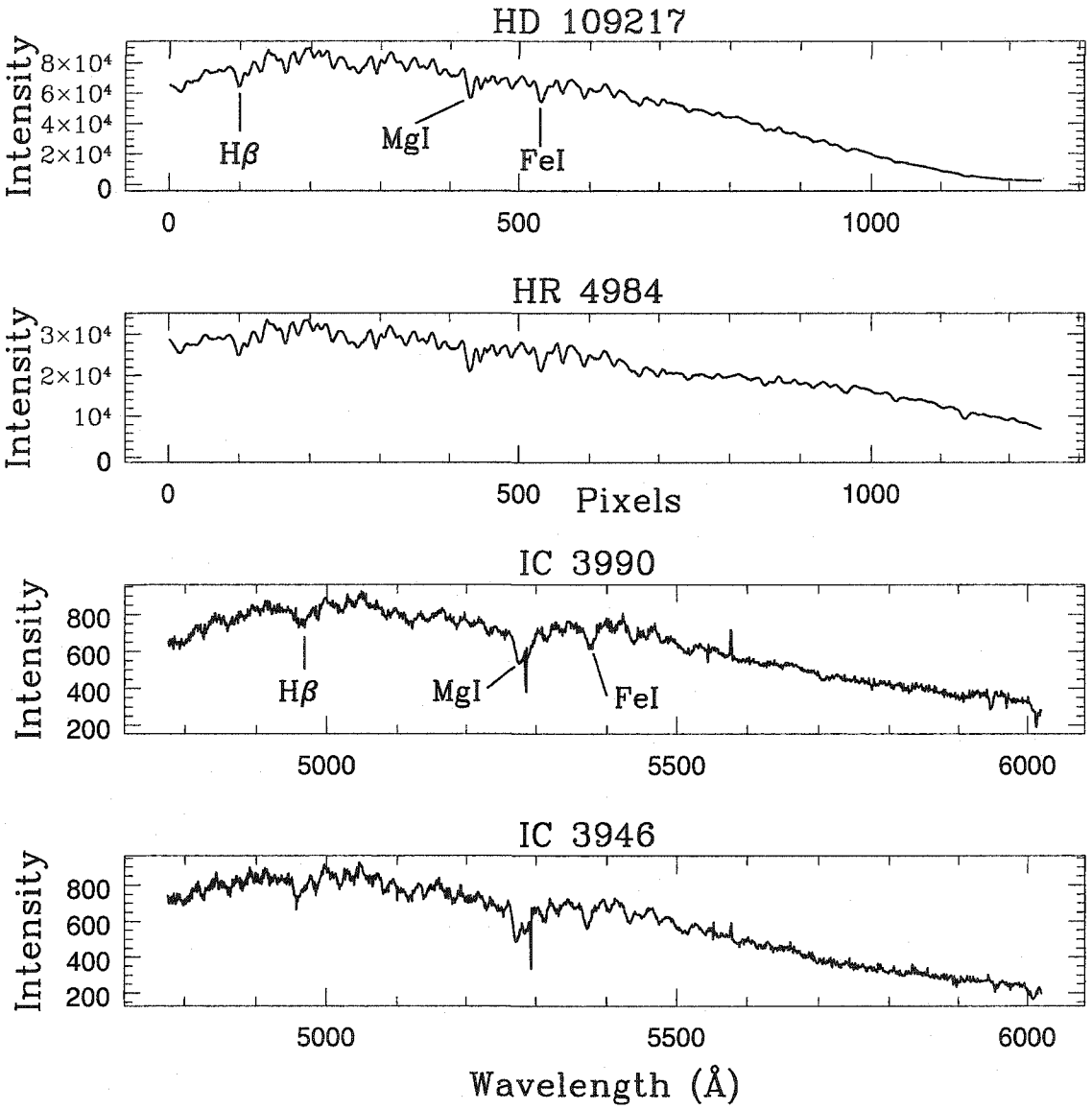

FIGURE 2.6. Two examples of K-Giant template star spectra and two sample Coma S0 spectra. The stellar spectra are boxcar smoothed by a factor of 5.

Isophotes are initialized in this task at a small semi-major axis specified in the parameter file. The semi-major axis length is increased by a factor of 1.1, and the process is repeated until the first *bad* isophote is reached. This bad isophote is determined by

$$I < S\sigma_I \tag{2.1}$$

where I is the mean intensity of an annulus, and σ_I is the RMS within that annulus, as outlined by Schlegel (1995). S is a constant chosen to be 2.5 in this case (other values can be chosen depending on the signal-to-noise of the data), which corresponds to ~ 20 mag arcsec^{-2}. The sum of the number of counts in each good isophote minus the sky background level is then converted to an I magnitude for each galaxy.

Two-dimensional models of the galaxies were created using an $R^{1/4}$ bulge and exponential disk fitting routine (Rix & Zaritsky 1995). In this way, the exponential scale radius of the disk and the effective radius of the bulge were obtained for each S0. Typically, a few pixels at the very centers of the galaxies were not included in the fit, because the fitting routine does not account for the seeing. Figure 2.7 shows the intensity profiles along the major-axes of the galaxies, along with their model counterparts. The jagged appearance of some of the data intensity profiles is most likely caused by a combination of rotating the image before taking the major-axis profile cut, based on an estimate of the position angle, and the 0.45 arcsec pixelation of the data.

2.2.3 Virgo Cluster Observations

Spectra of a sample of 10 Virgo S0s were taken at the Smithsonian Astrophysical Observatory Tillinghast 1.5-meter telescope at the Whipple Observatory in March and April of 2001 with the FAST instrument (Fabricant et al. 1998). We used the 600 lines mm^{-1} grating blazed at 5700 Angstroms and a 1.52" $\times$ 70" slit for a wavelength coverage of 3600-5600 Angstroms. Table 2.5 shows the Virgo cluster sample, apparent blue magnitude (Binggeli, Sandage & Tammann 1985), position angle of the major

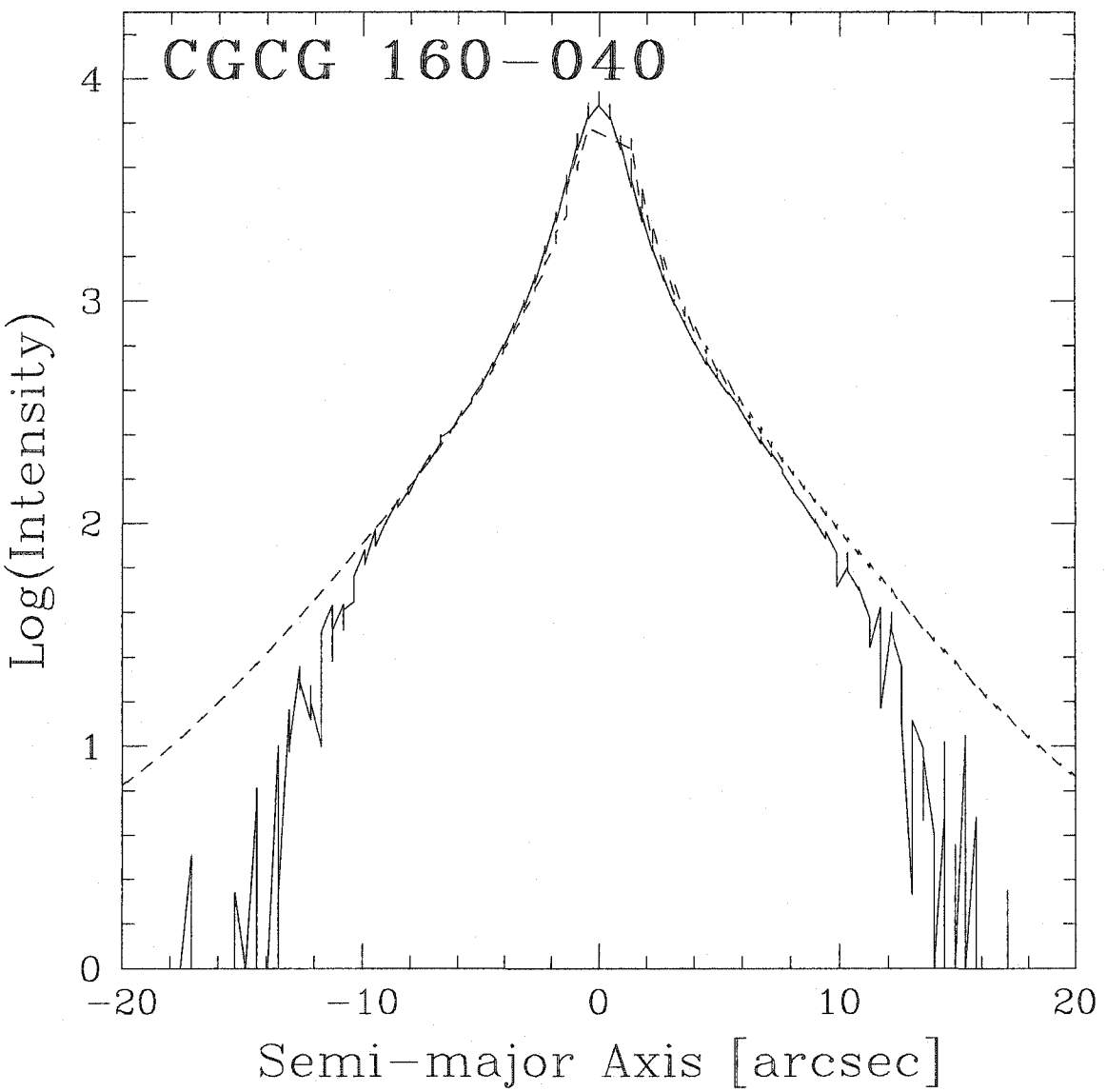
CGCG 160−040
Log(Intensity)
Semi−major Axis [arcsec]
0
1
2
3
4
−20
−10
0
10
20

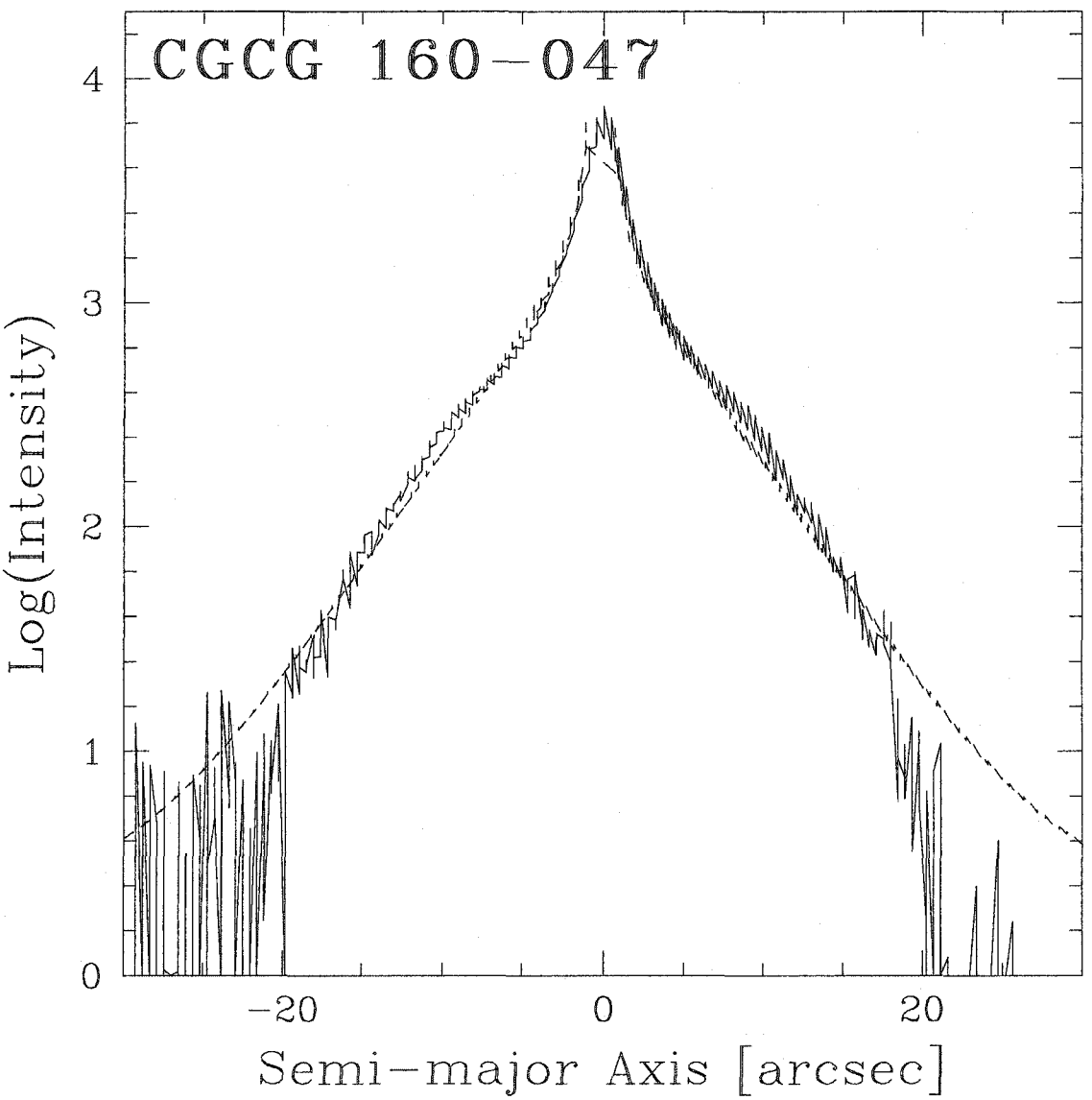
CGCG 160−047
Log(Intensity)
0
1
2
3
4
−20
0
20
Semi−major Axis [arcsec]

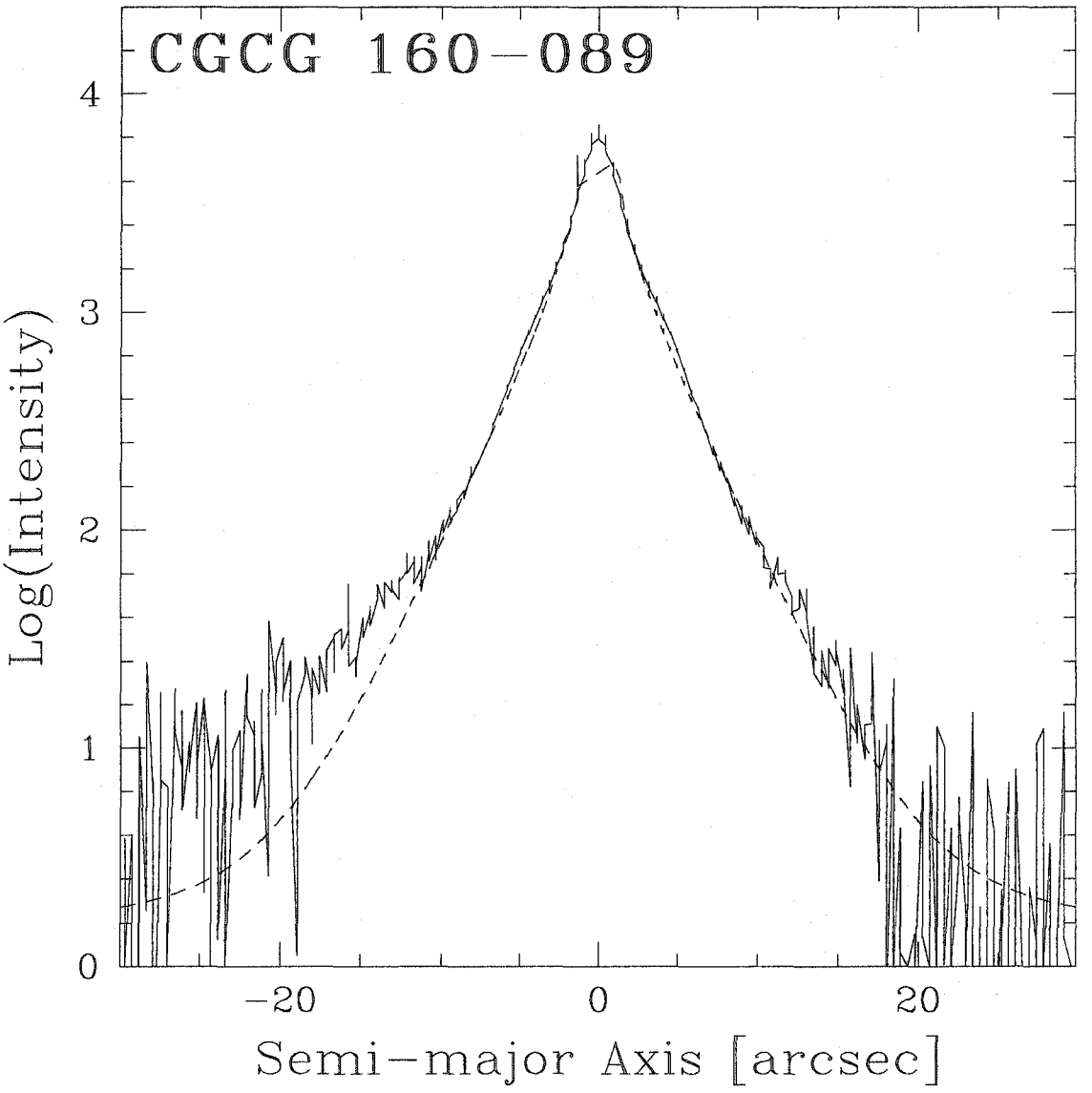
CGCG 160−089
Log(Intensity)
0
1
2
3
4
−20
0
20
Semi−major Axis [arcsec]

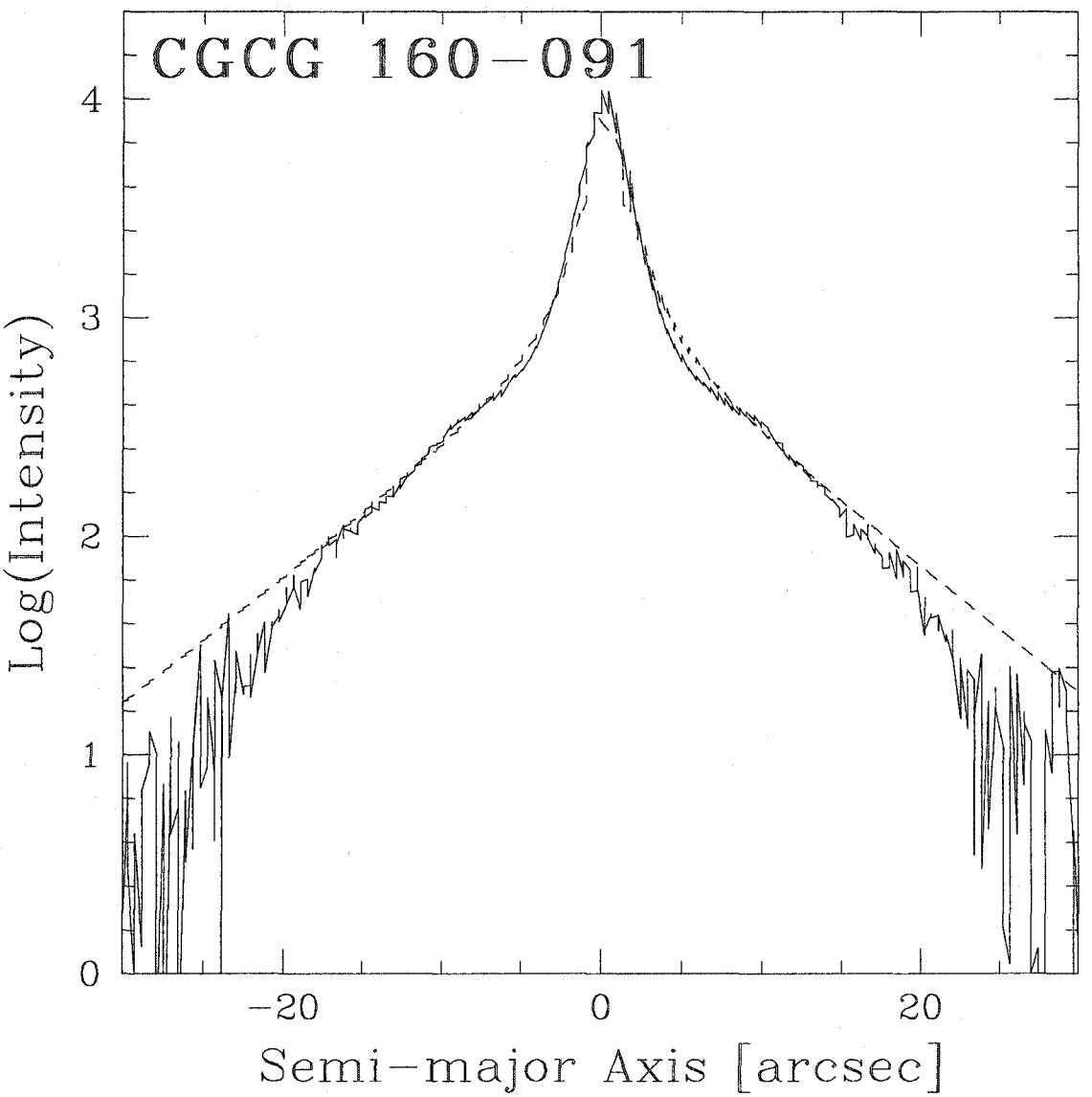
CGCG 160−091
Log(Intensity)
0
1
2
3
4
−20
0
20
Semi−major Axis [arcsec]

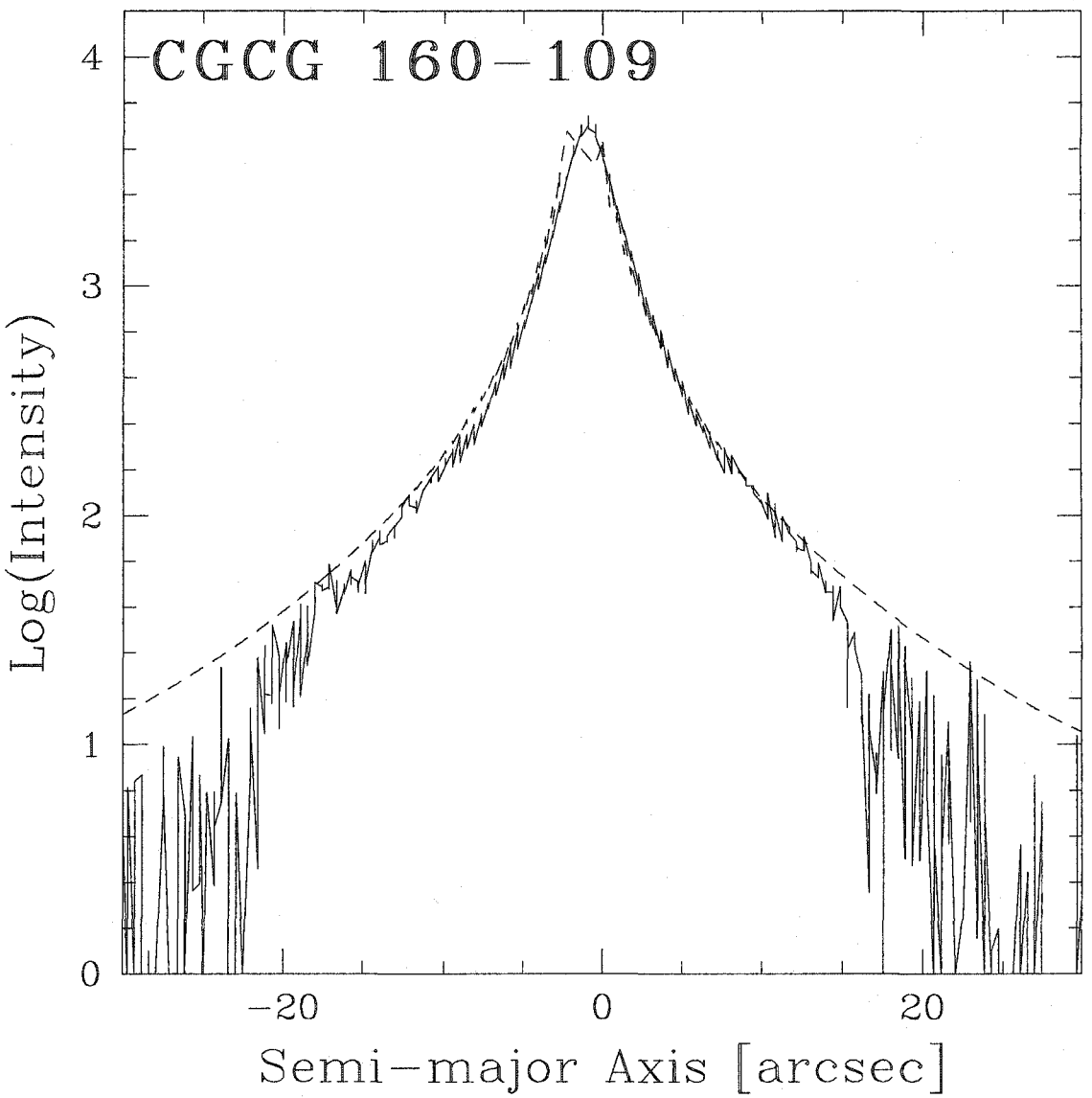
CGCG 160−109
Log(Intensity)
0
1
2
3
4
−20
0
20
Semi−major Axis [arcsec]

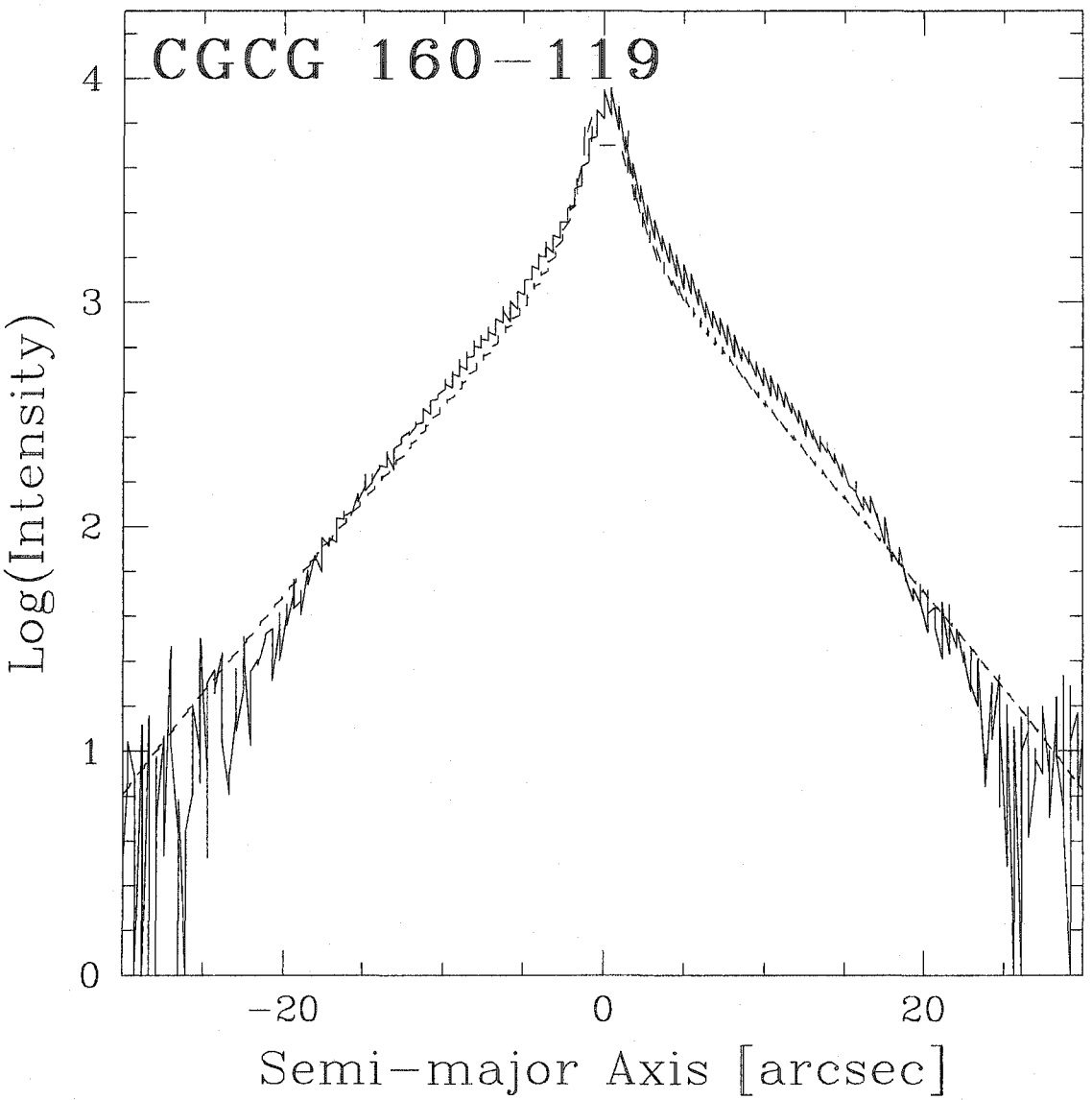
CGCG 160−119
Log(Intensity)
0
1
2
3
4
−20
0
20
Semi−major Axis [arcsec]

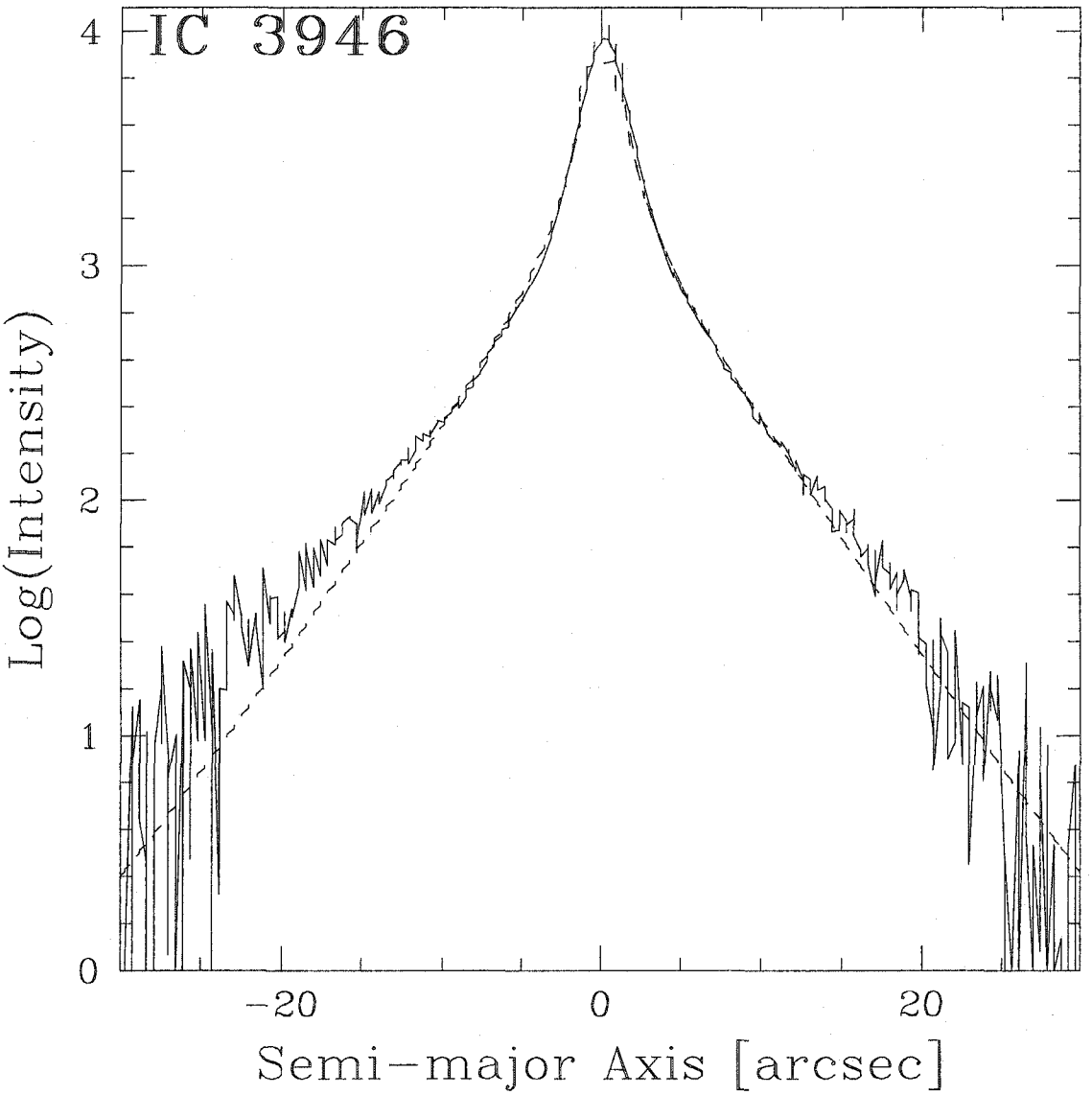
IC 3946
Log(Intensity)
Semi-major Axis [arcsec]
0
1
2
3
4
-20
0
20

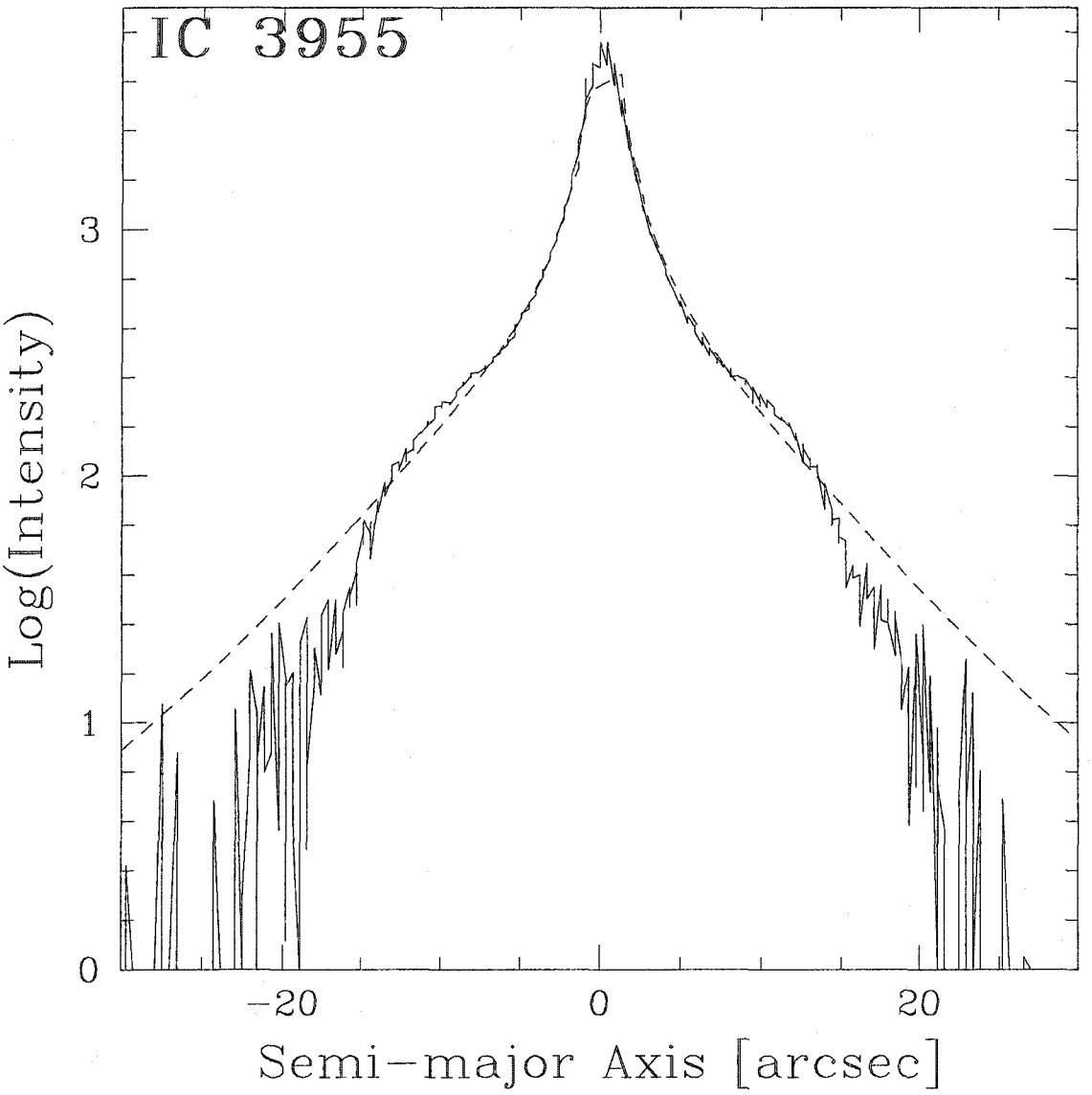
IC 3955
Log(Intensity)
0
1
2
3
−20
0
20
Semi−major Axis [arcsec]

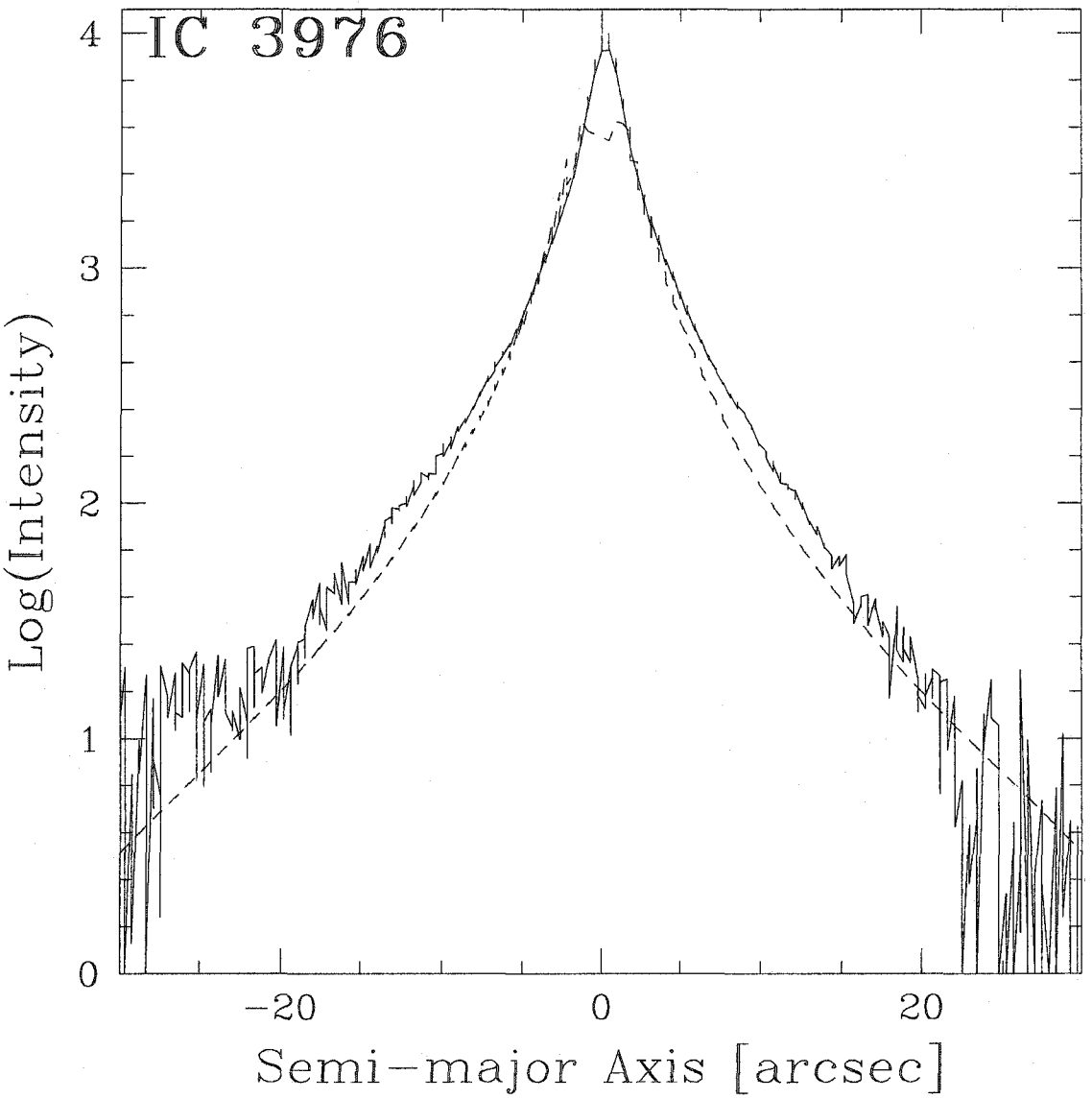
IC 3976
Log(Intensity)
Semi-major Axis [arcsec]
0
1
2
3
4
-20
0
20

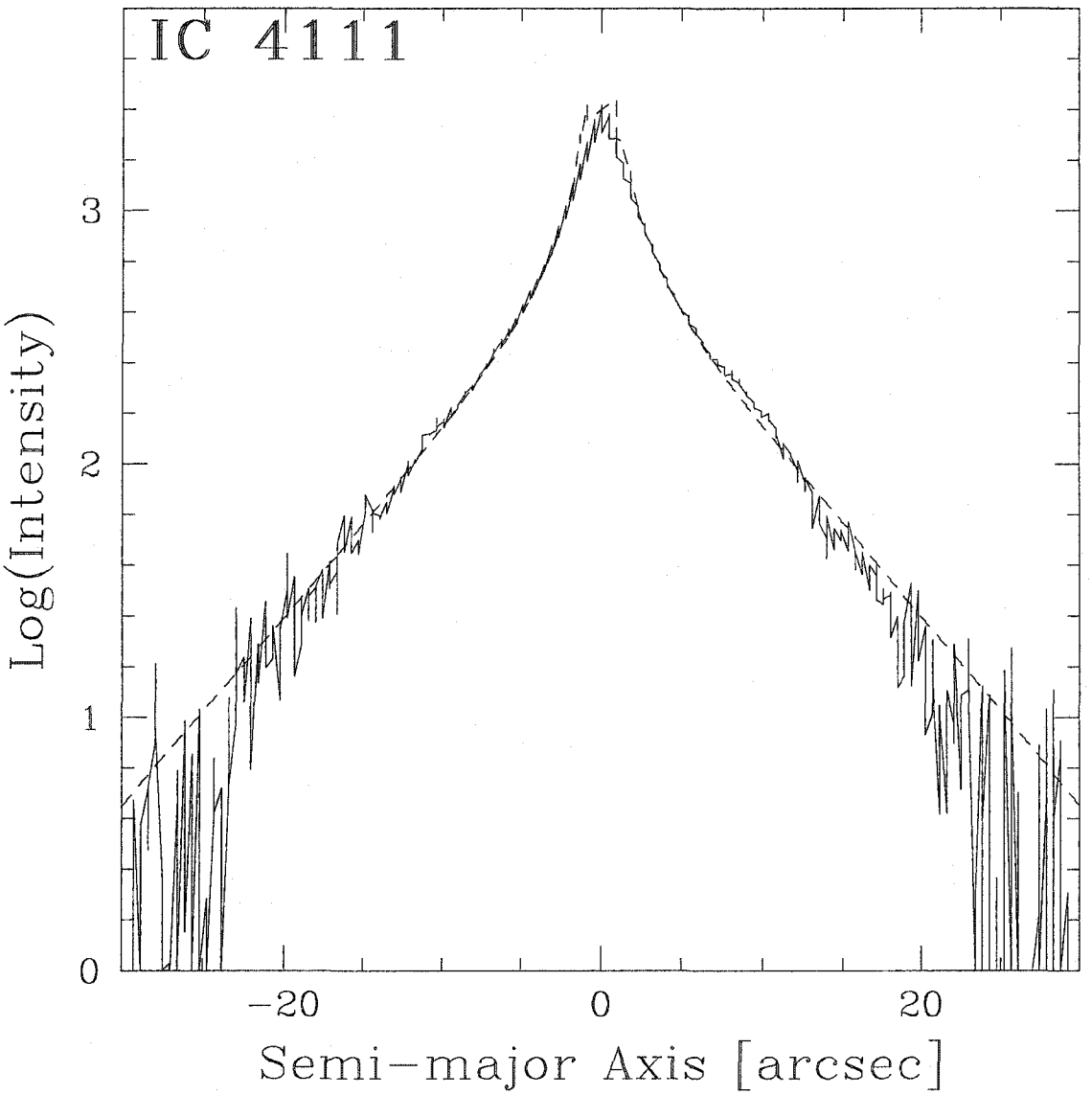
IC 4111
Log(Intensity)
0
1
2
3
−20
0
20
Semi−major Axis [arcsec]

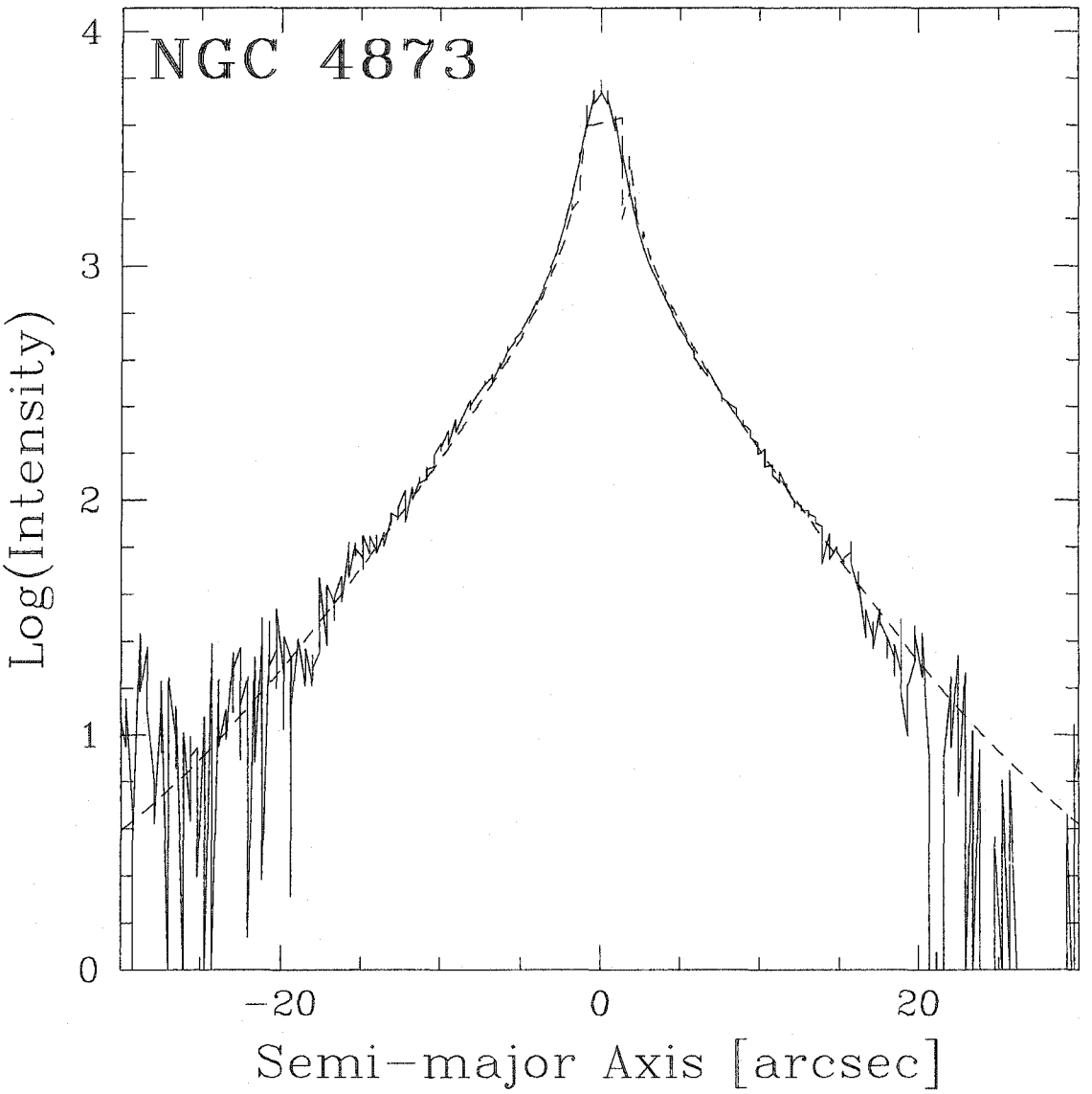
NGC 4873
Log(Intensity)
Semi-major Axis [arcsec]
0
1
2
3
4
-20
0
20

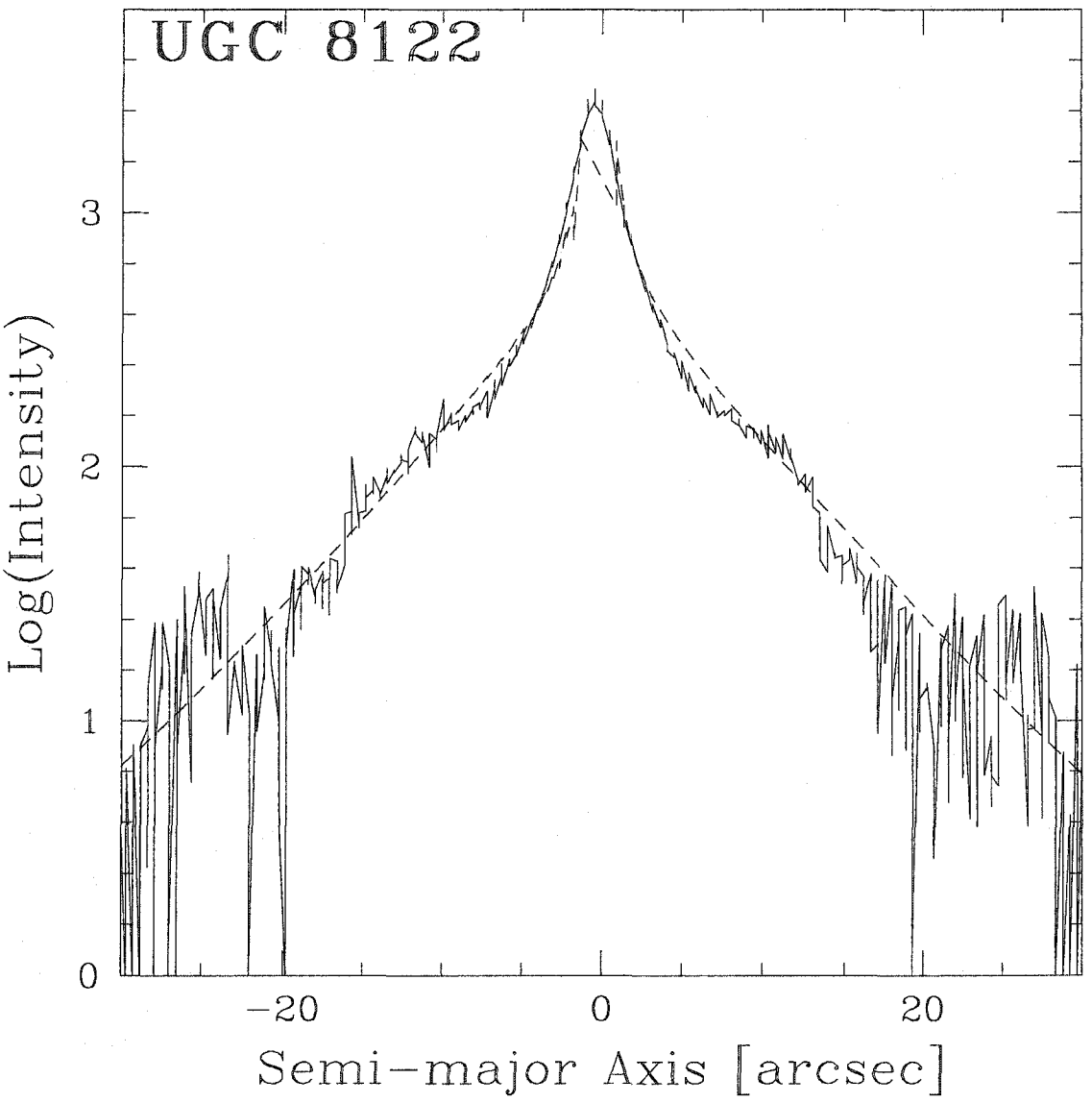

FIGURE 2.7. Observed log(Intensity) profiles along the major axis of each Coma S0 overlaid with the fitted bulge and disk decomposition.

Name	Type	RA	Dec	m_B	PA	Date	Time
*CGCG 160-040	S0	12:57:26	+27:32:45	14.9	-35	26 Apr 01	38
*CGCG 160-047	S0	12:57:47	+27:49:59	15.7	-88	13 Apr 02	40
*CGCG 160-089	SAB0	13:00:44	+28:20:13	15.2	50	17 Apr 02	40
*CGCG 160-091	SB0	13:00:52	+28:21:57	14.8	24	26 Apr 01	40
CGCG 160-109	SB0	13:02:09	+28:23:13	15.3	72	4 May 02	40
CGCG 160-119	S0	13:03:10	+28:35:01	15.1	38	4 May 02	20
CGCG 160-214	S0	12:59:02	+28:13:31	15.2	-68	5 May 02	40
IC 3946	SAB0/a	12:58:49	+27:48:37	15.4	73	5 May 02	30
IC 3955	SAB0/a	12:59:06	+27:59:48	15.4	25	26 Apr 01	40
IC 3976	SA0	12:59:29	+27:51:00	15.7	-29	9 May 02	40
IC 3990	SAB0/a	12:59:39	+28:53:44	15.3	23	9 Jun 02	15
IC 4088	Sab	13:01:43	+29:02:40	14.7	88	26 Apr 01	20
IC 4111	S0	13:02:56	+28:04:15	16.0	-47	9 May 02	40
NGC 4873	S0	12:59:33	+27:59:00	15.0	-80	26 Apr 01	40
UGC 8122	S0/a	13:00:50	+27:24:21	15.0	-20	15 Apr 02	40

TABLE 2.4. Coma S0 Sample. Column header explanations. Col. (1): Galaxy name. Col. (2): Morphological type. Col. (3): Epoch J2000 right ascension. Col. (4): Epoch J2000 declination. Col. (5): Apparent B-band magnitude. Col. (6): Position angle of major axis (degrees). Col. (7): Date of spectroscopic observation. Col. (8): Spectroscopy exposure time (minutes). Those galaxies marked with asterisks are not included in the final analysis; rotation curves for these four S0s were not of high enough quality at the scalelengths necessary to extract a maximum circular velocity for the TFR.

axis, date of observation, and exposure times for each galaxy. Observations were taken in a similar way to the Coma S0 galaxies at the MMT, with quartz flat and arc lamp spectra interspersed with S0 and template giant star observations. Data reduction was identical to the steps taken for the Coma spectroscopy. For two of the galaxies, VCC 1318 and VCC 1537, we could not extract rotation curves out to the regime where the rotational velocity is dominant. These were removed from the sample and are not discussed further, leaving us with eight remaining Virgo S0 galaxies in the sample.

Separate I-band images for the Virgo cluster S0 galaxies were not taken. Instead, we used H-band surface photometry from Gavazzi and collaborators. Calculated total H-band magnitudes, as well as H-band images, were obtained through the Galaxy On Line Database Milano Network (GOLD Mine; Gavazzi et al. 2003). To determine inclinations, we fitted the H-band data with IRAF's ELLIPSE task, as described in the previous section. Two-dimensional models of the galaxies were created in the same way as for the Coma sample, using Rix & Zaritsky (1995). The exception was VCC 1030, for which no H-band image was available from the database. Assuming that the dust extinction in an S0 galaxy in the near-infrared bands is negligible and assuming that the H- and K-bands trace the same underlying old stellar population, we determined inclination and scale-lengths for VCC 1030 using the K-band image.

Name	Type	RA	Dec	m_B	PA	Date	Time
VCC 698	S0	12:24:05.0	+11:13:06	13.60	-81	20 Mar 01	120
VCC 944	SB0	12:26:50.5	+09:35:02	12.08	50	18 Mar 01	120
VCC 1030	SB(s)0	12:27:40.5	+13:04:44	11.84	11	21 Mar 01	120
VCC 1062	SB(s)0	12:28:03.9	+09:48:14	11.40	83	21 Mar 01	120
VCC 1125	S0	12:28:43.4	+11:45:21	13.30	32	18 Mar 01	120
VCC 1242	S0	12:28:53.3	+14:04:06	12.60	79	19 Mar 01	120
VCC 1318*	SB(s)0/a	12:30:51.4	+08:21:36	12.86	-31	19 Mar 01	120
VCC 1535	SAB(s)0	12:34:03.1	+07:41:59	10.61	-65	20 Mar 01	90
VCC 1537*	S0	12:34:06.1	+11:19:17	12.70	6	20 Mar 01	120
VCC 1938	S0-	12:42:47.4	+11:26:33	12.11	-57	19 Mar 01	120

TABLE 2.5. Virgo S0 Sample. Column header explanations. Col. (1): Galaxy name. Col. (2): Morphological type. Col. (3): Epoch J2000 right ascension. Col. (4): Epoch J2000 declination. Col. (5): Apparent B-band magnitude. Col. (6): Position angle of major axis (degrees). Col. (7): Date of spectroscopic observation. Col. (8): Spectroscopy exposure time (minutes). Those galaxies marked with asterisks are not included in the final analysis; rotation curves for those two S0s were not of high enough quality at the scalelengths necessary to extract a maximum circular velocity for the TFR. All galaxies have H-band FITS images from the GOLD Mine database except for VCC 1030 which has K-band data only.

Chapter 3

TULLY-FISHER RELATION FOR CLUSTER S0'S

3.1 Determination of Rotation Curves

To determine rotation curves, each observed velocity along the major-axis of the galaxy, $v_{obs}(R)$, is corrected for inclination angle, i, using the output of the elliptical isophote fitting program and assuming a disk axis ratio, q_0, of 0.22 following Neistein et al. (1999). An asymmetric drift correction must be performed where there is significant velocity dispersion to obtain the circular velocity, $v_c(R)$, at each point. This correction is carried out as described in Hinz, Rix & Bernstein (2001). Following Binney & Tremaine (1987), application of the Jeans Equations and use of the relationship $v_c^2 = R(\frac{\partial \Phi}{\partial R})$ gives

$$v_c^2 = v_\phi^2 + \sigma_\phi^2 - \sigma_r^2 - \frac{R}{\nu}\frac{\partial(\nu v_R^2)}{\partial R} - R\frac{\partial(v_R v_z)}{\partial z}$$

where v_ϕ is the azimuthal velocity, σ_ϕ is the azimuthal velocity dispersion, and ν is spatial density of stars of the form $\nu = \nu_0 e^{-\frac{R}{R_{exp}}}$. If we neglect the $v_R v_z$ term and take $\sigma_\phi^2/\sigma_r^2 = 0.5$ for a flat rotation curve, we arrive at

$$v_c^2 = v_\phi^2 + \sigma_\phi^2[2(\frac{R}{R_{exp}} - \frac{\partial ln\sigma_R^2}{\partial ln R}) - 1].$$

For many of the S0 galaxies, $\frac{\partial ln\sigma_R^2}{\partial ln R}$ is small in the disk (see also Neistein et al. 1999) and can be neglected, leaving

$$v_c^2 = v_\phi^2 + \sigma_\phi^2(2\frac{R}{R_{exp}} - 1).$$

The magnitude of the asymmetric drift correction is dependent on the value of the velocity dispersion and is usually in the range $\sim 5 - 50$ km s^{-1}. Error bars on the

$v_c(R)$ data points include propagation of the uncertainties in v_{obs}, σ_{obs}, and inclination angle, i.

To obtain a single maximum circular velocity value for each galaxy, we calculate a series of theoretically predicted rotation curves based on the bulge-disk decompositions. This "maximal disk" fitting (e.g., Courteau & Rix 1999) has been shown to successfully trace the total mass of the inner parts of spirals, even though it is simply a fit to the stellar light. We use an infinitely thin, exponential disk of the form

$$v_c^2(R) = 4\pi G\Sigma_0 R_d y^2[I_0(y)K_0(y) - I_1(y)K_1(y)],$$

where Σ_0 is the central surface density, R_d is the disk scale length, I_0, I_1, K_0 and K_1 are modified Bessel functions, and $y = \frac{R}{2R_d}$.

From Hernquist (1990), the bulge rotation curve can be modeled by

$$v_c^2 = \frac{GM(<R)}{R} = \frac{GM_{tot}}{R}\frac{R^2}{(R+a)^2}.$$

The scale length, a, is related to the effective radius of the bulge, R_e, by $a \sim R_e/1.8153$. We then add the disk and bulge components in quadrature to produce a model rotation curve for each S0. The only free parameter, the effective mass-to-light ratio, is then adjusted, and the best-fitting model circular velocity curve is extracted through a chi-squared minimization. Only rotation-dominated points, where $v_\phi > \sigma_\phi$, are included in the fit, because the approximations and systematics involved in the drift correction may lead to large errors in the calculated v_c if σ_ϕ is large. Figures 3.1-3.11 show the bulge and disk model components (upper panels), the velocity dispersion data points (lower right panels), the circular velocity data points, and the fitted model rotation curve for each galaxy (lower left panels). These plots show the predicted rotation curves at all radii; however, in the inner parts of the S0 galaxies where the dispersion dominates, a match should not be expected.

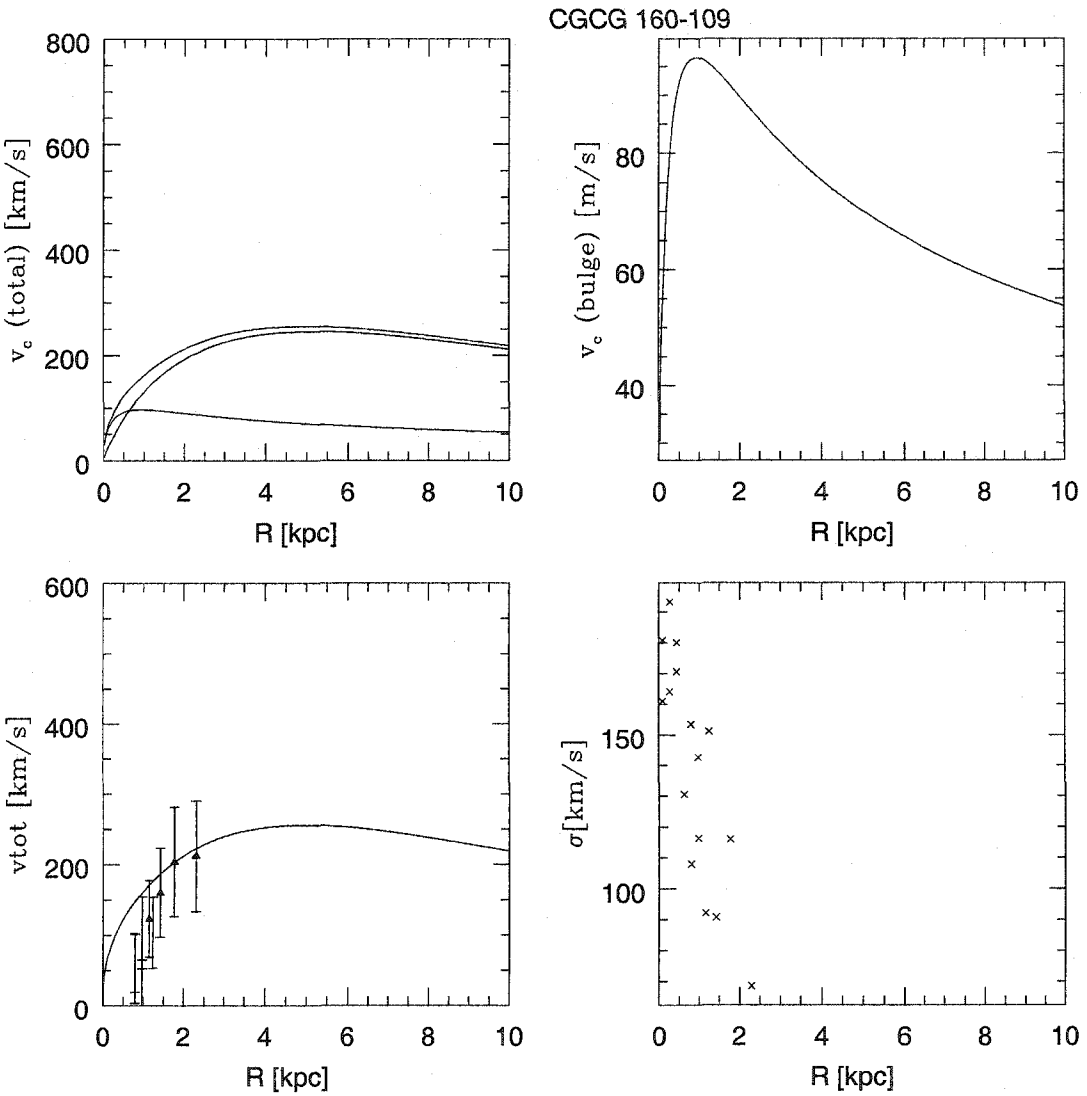

FIGURE 3.1. Rotation curve for CGCG 160-109.

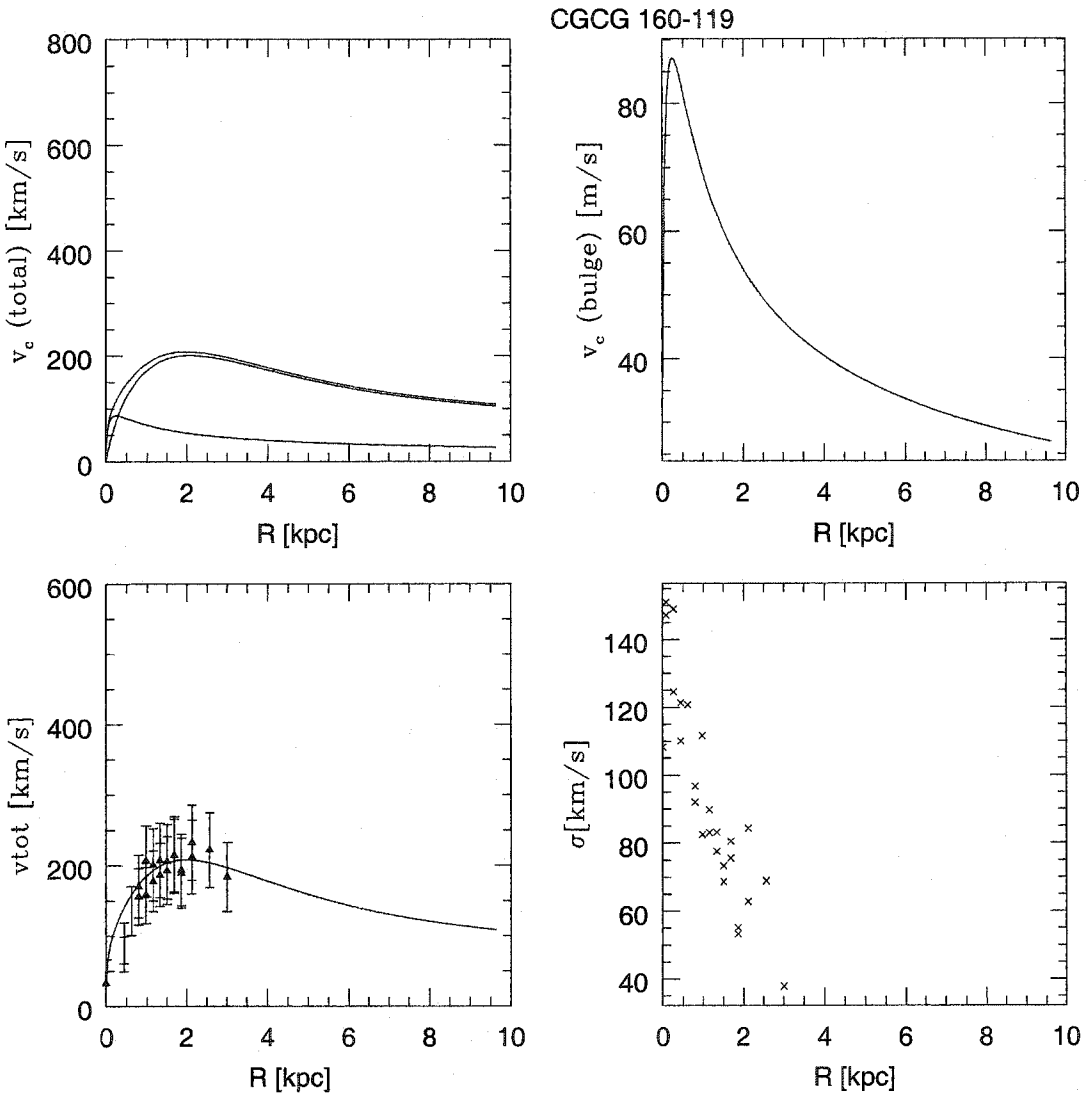

FIGURE 3.2. Rotation curve for CGCG 160-119.

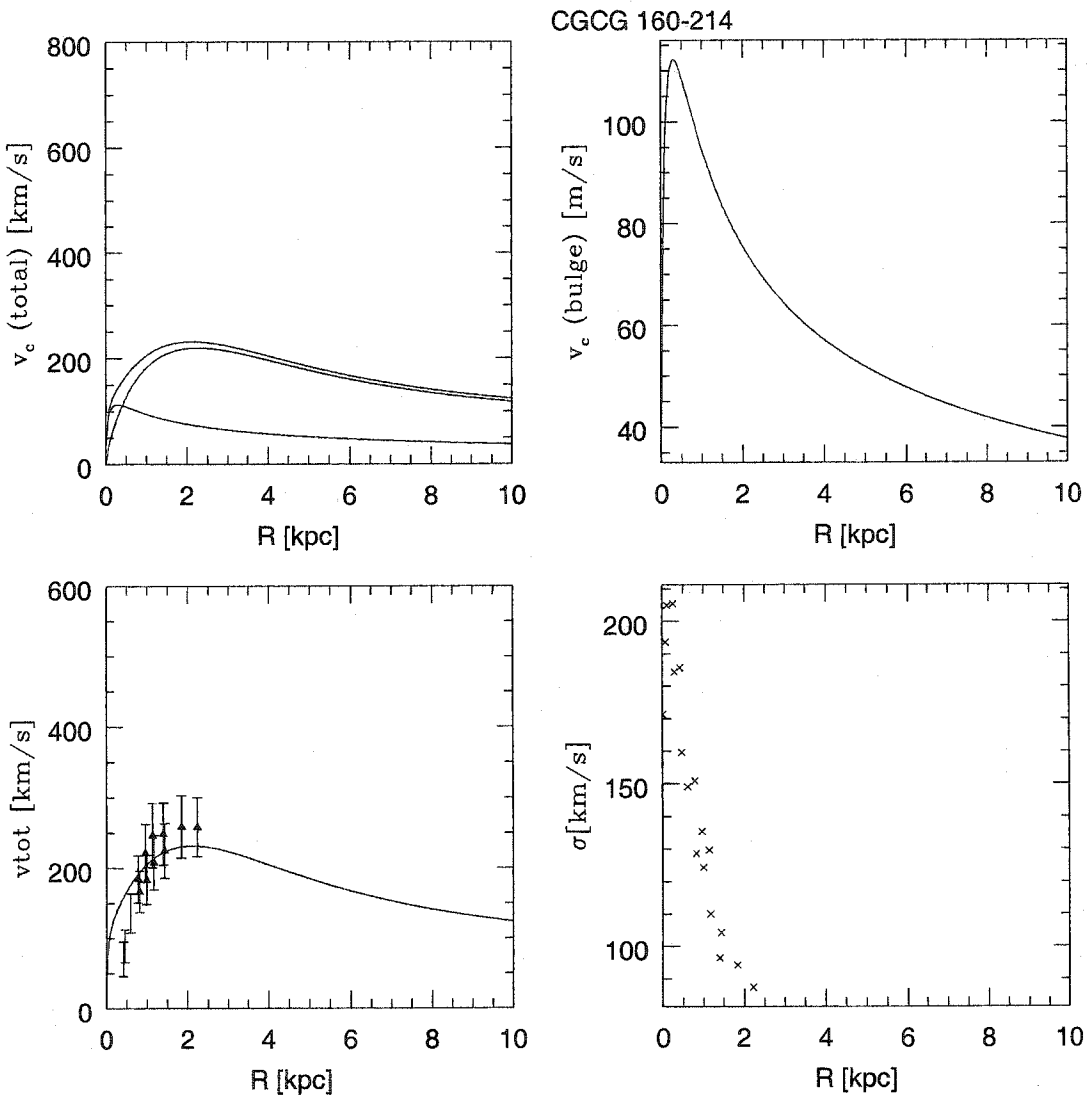

FIGURE 3.3. Rotation curve for CGCG 160-214.

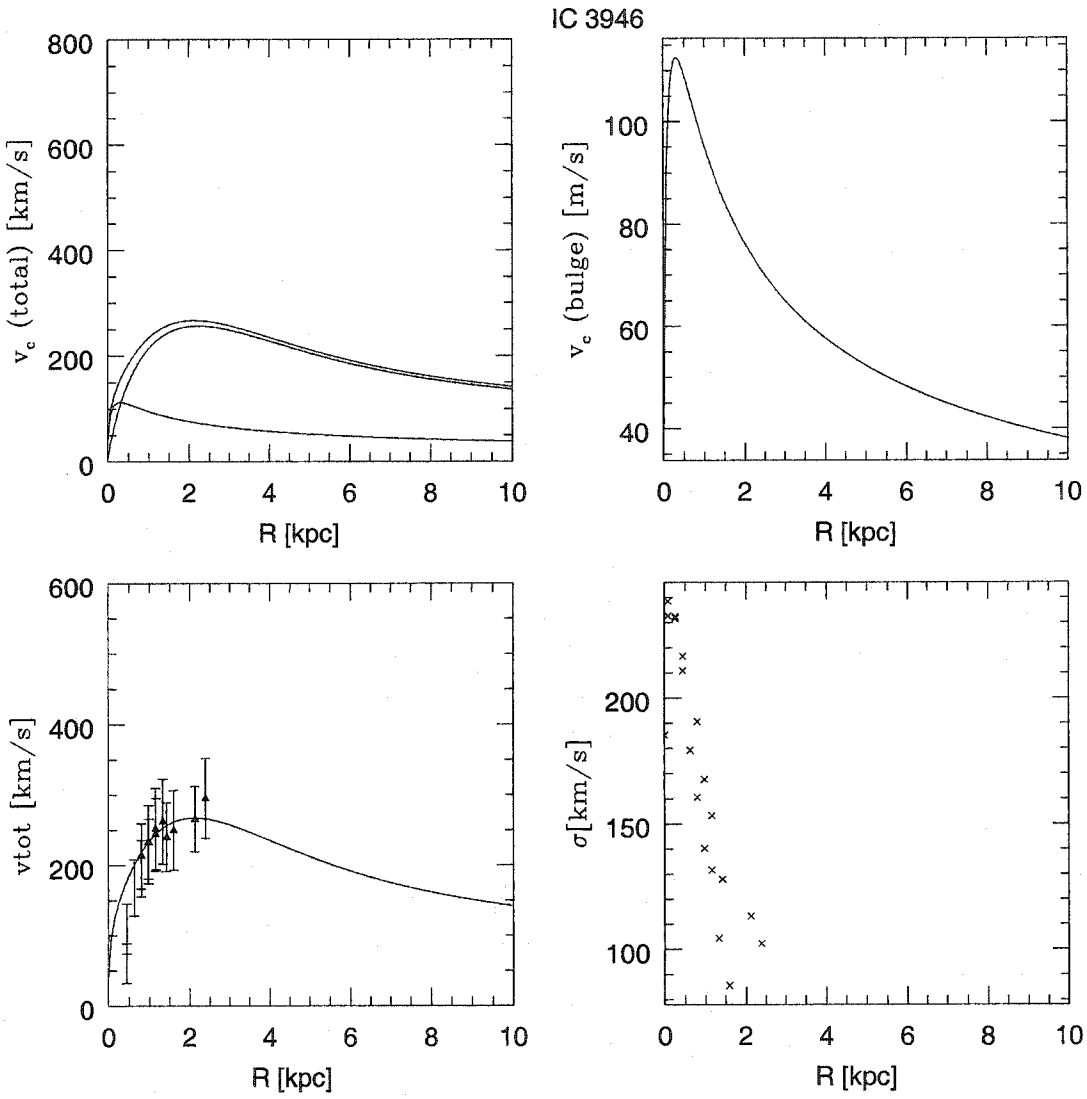

FIGURE 3.4. Rotation curve for IC 3946.

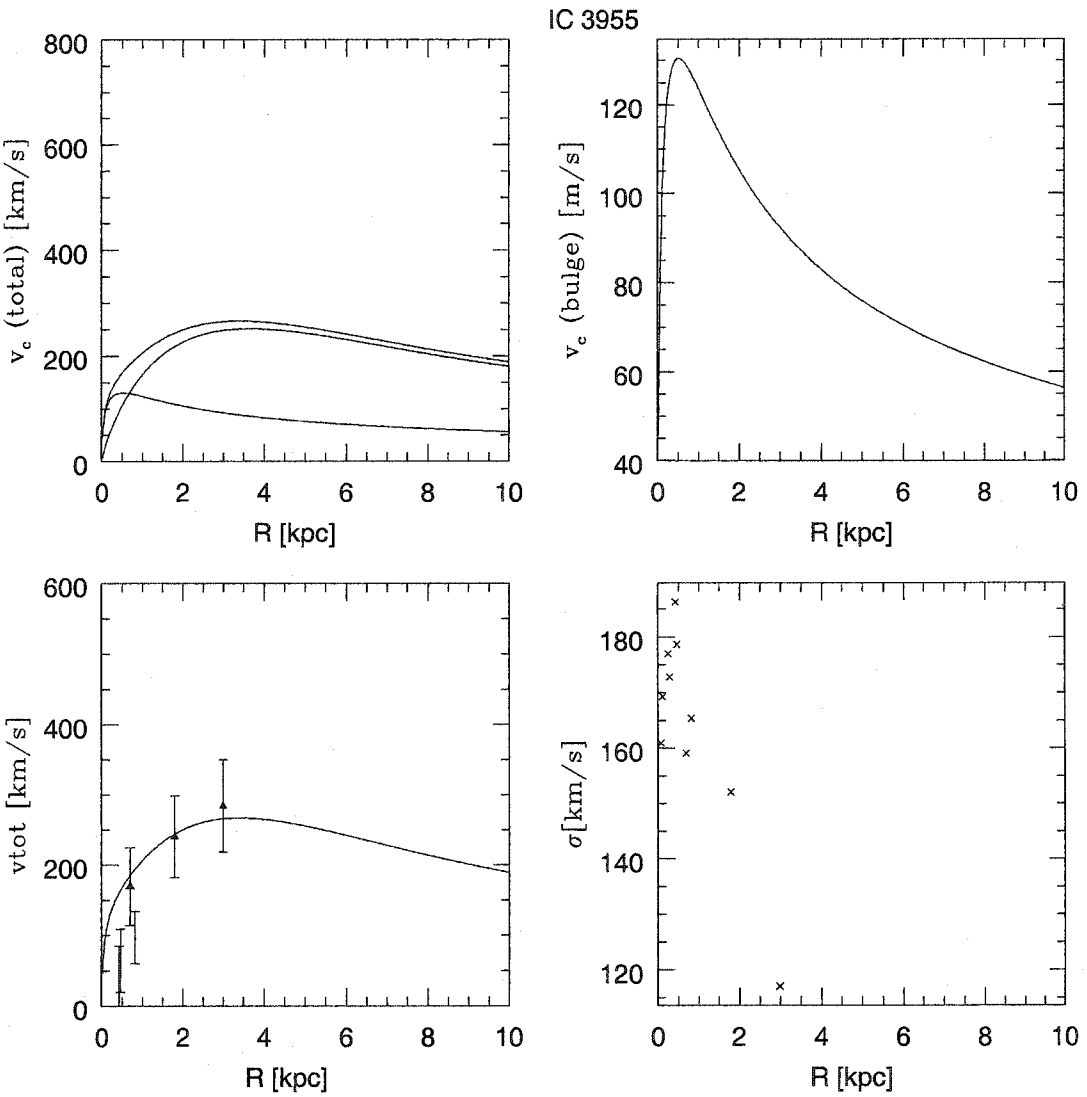

FIGURE 3.5. Rotation curve for IC 3955.

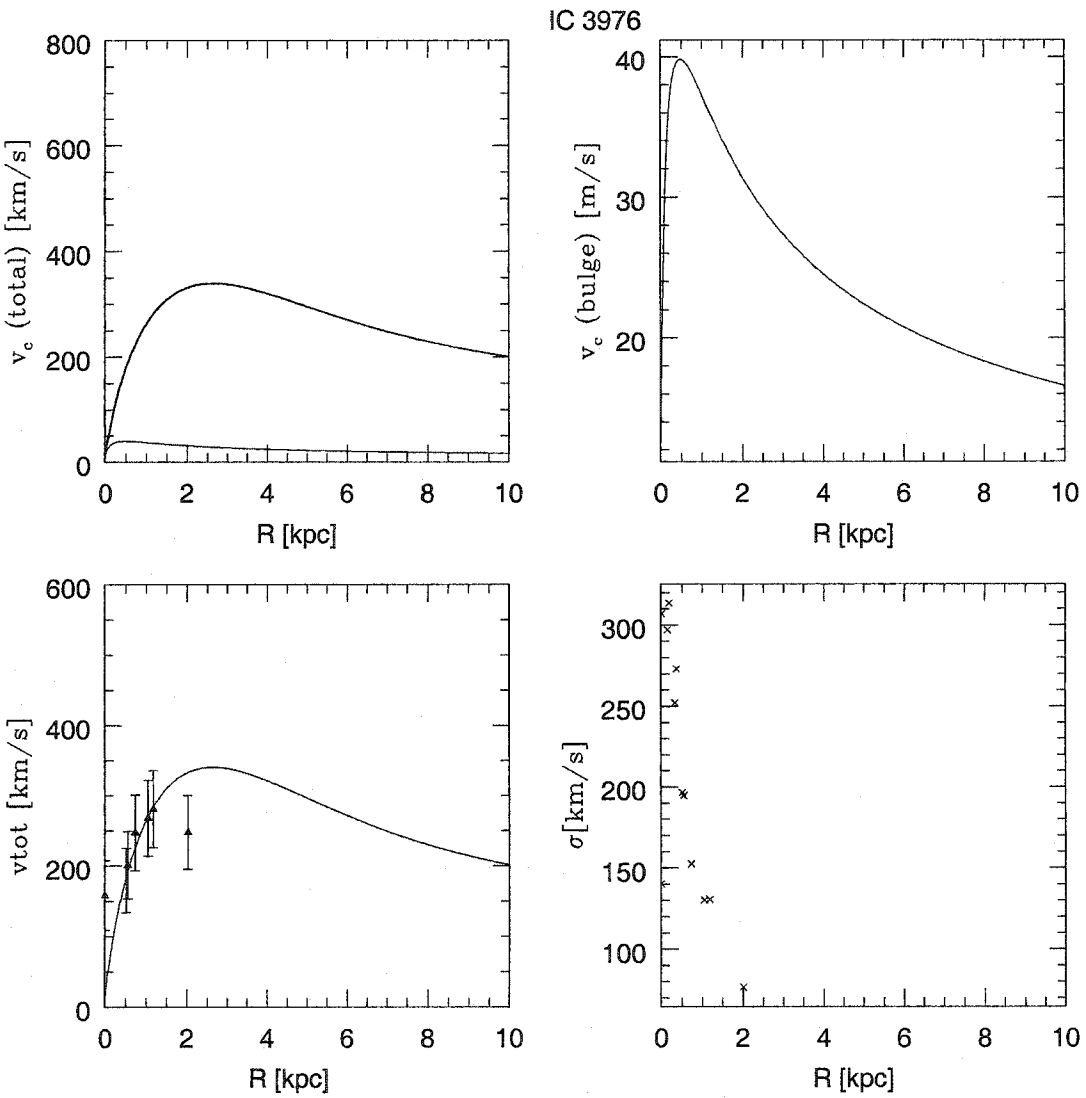

FIGURE 3.6. Rotation curve for IC 3976.

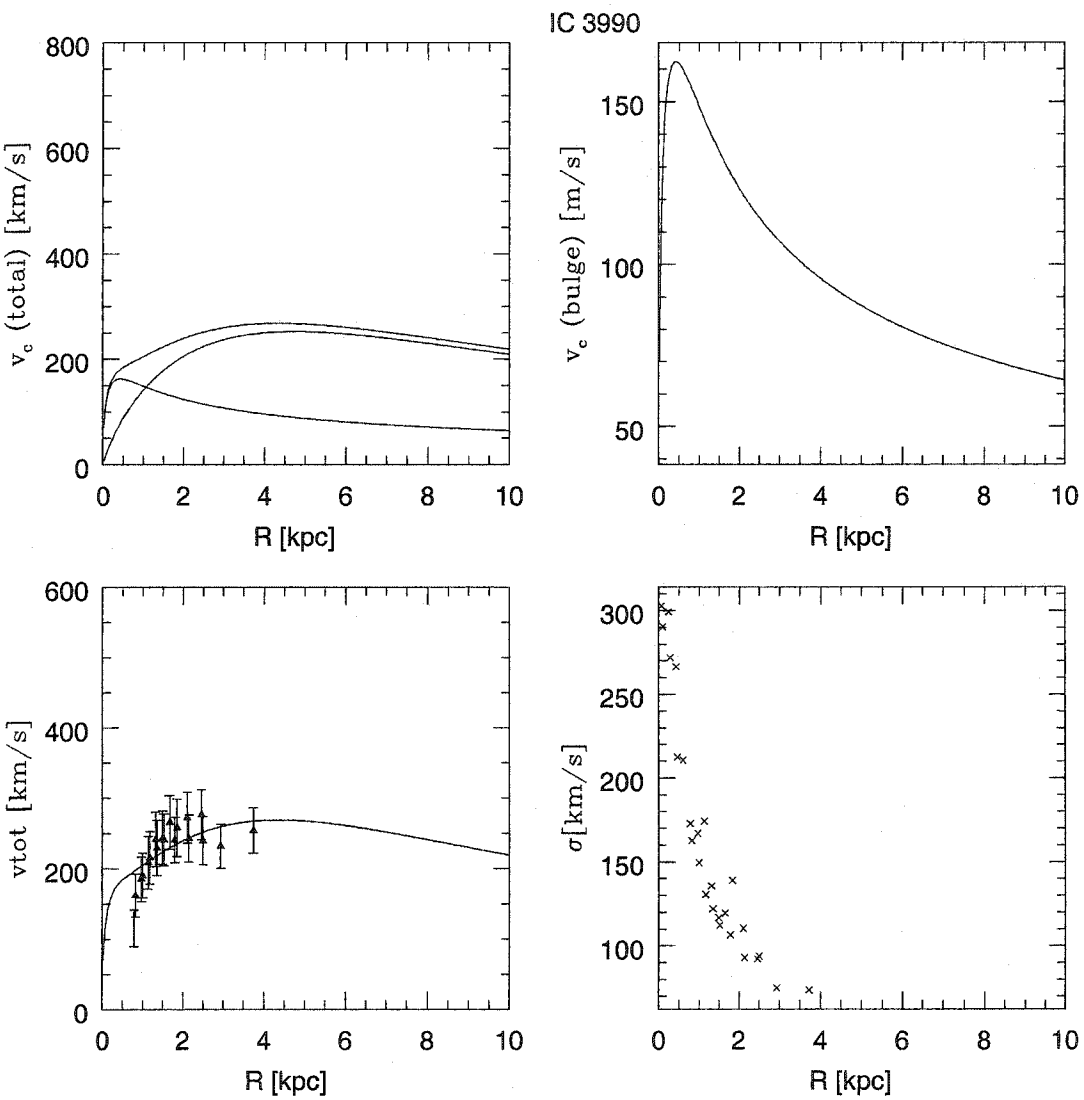

FIGURE 3.7. Rotation curves for IC 3990.

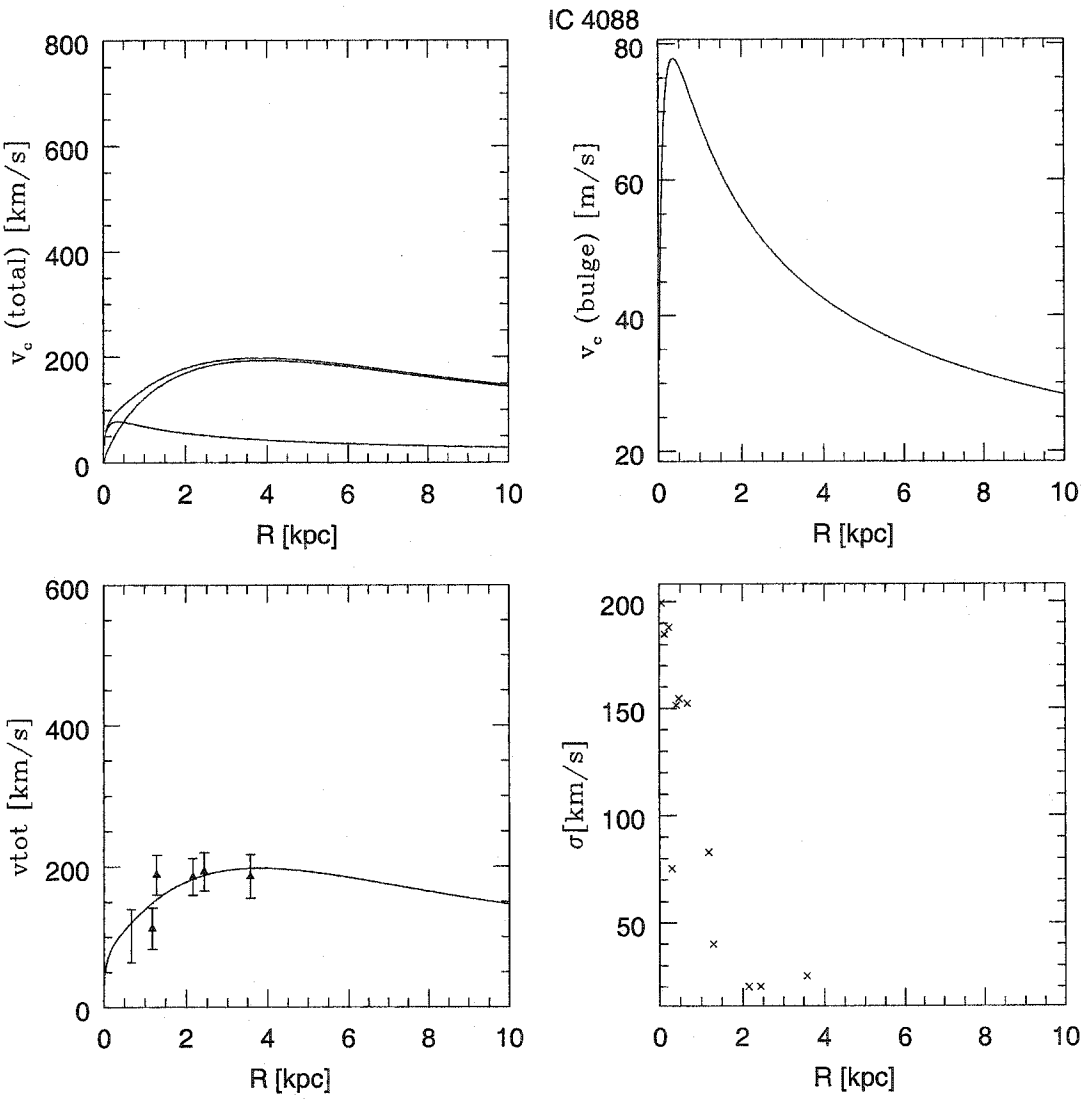

FIGURE 3.8. Rotation curve for IC 4088.

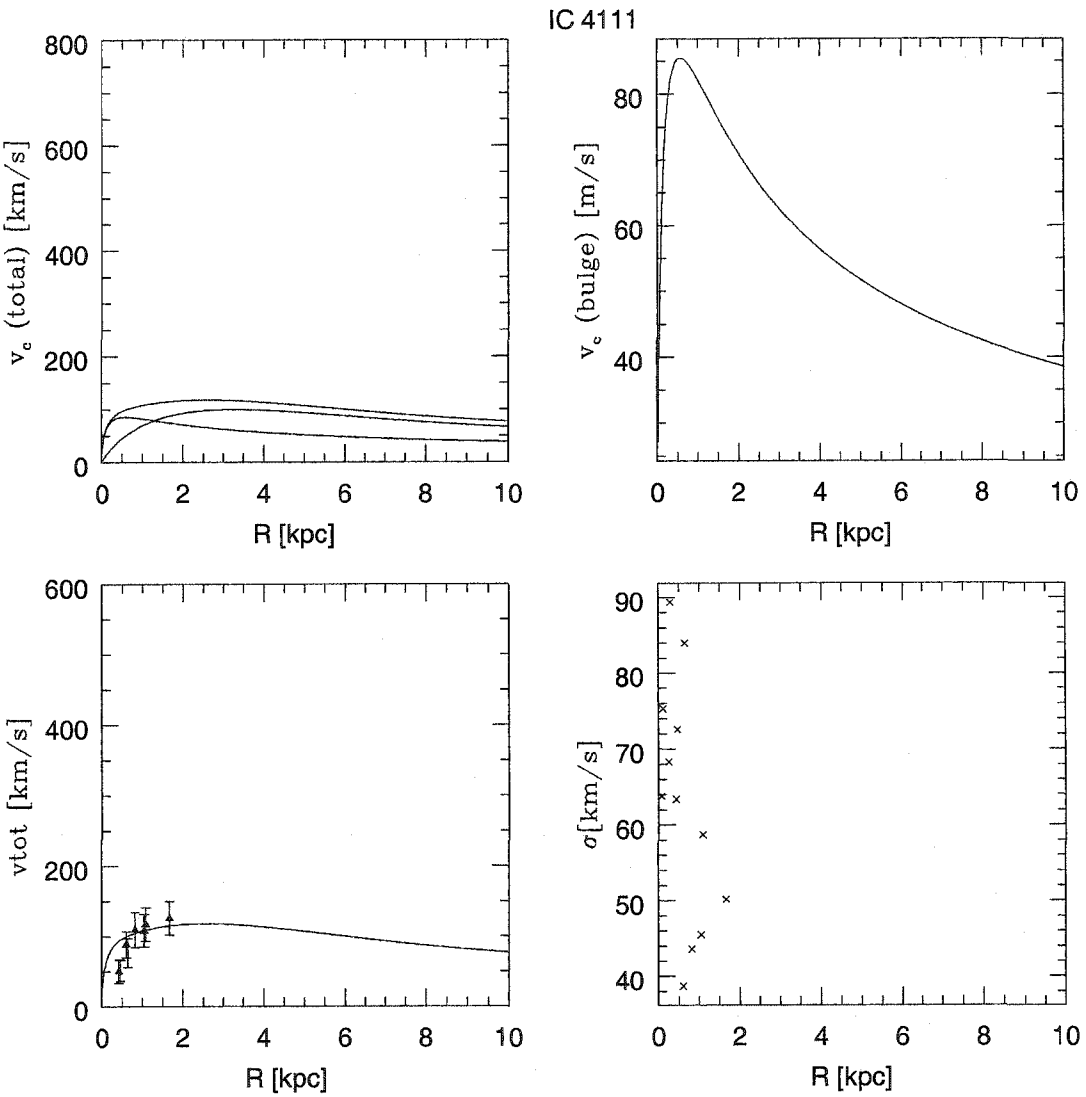

FIGURE 3.9. Rotation curve for IC 4111.

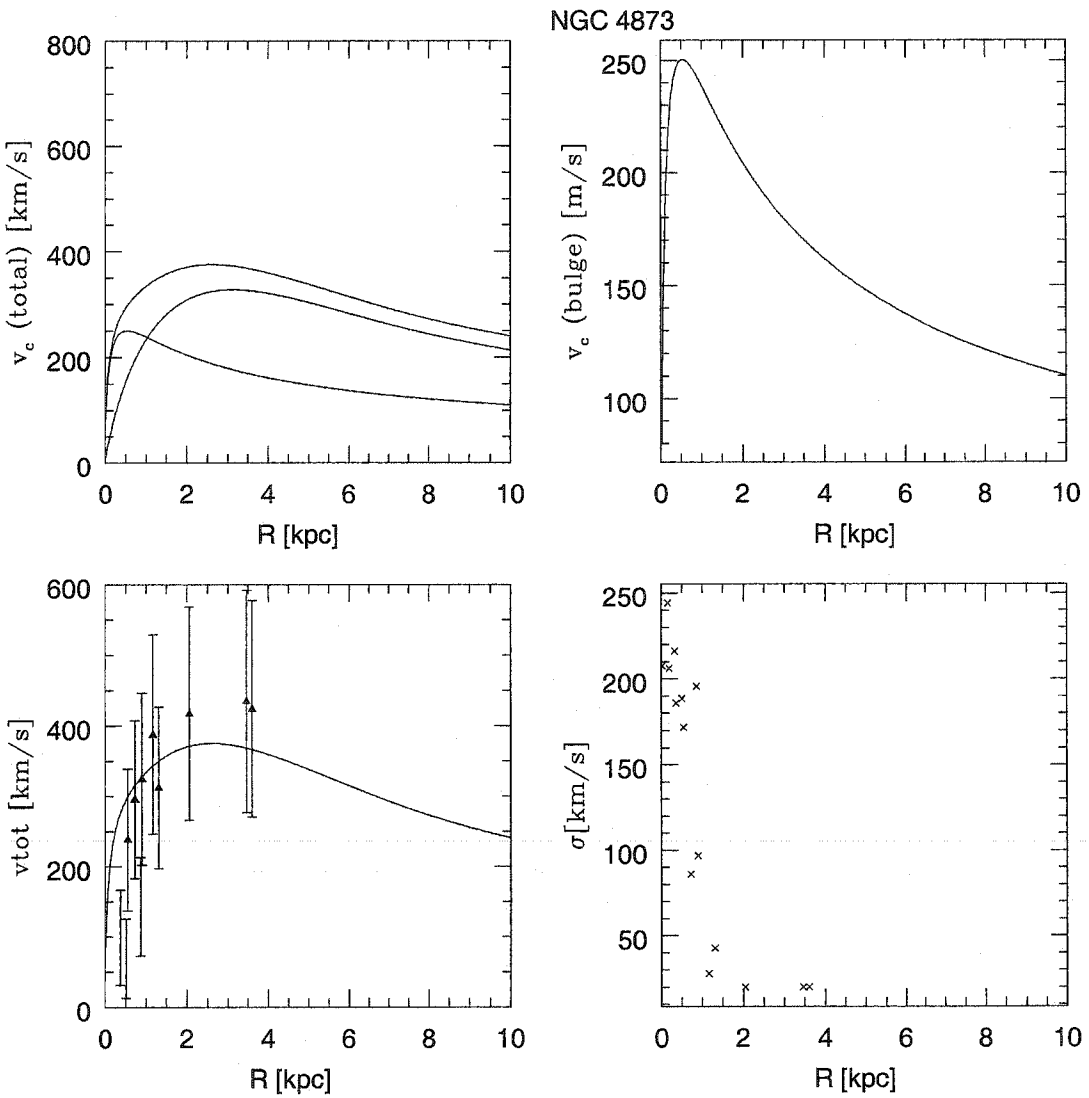

FIGURE 3.10. Rotation curves for NGC 4873.

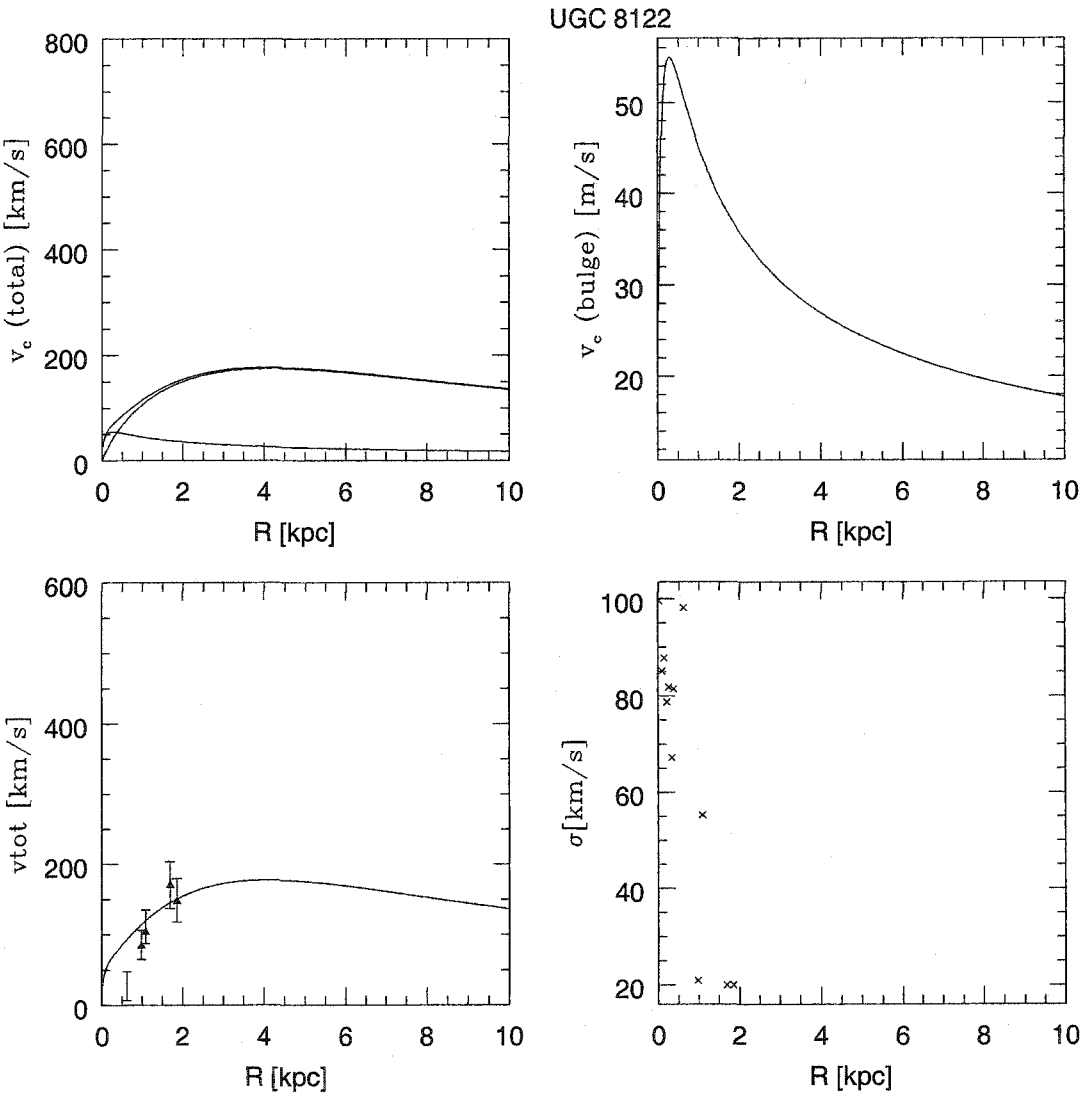

FIGURE 3.11. Rotation curve for UGC 8122.

3.2 Rotation-Luminosity Relations

Figure 3.12 shows our absolute I-band magnitudes versus the maximum predicted circular velocities resulting from our analysis for the Coma S0 sample, and Table 3.1 lists the values with error bars. Both the Hinz, Rix & Bernstein (2001) sample and the additional Coma S0s from this work are represented. We assume a radial velocity of $v_z = 6942$ km s^{-1} for Coma (Zabludoff et al. 1993) and $H_0 = 80$ km s^{-1} Mpc^{-1} as used by Neistein et al. (1999). Velocity error bars are calculated from a likelihood ratio test, i.e. $\delta v_{max} = |v_{max}(\chi^2_{min}) - v_{max}(\chi^2_{min} + 1)|$. A linear best fit to the data is performed to determine the slope, zero-point, and scatter of any TFR. A specified velocity-luminosity parameter box is searched to find a best likelihood given by $p_{data}(x, y) \times p_{model}(x, y)$, where $p_{data}(x, y)$ reflects the measurement errors and $p_{model}(x, y)$ reflects the model probability, which is the TFR with its scatter (Rix et al. 1997). The linear best fit (Rix et al. 1997) performed by Hinz, Rix & Bernstein (2001) on the *original* Coma sample of the form

$$M_I(\log v_c) = M_I(2.3) - \alpha(\log v_c - 2.3)$$

yielded $\alpha = 3.33^{+3.10}_{-2.79}$, with a zero-point of $M_I(2.3) = -21.83 \pm 0.30$ mag and a scatter of $\sigma = 0.44^{+0.32}_{-0.15}$. When the slope was fixed to that of late-type spirals, $\alpha = 7.46$ (Mathewson et al. 1992), they obtained a zero-point of $M_I(2.3) = -21.65 \pm 0.35$ mag, with an intrinsic scatter of $\sigma = 0.53^{+0.30}_{-0.20}$. These results were compromised by the small sample size and uncertainties in the derived rotation curves due to the fact that the velocity data did not extend very far into the disks of the S0s.

Adding 10 new Coma S0s to the Hinz, Rix & Bernstein (2001) sample and using the same fitting program as before, with no slope restriction, produces the following relations: for the new S0s only, $\alpha = 1.12^{+1.47}_{-1.64}$, $M_I(2.3) = -21.33^{+0.23}_{-0.24}$, and $\sigma = 0.34^{+0.28}_{-0.13}$; for all S0s, both new and old samples, $\alpha = 1.45^{+1.81}_{-1.99}$, $M_I(2.3) = -21.62^{+0.25}_{-0.24}$, and $\sigma = 0.52^{+0.23}_{-0.14}$. The slope of this relation is obviously not well constrained by the

Name	M_I	M_H	v_{max}
CGCG 160-109	-21.56 ± 0.10	-23.24 ± 0.15	$255.65^{+50.04}_{-50.39}$
CGCG 160-119	-21.32 ± 0.10	-23.08 ± 0.15	$207.83^{+7.65}_{-16.22}$
CGCG 160-214	-21.29 ± 0.10	-23.40 ± 0.15	$233.90^{+12.65}_{-30.59}$
IC 3946	-21.83 ± 0.10	-23.37 ± 0.15	$267.22^{+19.34}_{-18.45}$
IC 3955	-21.10 ± 0.10	-23.20 ± 0.15	$266.80^{+39.67}_{-40.06}$
IC 3976	-21.18 ± 0.10	-23.03 ± 0.15	$317.39^{+31.59}_{-29.83}$
IC 3990	-22.09 ± 0.10	-23.95 ± 0.15	$268.61^{+9.89}_{-6.80}$
IC 4088	-21.75 ± 0.10	-23.62 ± 0.15	$197.70^{+13.42}_{-14.40}$
IC 4111	-20.62 ± 0.10	-22.46 ± 0.15	$106.61^{+9.91}_{-9.29}$
NGC 4873	-21.31 ± 0.10	-23.53 ± 0.15	$375.17^{+50.03}_{-50.38}$
UGC 8122	-21.37 ± 0.10	-22.99 ± 0.15	$177.06^{+55.07}_{-59.95}$
VCC 698	—	-20.72 ± 0.15	$180.61^{+14.00}_{-14.04}$
VCC 944	—	-22.23 ± 0.15	$155.66^{+17.98}_{-17.98}$
VCC 1030	—	-22.73 ± 0.15	$199.40^{+14.30}_{-14.55}$
VCC 1062	—	-23.13 ± 0.15	$209.98^{+9.77}_{-10.25}$
VCC 1125	—	-21.34 ± 0.15	$87.95^{+3.24}_{-3.36}$
VCC 1242	—	-21.62 ± 0.15	$84.45^{+6.99}_{-4.49}$
VCC 1535	—	-24.00 ± 0.15	$343.19^{+10.19}_{-8.73}$
VCC 1938	—	-22.18 ± 0.15	$211.21^{+12.52}_{-12.66}$

TABLE 3.1. The S0 galaxy sample magnitudes and derived maximum velocities. Column header explanations. Col. (1): Galaxy name. Col (2): I-band absolute magnitude. Col. (3): H-band absolute magnitude. Col. (4): Maximum circular velocity (km s^{-1}).

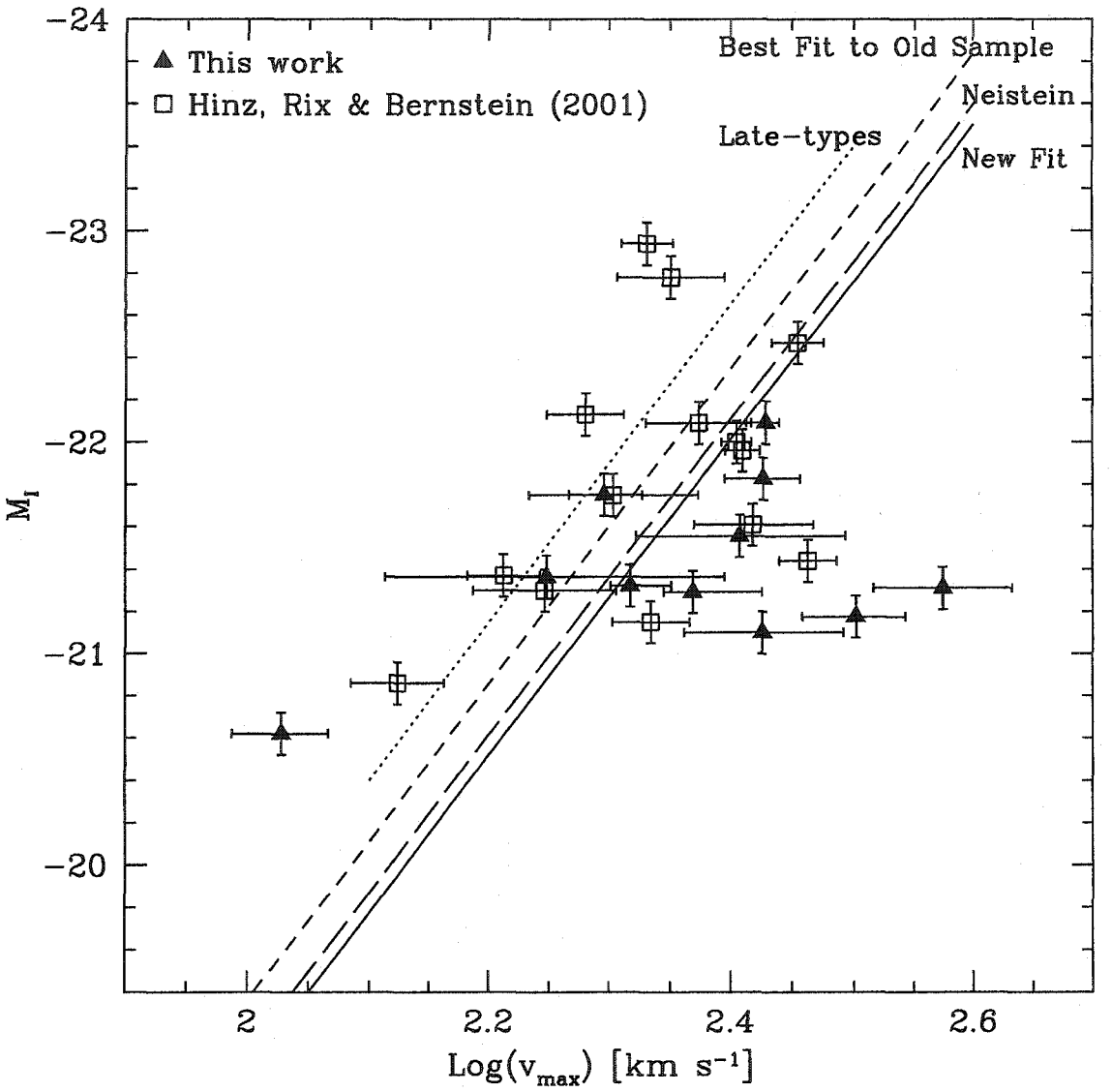

FIGURE 3.12. A Tully-Fisher-type fit to I-band photometry of Coma S0 galaxies. The late-type relation (left dotted line) is from Mathewson et al. (1992). The short-dashed line is the best fit line to the original Coma sample. The long-dashed line is the Neistein et al. (1999) fit to their sample of field S0s. The right solid line is the best fit to all the Coma S0s plotted.

data. To make a direct comparison with the TFR for late-type spirals, we choose also to fit the relation by holding the slope at the late-type spiral value, $\alpha = 7.46$. This slope value from Mathewson et al. (1992) is based on I-band photometry and Hα and H I rotation curves of 1355 galaxies and is used to fix the slope in the Neistein et al. (1999) study of field S0s. For this value, for the new Coma S0s, the best fit becomes $M_I(2.3) = -20.87^{+0.67}_{-0.66}$ and $\sigma = 0.89^{+0.81}_{-0.38}$ and for all Coma S0s, $M_I(2.3) = -21.27 \pm 0.40$ and $\sigma = 0.82^{+0.39}_{-0.25}$. Figure 3.12 includes the late-type I-band TFR from Mathewson et al. (1992) as well as a best fit line to field S0s calculated by Neistein et al. (1999). Also shown are the best-fit lines to our data, both the fit to the original Coma sample and the fit to all Coma S0s with $\alpha = 7.46$. A Spearman rank test, a non-parametric estimator of the correlation between two variables, on the new sample gives a $\sim 65\%$ probability that the relation was drawn from a random sample (one that is uncorrelated). For the entire sample, this probability is $\sim 31\%$.

The two Coma objects from the Hinz, Rix & Bernstein (2001) sample that were re-observed, IC 3990 and IC 4088, were probed out to much further in the disk in the new observations. The new rotation curve for IC 3990 goes out to 3.7 kpc, compared to 1.6 kpc in the previous observations. Likewise, the new rotation curve for IC 4088 goes out to 3.6 kpc instead of 1.4 kpc. The maximum velocities acquired from both sets of observations agree well. From Hinz, Rix & Bernstein (2001), $v_{max}(R) = 236.62 \pm 23.56$ km s^{-1} for IC 3990 and 201.13 ± 32.43 km s^{-1} for IC 4088. The new observations give $v_{max}(R) = 268.61 \pm 9.89$ km s^{-1} for IC 3990 and 197.696 ± 14.40 km s^{-1} for IC 4088. Even without probing further into the disk, the maximal disk fitting routine seems to predict the maximum velocity fairly well. Therefore, we can be reasonably confident in the values for the other S0s observed in the Hinz, Rix, & Bernstein (2001) sample.

There are some objects that are far outliers from the late-type TFR. Three objects, NGC 4873, IC 3976, and IC 3955 appear to be rotating much faster than expected for their luminosities, or, alternatively, are much too faint for their rotation velocities,

appearing to the lower right of the late-type spiral TFR. This behavior cannot be an artifact of an insufficient pressure support correction, but indicates a differing M/L when measured over the whole galaxy. Since the colors and stellar populations of S0 galaxies do not show great variance, this may reflect a different mix of luminous (or stellar) to dark matter, perhaps due to a peculiar merging history. Note that Neistein et al. (1999) showed that analogous field S0 galaxies in their sample satisfy the fundamental plane relation, indicating normal M/L at the center.

It is obvious that the value of the M_I-v_c scatter for the Coma S0s, $\sigma = 0.82^{+0.39}_{-0.25}$, is much larger than that found in the I-band for late-type spirals and also larger than that predicted by numerical simulations (e.g., Steinmetz & Navarro 1999). The values for late-type spirals from the literature for comparison are $\sigma = 0.2$ mag (Sakai et al. 2000), $\sigma = 0.1$ mag (Bernstein et al. 1994), $\sigma = 0.32$ mag (Mathewson et al. 1992), and $\sigma = 0.35$ mag (Giovanelli et al. 1997). The S0 scatter is consistent, however, with two previous studies of a possible TFR in these galaxies: the Neistein et al. (1999) study of field S0s found $\sigma = 0.7$ mag and Hinz, Rix & Bernstein (2001) found $\sigma = 0.53^{+0.30}_{-0.20}$.

A third study of S0s using different techniques to recover the kinematics (Mathieu, Merrifield, & Kuijken 2002) finds a scatter about the best-fitting line of only ~ 0.3 mag with a sample of six S0s. One explanation for the lower scatter is the sparse statistical significance that can be achieved with only six cases. Another possibility is that the Mathieu et al. (2002) S0s are not representative because they were specifically chosen to contain small bulges. Such S0 galaxies may be the "prime candidates" to have formed from gas-stripped spirals. The original sample of Hinz, Rix & Bernstein (2001) consisted mainly of S0/a type galaxies, not E/S0 types, so that a similar bias towards S0s that are stripped spirals, and, therefore, a bias towards a small scatter in the TFR, may have occurred; this, however, was not reflected in the large scatter found for that sample. Again, in the new sample, most are of the S(AB)0 type, with four S0/a types, but the scatter in the TFR remains large. Figure 3.13 shows

the offset from the late-type I-band relation for each of the Coma S0s versus the ratio of the bulge scalelength to the disk scalelength. Although the relation is not tight, we can see that, in general, S0s with large bulges tend to be more offset from the late-type relation than those with small bulges and that there is more scatter in this relation for S0s with large bulges. The reliability of this plot depends strongly the two-dimensional model fits to the I-band S0 images. The two outlier points in Figure 3.13, at $R_{BULGE}/R_{DISK} \sim 0.7$ and offsets of 0.7 and 1.1, correspond to CGCG 160-109 and IC 4111. These two galaxies are fit well by their models, as shown in the comparison profiles of Figure 2.7. Similarly, the S0 galaxy in Figure 3.13 at $|\Delta M_I| \sim 2.6$, NGC 4873, has a model fit that is among the best in the sample. It seems unlikely, then, that the spread in R_{BULGE}/R_{DISK} values could be caused by poor two-dimensional fits.

Furthermore, Mathieu et al. (2002) find an offset from the late-type TFR of ~ 1.8 mag in the I-band. They propose this offset is expected (using Charlot & Bruzual models from 1991) if star formation had been suddenly switched off a few Gyr ago, so that the S0 galaxies contained just the old stellar population of a normal spiral galaxy. Hinz, Rix & Bernstein (2001) found that there was at most a small offset, $\Delta m_I \leq 0.2$, in the I-band luminosity at a given circular velocity, $v_c \sim 200$ km s^{-1}, between late-type spirals and the S0s. This was interpreted as implying that the zero-point is weakly, if at all, dependent on galaxy type; a suggested explanation of this result was that S0s contain a smaller dark matter fraction than late-type spirals. The offset for the combined Coma samples is nearly identical to that found by Neistein et al. (1999) and corresponds to ~ 0.6 mag at $v_c \sim 200$ km s^{-1}. We still do not find an offset as large as the ~ 1.8 mag value of Mathieu et al. (2002). Using stellar population models (Worthey 1994), we expect an S0 galaxy comprised of a 5 Gyr old single burst population to be ~ 0.53 mag fainter in the I-band than a late-type spiral with the same age population with star formation bursts every 1 Gyr. Our Coma results would agree with differences in star-forming history of this general

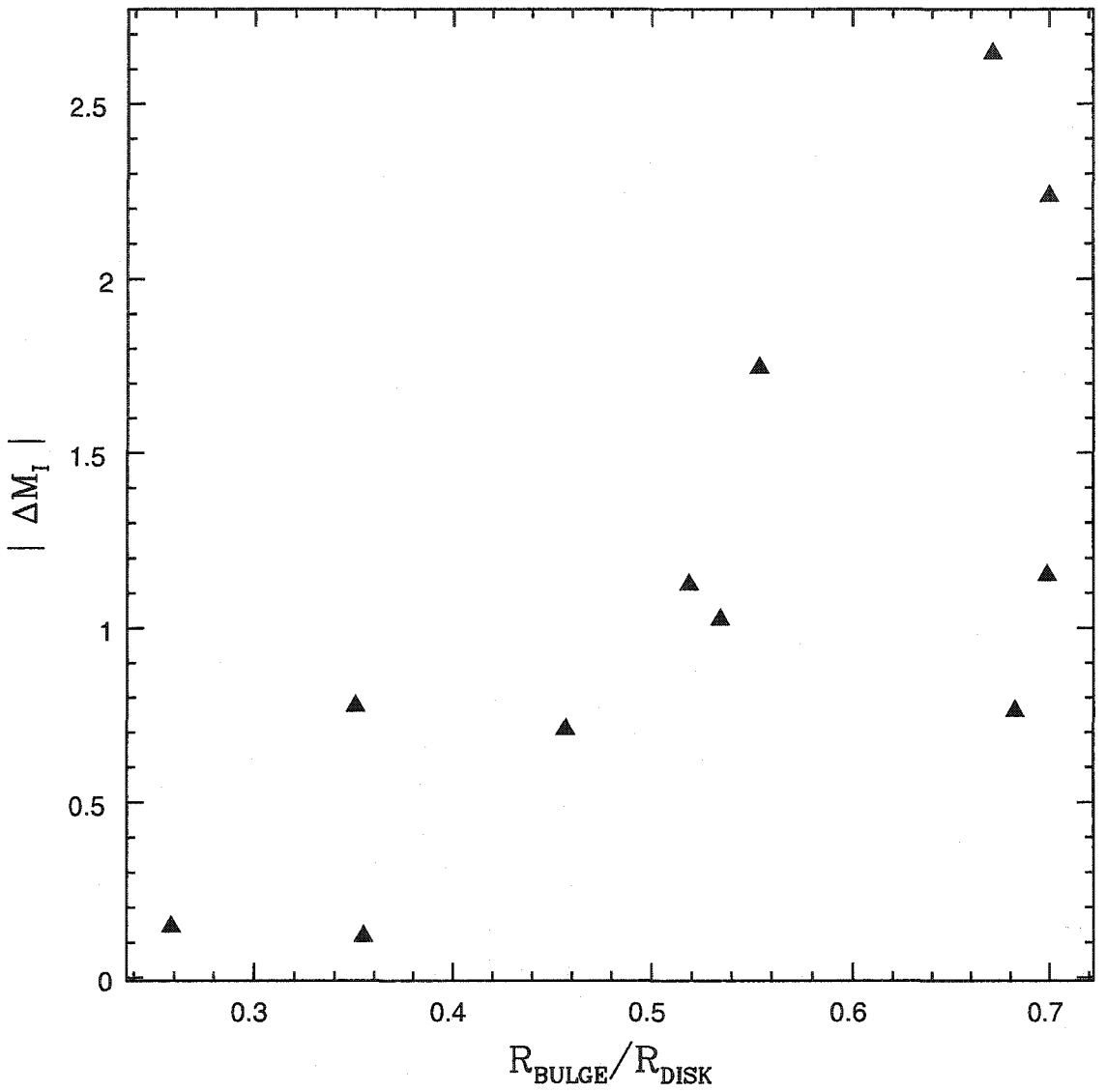

FIGURE 3.13. The offset of each Coma S0 galaxy from the late-type I-band TFR versus the ratio of the bulge and disk scalelengths.

type, although both the scatter in our data and the simplicity of this modeling would allow substantial variation.

Our I-band TFR for the Coma S0s can be compared to other photometry that samples the underlying old stellar population, such as H-band. The H-band TFR for late-type spirals has been explored in a variety of environments. The first such studies were conducted by Aaronson and collaborators in the 1970s and 1980s. In particular, a sample of 13 Coma spirals was determined by Aaronson et al. (1986) to have a slope of -9.9±0.8 and a scatter of 0.76 magnitudes. Bernstein et al. (1994) found an RMS scatter of 0.20 magnitudes using a sample of 17 Coma galaxies, some of which overlapped with the Aaronson et al. (1986) study. Pierce & Tully (1992) find a relation of $M_H = -9.50(\log W - 2.50) - 21.67 \pm 0.08$ for 15 spirals, with a dispersion of ~ 0.3 magnitudes. Gavazzi et al. (1999) constructed a TFR for both a sample of Virgo galaxies and a combination of 73 galaxies from the clusters Abell 262, Cancer, Coma, and Abell 1367. They find a scatter of 0.35 magnitudes for the cluster combination and 0.70 magnitudes for the Virgo late-type galaxies. A large study was presented by Sakai et al. (2000) as part of an HST Key Project. The observed dispersion of the H-band TFR appeared to be 0.36 magnitudes, with the best fitting relation given by $H_{-0.5} = -(11.03 \pm 0.86)(\log W_{20} - 2.5) - (21.74 \pm 0.14)$, where W_{20} is the width in km sec^{-1} of the H I profile measured at 20% of the peak of the H I flux. There have also been studies using the Two Micron All Sky Survey (2MASS) J, H, and K_s photometric magnitudes for the TFR (Bouche & Schneider 2000; Bamford 2002). They find that the scatter in the TFR in the 2MASS bands is comparable to that for the I-band (e.g., Giovanelli et al. 1997) and that the intrinsic scatter is similar for all these bands (0.375 magnitudes for I, 0.474 for J, 0.478 for H, and 0.504 for K_s). Thus, previous studies of the H-band TFR generally indicate scatter values consistent with the I-band value of ≤ 0.5 mag.

Gavazzi et al. (2000) present 1.65 μm (H-band) surface photometry of all of the galaxies in our Coma. In Figure 3.14, we show our I-band magnitudes versus the

Gavazzi et al. H-band magnitudes. There is little scatter in the H versus I-band figure, with no obvious outliers that would signal spurious errors in our photometry. A best fit line has a slope of 1.05±0.11 and an intercept of -2.46±1.55. We also plot I versus $I-H$ in Figure 3.15 to double-check for errant photometric points and find none. The data are consistent with a single $I-H$ color of $\sim$1.8 for almost all members of the sample. Figure 3.16 shows the new Coma sample H-band TFR using the Gavazzi et al. H-band photometry and our maximum velocity points. The solid line is an H-band relation fit from Pierce & Tully (1992), which was also used by Mathieu et al. (2002). A free fit to the H-band data points yields $\alpha = 0.84^{+1.80}_{-1.59}$, $M_H(2.3) = -23.17^{+0.25}_{-0.26}$, and $\sigma = 0.37^{+0.31}_{-0.14}$. Again, the slope here is poorly constrained. If we fix the slope at the Pierce & Tully (1992) value for late-type spirals ($\sim$9.8), we find the following values for our Coma S0s: $M_H(2.3) = -22.58^{+0.85}_{-0.86}$ and $\sigma = 1.18^{+0.97}_{-0.46}$. The scatter is much larger than that found for late-type galaxies by any of the studies above. Despite the large scatter, the Coma S0 galaxies do seem to lie quite close to the late-type H-band relation. Mathieu et al. (2002) interpret a similar result as showing that, as H-band is dominated by old stellar populations, the old populations of S0 and late-type spirals are similar.

Figure 3.17 shows the absolute H-band magnitudes versus the maximum predicted circular velocities resulting from our analysis for the Virgo S0 sample (solid triangles), the H-band relation fit from Pierce & Tully (1992) (solid line), and the H-band Coma S0 sample (open squares). We assume a radial velocity of $v_z = 1079$ km s^{-1} for Virgo (Ebeling et al. 1998) and $H_0 = 80$ km s^{-1} Mpc^{-1}. A free fit to the Virgo H-band data points yields $\alpha = 3.67^{+2.54}_{-2.62}$, $M_H(2.3) = -22.52^{+0.52}_{-0.53}$, and $\sigma = 0.67^{+0.65}_{-0.26}$. Fixing the slope at the Pierce & Tully (1992) value for late-type spirals (9.8), we find that the Virgo S0 sample yields $M_H(2.3) = -22.97 \pm 1.06$ and $\sigma = 1.33^{+1.28}_{-0.52}$. The scatter for both fits is very large, similar to the slope-restricted Coma sample, and is much greater than the observed scatter of the late-type spiral H-band relation. There does not seem to be a significant change in either the values for the zero-point or the scatter

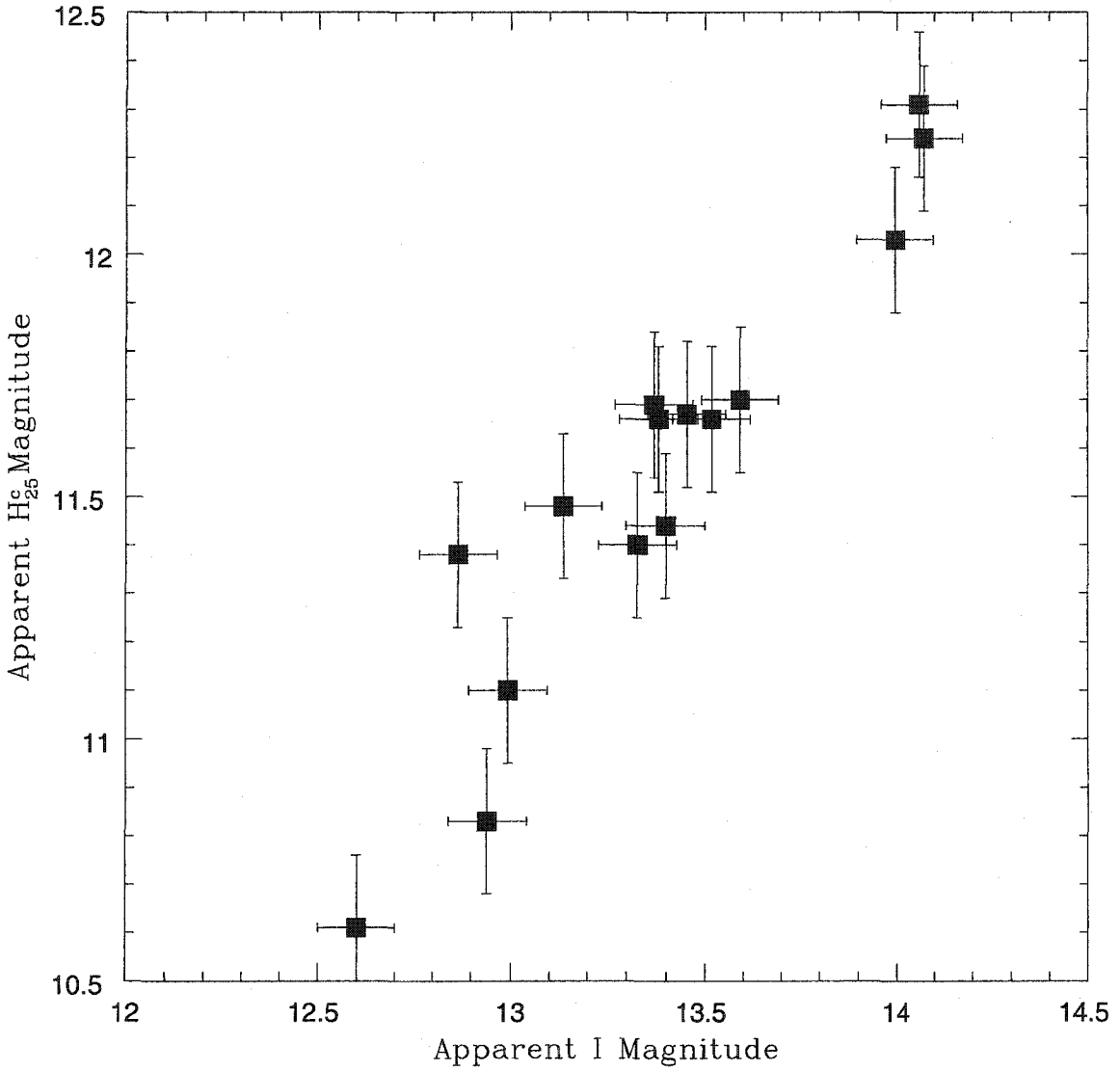

FIGURE 3.14. H-band magnitudes from Gavazzi et al. (2000) versus I-band magnitudes from this work.

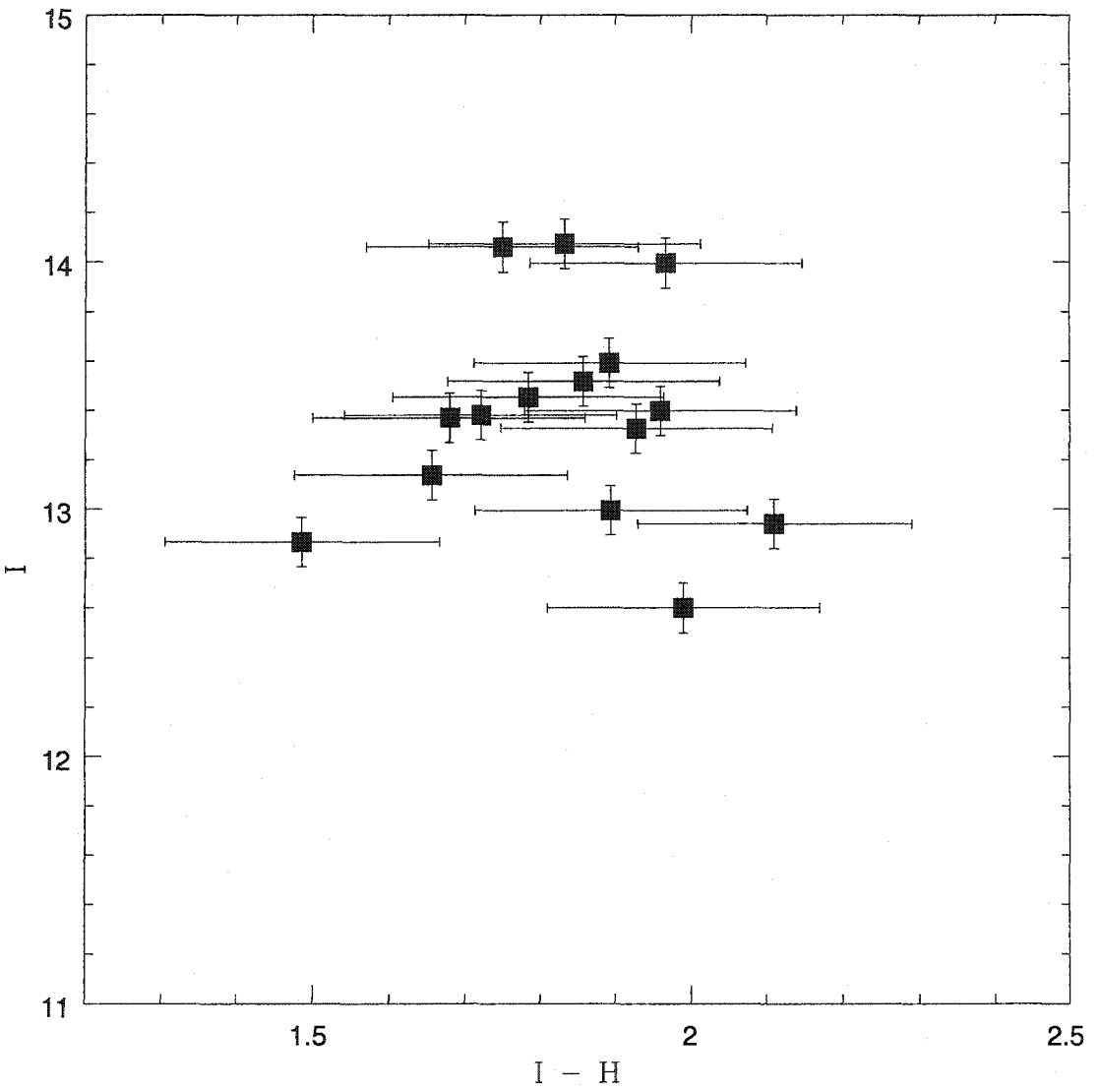

FIGURE 3.15. I versus $I - H$ for the Coma S0s.

found for Virgo S0s as compared to Coma S0s, despite the difference in population and richness of the clusters. A fit to both the new Coma and Virgo cluster H-band S0 data with the Pierce & Tully (1992) fixed slope has a scatter of $\sigma = 1.27^{+0.67}_{-0.39}$ and a zero-point of $M_H(2.3) = -22.76^{+0.68}_{-0.66}$. Echoing the findings of Hinz, Rix, & Bernstein (2001), the relation between H-band luminosity and v_c for cluster S0s is poorly defined, and there is a small offset, $\Delta m_H \sim 0.2$, in the H-band luminosity at a given circular velocity, $v_c \sim 200$ km s^{-1}, between late-type spirals and S0s.

Figure 3.18 includes both the cluster S0s and the Neistein et al. (1999) field S0s. The photometry for the Neistein et al. (1999) sample was originally taken in the I-band. For the purposes of comparing their data to our own, we have converted their I-band magnitudes to H-band, assuming an average $I - H$ value for an S0 galaxy of 1.8 based on Figure 3.15. The cluster S0s seem to occupy approximately the same parameter space as the field S0s, with a similarly large scatter and poorly determined slope. The faintest galaxies in the cluster samples, for instance, seem to lie just as far away from the late-type relation as the field galaxies. We interpret this similarity in the relation between field and cluster S0 galaxies to mean that cluster S0s are not solely produced by an evolutionary scenario in which spirals are stripped of their gas upon entering the cluster potential but are instead the outcome of minor mergers or of multiple possible formation histories, just as we might expect of field S0s. In support of this, for example, simulations by Kodama & Smail (2001) have shown that the bulges of late-type spirals (Scdm) are not luminous enough to evolve into the bright bulges of S0 galaxies simply as a result of stopping the star formation in the disk or by harassment in the cluster environment. They suggest that one possible way to form S0s in clusters might be to accrete field populations that are not the same as a 'pure' field population, that S0s could be formed if the galaxies accreted into clusters are 'pre-processed' in subcluster units or somehow instrinsically biased toward earlier type galaxies. They comment that most of the small bulge Scdm galaxies may have already been transformed to bulge-strong galaxies by minor mergers or through bar-

formation due to strong galaxy-cluster interactions. In this case, we would not expect a purely late-type spiral TFR to hold for S0s. It seems likely, then, from the S0 TFR constructed here, that multiple processes are involved in the formation and evolution of S0s.

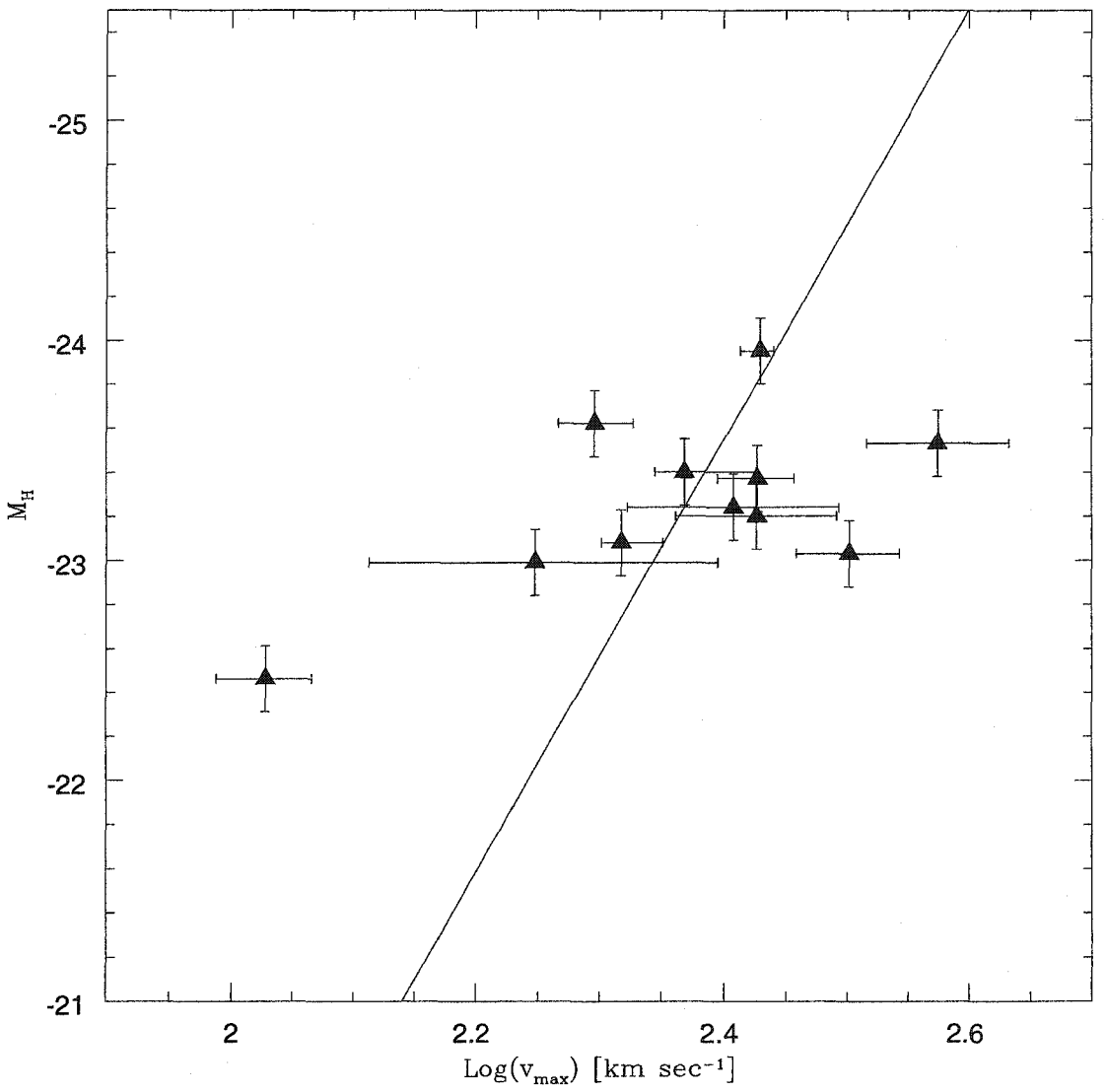

FIGURE 3.16. A Tully-Fisher-type fit to H-band photometry of Coma S0 galaxies. H-band magnitudes are from Gavazzi et al. (2000). The solid line is an H-band late-type spiral relation from Pierce & Tully (1992), which was also used by Mathieu et al. (2002).

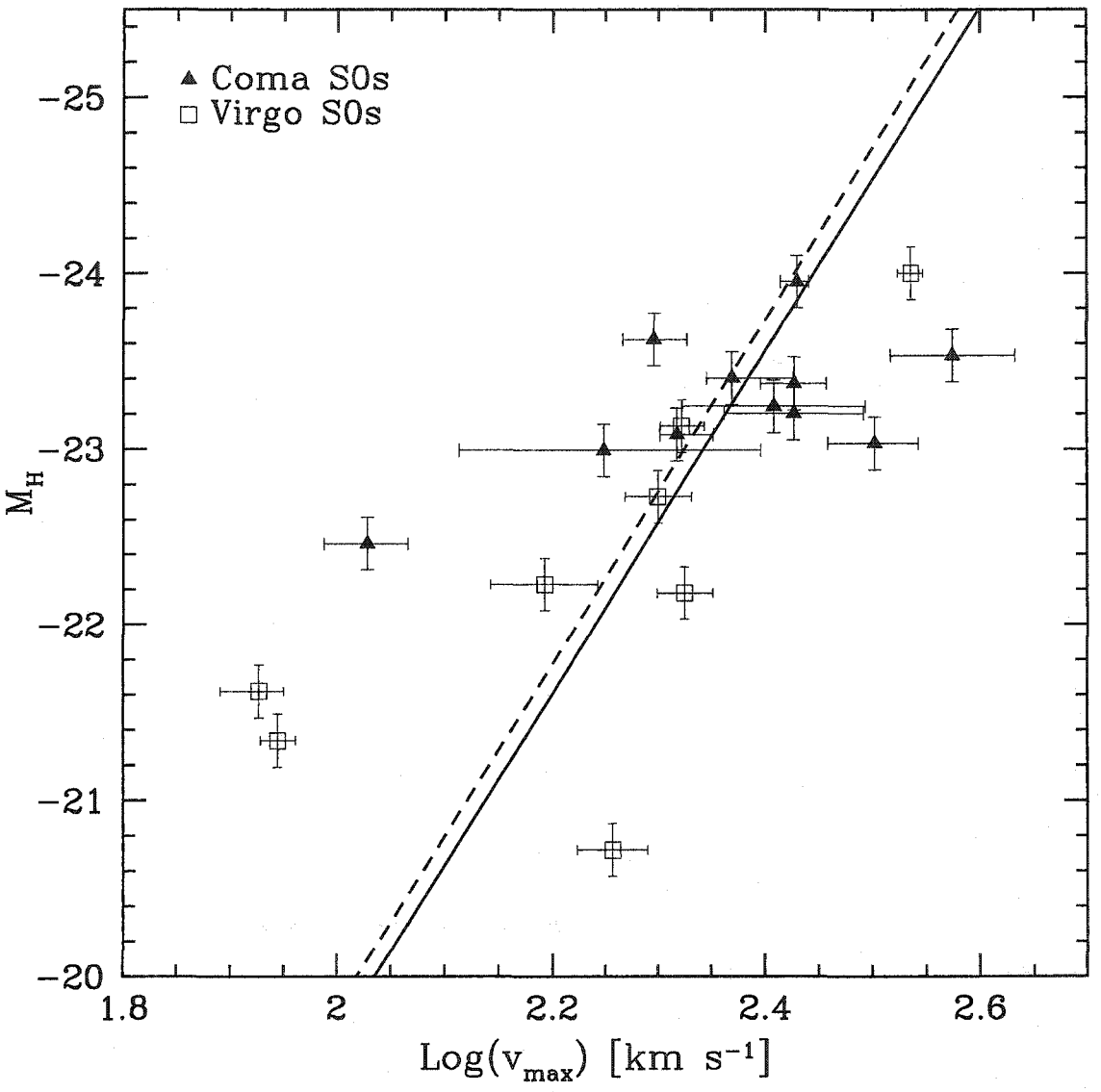

FIGURE 3.17. A Tully-Fisher-type diagram of H-band photometry of the Virgo (solid triangles) and Coma (open squares) S0 sample. H-band magnitudes are from Gavazzi et al. (2003). The solid line is the Pierce & Tully (1992) late-type spiral relation. The dashed line is a fit to the data holding the slope at the Pierce & Tully (1992) value.

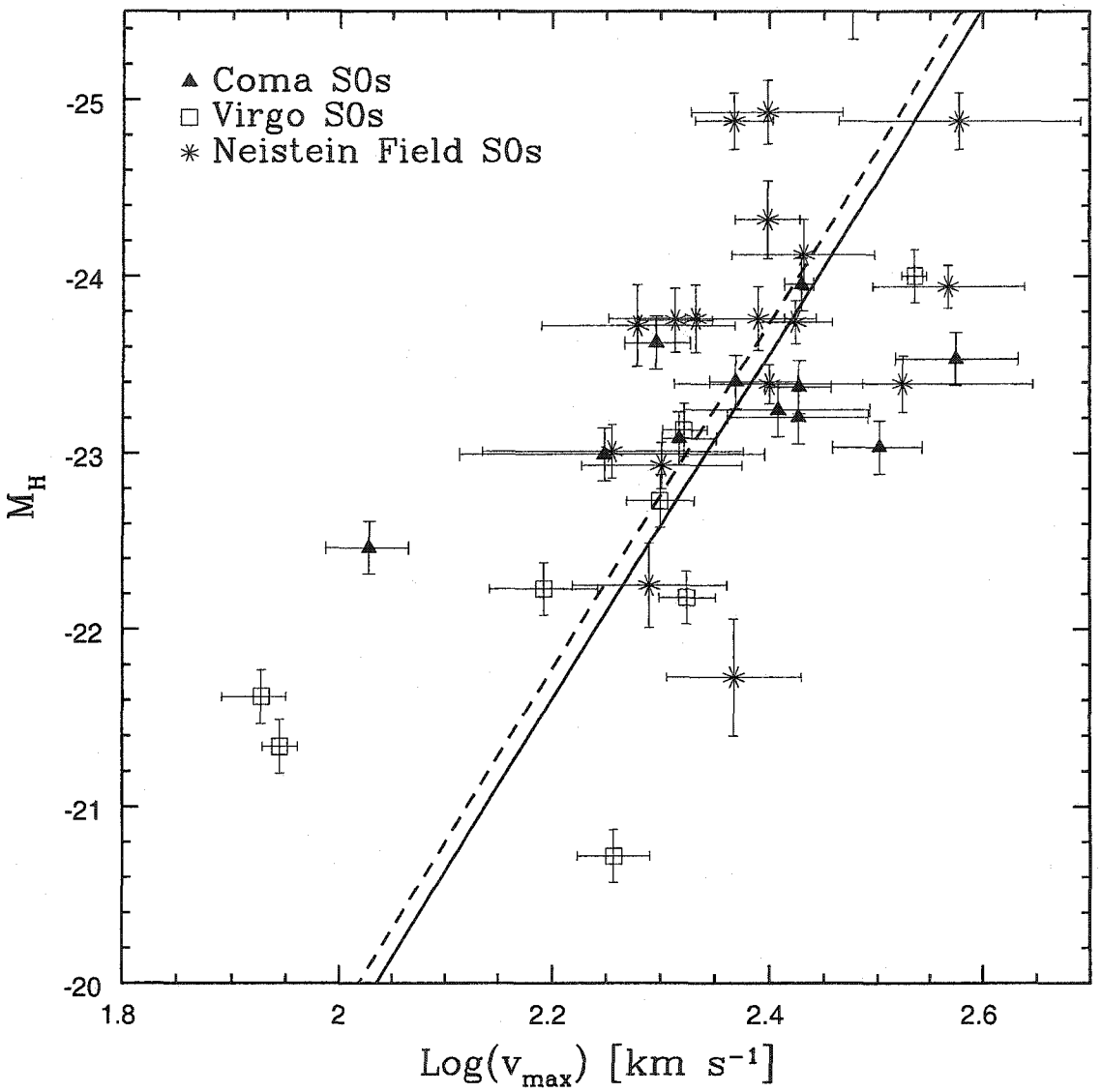

FIGURE 3.18. An H-band Tully-Fisher type diagram of the Virgo and Coma cluster S0s, with the Neistein et al. (1999) field S0 sample. The solid line is the Pierce & Tully (1992) late-type spiral relation. The dashed line is a fit to the cluster S0 data holding the slope at the Pierce & Tully (1992) value.

Chapter 4

DYNAMICAL MASSES OF ULIRGS

4.1 Calculation of Dynamical Masses

4.1.1 Light Profiles

To obtain dynamical masses for the ULIRG sample, bulge and/or disk scale-lengths must be fitted to the large-scale near-infrared images. Two-dimensional models were created using an $r^{1/4}$ bulge and exponential disk fitting routine (Rix & Zaritsky 1995). The routine rebins the images onto a cylindrical grid, given a specified minimum and maximum radius and the coordinates of the galaxy center. Fed an initial guess for a set of bulge and disk parameters, the program begins a "biased random walk" within a parameter box until it finds the combination of parameters which minimize chi-squared. Typically, a few pixels at the very centers of the galaxies are not included in the fit, because the fitting routine does not account for the seeing. Although both H and K_s-band images were fitted where available, we report the results for H-band, since we have images at this wavelength for the whole sample. Exponential disk and effective bulge H-band radii with errorbars are listed in Table 4.1.

4.1.2 Mass Models

As ULIRGs are the products of mergers or are mergers in progress, it is not clear whether the inner regions of the galaxies should be expected to be hot spherical systems or cold disk systems. Radial profile fits to a large sample of ULIRGs (e.g., Scoville et al. 2000) show that the best fitting models can be $r^{1/4}$, exponential, or neither. If the ULIRGs are ellipticals in formation, then we might expect their centers to be kinematically hot spheroids, but young stars, with strong CO lines, formed in

Name	R_{exp} (pc)	R_{eff} (pc)
NGC 1614	85.8 ± 58.9	58.9 ± 105.1
NGC 2623	1883.0 ± 399.8	1007.8 ± 149.2
NGC 7674	4420.5 ± 215.0	890.8 ± 181.5
IRAS 10565+2448	1454.3 ± 643.6	455.5 ± 87.8
IRAS 17208-0014	1618.6 ± 25.9	932.1 ± 73.2
IC 694	686.5 ± 28.9	12.15 ± 4.19
IC 883	224.6 ± 18.4	19.0 ± 48.9
VII Zw 31	1533.3 ± 53.4	416.7 ± 320.6
Mkn 231	573.6 ± 21.1	400.7 ± 46.4
Mkn 273N	1317.0 ± 10.8	732.4 ± 82.0

TABLE 4.1. Scale radii for the ULIRG sample. Column header explanations. Col. (1): Galaxy name. Col. (2): H-band exponential disk scale-length in parsecs. Col. (3): H-band effective radius of the bulge in parsecs.

the gas which falls to the center of the galaxy, may settle into a ring or disk (Barnes & Hernquist 1991). Also, a remnant disk consisting of the old stellar population of an original merging spiral galaxy may still be intact. Therefore, we calculate dynamical masses based on both a series of spherical models and a disk model. These models are also described in detail in Shier (1995).

The question of modeling systems in this way that may not be in dynamical equilibrium is a difficult one. Clearly, ULIRGs with tidal streams and tails are not in equilibrium in their outer parts. However, the following models are generated exclusively for the inner 1 kpc of each galaxy, where more stability might be expected and where the dynamics have been shown to adhere well to the fundamental plane (see Section 1.2). High resolution H I measurements of ULIRGs could be used confirm the relative equilibrium of the inner parts of the ULIRG systems and confirm the values of the velocity dispersion obtained from the 2.3 μm CO bandheads.

Spherical Models The mass density distributions in the spherical models are taken from Tremaine et al. (1994), who analytically derive a family of "η-models", where

the central density cusps are described by $\rho \propto r^{3-\eta}$, where ρ is the mass density. All η models have $\rho \propto r^{-4}$ as $r \to \infty$. The general form of the density distribution function is

$$\rho_\eta \equiv \frac{\eta}{4\pi} \frac{1}{r^{3-\eta}(1+r)^{1+\eta}}, \; 0 < \eta \leq 3. \tag{4.1}$$

Models with $\eta = 1$ resembles a singular isothermal sphere, $\eta = 2$ models have $\rho \sim 1/r$ at small radii, and $\eta = 3$ models have constant density cores. We consider only the $\eta = 2$ and the $\eta = 3$ models for the rest of this work, following Shier (1995). The mass interior to the radius is given by

$$M_\eta(r) \equiv 4\pi \int_0^r r^2 \rho_\eta(r)\, dr = \frac{r^\eta}{(1+r)^\eta}\,, \tag{4.2}$$

We combine these models with the hydrostatic equilibrium equation,

$$\frac{d(\rho\sigma_{los}^2)}{dr} = -\rho \frac{d\Phi}{dr} \tag{4.3}$$

where σ_{los} is the line-of-sight velocity dispersion and Φ is the gravitational potential, and solve for the integral form of the velocity dispersion,

$$\sigma_{los}^2(r) = \frac{G}{\rho(r)} \int_r^\infty \frac{M(r)\rho(r)\, dr}{r^2}\,. \tag{4.4}$$

However, stars at all different radii in the galaxy contribute to the observed velocity dispersion within the slit size of the spectrograph, in essence taking an average of all of the velocities. This average is weighted by the flux from each volume element. In terms of the mass-to-light ratio, γ, and the extinction along the line-of-sight, $e^{-\tau}$, the observed velocity dispersion is given in terms of the line-of-sight dispersion by

$$\sigma_a^2 = \frac{\int_a \sigma_{los}^2(r)\rho/\gamma e^{-\tau} dV}{\int_a \rho/\gamma e^{-\tau} dV}\,. \tag{4.5}$$

This is a volume integral that covers the portion of the ULIRG seen through the aperture.

We can rewrite the form of ρ in terms of an effective or scale radius, R_{eff}, that describes the physical size of the model galaxy and the radius at which the density power law changes. This form is

$$\rho(r) = \frac{\rho_0}{(r/R_{eff})^{\eta-3}(1+r/R_{eff})^{1+\eta}} \ . \tag{4.6}$$

We can then write the mass interior to a radius r as

$$M(r) = \frac{R_{eff}\sigma_a^2}{G} \frac{(r/R_{eff})^{\eta}}{(1+r/R_{eff})^{\eta}} \frac{\int_a \rho/\eta e^{-\tau} dV}{\int_a v_{r,\eta}^2(r)\rho/\eta e^{-\tau} dV} \ . \tag{4.7}$$

In this case $v_{r,\eta}^2(r)$ is a dimensionless velocity dispersion calculated by Tremaine et al. (1994). The definition is given by

$$v_{r,\eta}^2(r) = GM_T/R_{eff}\sigma(r), \tag{4.8}$$

where M_T represents the total mass of the galaxy. Table 4.2 lists the calculated ULIRG masses for $\eta = 2$ and $\eta = 3$ spherical models based on our measured velocity dispersions and scale-lengths.

Disk Models For the purpose of creating a simple disk model, we assume that the local velocity dispersion is small in comparison to the circular velocity, v_c, so that the stars in the disk are on nearly circular orbits, given by

$$v_c^2(r) = \frac{GM(r)}{r} \ . \tag{4.9}$$

The inclination reduces the line-of-sight velocity by $\cos i$. Also, stars that are not on the observed major axis have components of their motion in the plane of the sky, so that the observed velocity is actually given by

$$v_{los}(r,\theta) = v_c \cos i \sin\theta \ , \tag{4.10}$$

where θ is the azimuthal coordinate in the galaxy. As we have no direct information about the inclination angles for the ULIRGs, we set i equal to 30°, which is the median

inclination for a set of randomly oriented disks. The observed velocity dispersion is the standard deviation of the velocities of the stars within one spectrograph aperture width. This standard deviation is weighted by the flux received at each point along the aperture, so that the observed velocity dispersion, σ_a, is given by

$$\sigma_a^2 = \frac{\int_a \frac{GM(r)}{r} \cos^2 i \sin^2 \theta \rho/\gamma dA}{\int_a \rho/\gamma dA} . \quad (4.11)$$

Assuming that the ULIRG has an exponential surface mass density, i.e., $\Sigma = \Sigma_0 e^{r/r_{exp}}$, the mass of the galaxy within a specific radius is

$$M(r) = \frac{r_{exp}\sigma_a^2}{G \cos^2 i}[1 - e^{-r/r_{exp}}(1 + r/r_{exp})] \frac{\int_a \Sigma/\gamma \, dA}{\int_a \frac{1-e^{-r/r_{exp}}(1+r/r_{exp})}{r/r_{exp}} \sin^2 \theta \Sigma/\gamma \, dA} . \quad (4.12)$$

4.2 Comparing Molecular Masses to Dynamical Masses

Table 4.2 shows the molecular gas masses from millimeter CO measurements (Scoville et al. 2000), dynamical masses from other works (Shier et al. 1996; Alonso-Herrero et al. 2001; Tacconi et al. 2002), and the dynamical masses from this work for the disk, $\eta = 2$, and $\eta = 3$ models. All dynamical masses are the values for the galaxy mass within the central 1 kpc, for direct comparison with the Shier et al. (1996) values. The mass errors are calculated from the errors in the velocity dispersions derived from the near-IR spectroscopy. For half (5) of galaxies in the ULIRG sample, we find total dynamical masses which are lower than the molecular gas masses predicted from millimeter CO measurements using the standard conversion between CO and H_2. The gas masses range from $\sim$ 1.5-10 times the dynamical masses in these ULIRGs. This is not reasonable, assuming that at least some of the mass in the inner regions of these galaxies is in the form of stars. For two other galaxies, IC 694 and Mkn 273, almost the entire dynamical mass budgets would have to be taken up by molecular gas in order for the estimates to agree.

For the galaxies that overlap with the Shier et al. (1996) sample, we calculate higher dynamical masses, mainly due to the higher velocity dispersions drawn from

the near-infrared spectroscopy. In the cases of NGC 1614 and NGC 2623, the higher dynamical mass estimates now allow for the molecular gas portion calculated by Scoville et al. (2000). The combined estimates leave $\sim 3\times10^9\,M_\odot$ for the stellar population in NGC 1614 and $\sim 7\times10^9\,M_\odot$ for NGC 2623. The difference in velocity dispersion estimates is almost certainly due to the higher signal-to-noise spectra obtained at the 6.5-meter MMT as opposed to the Shier et al. (1996) spectra which were taken with the 2.3-meter Bok telescope.

Another comparison value of the dynamical mass for NGC 1614 comes from Alonso-Herrero et al. (2001). They used Brγ spectroscopy (Puxley & Brand 1999) and NICMOS-2 images in Paα of an emitting ring region to calculate a dynamical mass independent of the CO bandheads. They assumed that the ring was associated with a Lindbland resonance or similar dynamical feature and that the ring was close to round. They obtained a rotational velocity for the ring by modeling the line profile expected for a rotating ring and also calculated an inclination for the ring based on its observed ellipticity ($i = 51°$). They then used the virial theorem to convert the ring's rotational velocity to a mass. They found a dynamical mass of $1.4\times10^8\,M_\odot$ within $\sim$620 pc. They also estimated the mass in old stars as $1.2\times10^9\,M_\odot$, and the modeled starburst mass as $0.55\times10^9\,M_\odot$, both of which fit within our mass budget for the stellar population in that region in addition to the Scoville et al. (2000) gas mas estimate. There is no obvious reason why the results from this work disagree with the Alonso-Herrero et al. (2001) estimates of the dynamical mass. Changes in the estimate of the inclination angle of the system do not increase their dynamical mass by a large enough factor to make up the difference in estimates. They use the Shier et al. (1996) scalelengths for their mass models, but even adopting those scalelengths with our value for the velocity dispersion does not bring the estimates into agreement. One possibility is that, for this galaxy in particular, CO measurements are strongly weighted by the center of the ULIRG and overestimate the dispersion. That the CO photometric index is extremely large in the inner 0.4" in comparison to

the Paα emission is shown by Alonso-Herrero et al. (2001).

The results for these 10 ULIRGs have strong implications for theories on the efficiency and mechanisms for star formation in extreme environments such as the inner portions of ULIRGs. The most widely applied star formation law is the Schmidt law (Schmidt 1959), where the star formation rate is given by a gas density power law,

$$\Sigma_{SFR} = A\Sigma_{gas}^{N} \ , \tag{4.13}$$

where A is the absolute star formation rate efficiency. Observations generally place the value of N in the range 1-2, depending on which star formation tracers are used. Kennicutt (1998) explored the changes in A and N in the high density environments of a sample of luminous infrared starburst galaxies, including several ULIRGs in our sample. He found a well-defined Schmidt law for the starbursts, with $N = 1.3 - 1.4$, and calculated that the global star formation efficiencies are much larger than for a sample of normal spirals by a median factor of 6. However, he cautioned that the CO/H_2 standard conversion factor led to scatter in correlations between the star formation rate and molecular gas density. For instance, it may be that the conversion factor is valid in regions with solar metallicity but that it underestimates the H_2 mass in metal-poor galaxies. He found that metal-rich spirals show a better defined star formation rate versus molecular hydrogen gas density, in support of the fact that the CO/H_2 conversion might indeed be wrong for some environments. He further showed that lowering gas masses in the starburst galaxies by a factor of 2, allowing for the possibility that the standard conversion ratio is actually lower than usually stated, would increase N from 1.4 to 1.5, for an increased star formation rate in these galaxies. Therefore, if we are correct in our assessment of the dynamical masses of the ULIRGS, the gas masses must be lower and the star formation rate must be higher in these galaxies than predicted by the standard conversion.

Our results may also shed light on what types of mechanisms control the star

Name	$\log M(H_2)$ ($M_\odot$)	$\log M_{dyn}$ ($M_\odot$)	$\log M_{dyn}^{disk}$ ($M_\odot$)	$\log M_{dyn}^{\eta=2}$ ($M_\odot$)	$\log M_{dyn}^{\eta=3}$ ($M_\odot$)
NGC 1614	9.68	9.32±0.25[a]	10.01±0.05	9.72±0.06	9.84±0.07
NGC 2623	9.77	9.46±0.21[b]	10.00±0.06	10.22±0.07	10.11±0.07
NGC 7674	10.12	—	9.52±0.29	9.82±0.28	9.73±0.28
IRAS 10565+2448	10.34	—	10.03±0.10	10.16±0.10	10.17±0.10
IRAS 17208-0014	10.71	—	9.92±0.22	10.09±0.22	9.99±0.22
IC 694	10.00	9.76±0.24[b]	10.01±0.11	10.13±0.11	10.09±0.11
IC 883	9.87	—	10.09±0.03	9.22±0.03	9.29±0.03
VII Zw 31	10.69	—	9.73±0.12	9.60±0.12	9.09±0.12
Mkn 231	10.33	10.60[c]	9.90±0.08	9.97±0.08	10.00±0.08
Mkn 273N	10.58	—	10.47±0.18	10.62±0.18	10.57±0.18

TABLE 4.2. Masses for the ULIRG sample. Column header explanations. Col. (1): Galaxy name. Col. (2): Log of the molecular hydrogen mass from Scoville et al. (2000) in solar masses. Col. (3): Log of the dynamical mass in solar masses from a.) Alonso-Herrero et al. (2001), b.) Shier et al. (1996), c.) Tacconi et al. (2002). Col. (4): Log of the calculated dynamical mass in solar masses from this work for a disk model. Col. (5): Log of the calculated dynamical mass in solar masses from this work for a spherical, $\eta = 2$ model. Col. (6): Log of the calculated dynamical mass is solar masses from this work for a spherical, $\eta = 3$ model.

formation processes in merging starbursts on their way to becoming ellipticals. There are three basic physical processes behind intense starbursts such as the ones observed in ULIRG environments: gravitational instabilities in nuclear gas disks (Kennicutt 1998), efficient cloud-cloud collisions driven by gas motion in their central regions which are proportional to a power of local volumic density, $\propto \rho^2$ (Scoville et al. 1991), and dynamical disturbances or tidal forces, perhaps, for example, from supermassive binary black holes (Taniguchi & Wada 1996). Schmidt laws with $N \sim 1 - 1.5$ favor the gravitational instability scenario, while laws with $N \sim 2$ favor star formation triggered by cloud-cloud collisions. The third mechanism of dynamical disturbances also relies on gravitational instability formalism, so is generally associated with lower values of N.

Taniguchi & Ohyama (1998) found that, for two samples of high luminosity starburst galaxies with millimeter CO measurements, the surface density of the far-infrared luminosity was proportional to the derived H_2 surface mass density, with $N \sim 1$, implying that the most likely star formation mechanism is gravitational instability in nuclear gas disks when the standard ratio is used. However, Scoville, Sanders, & Clemens (1986) suggested that cloud-cloud collisions account for the high rates of star formation in ULIRGs, with this process being the dominant mode for the formation of high-mass stars. They explored CO data on a large sample of giant molecular clouds and suggested that any model attempting to mimick massive star formation must account for both the formation of stars deep in the interior of clouds and the lower efficiency in high-mass clouds. One model that accounted for both of these factors was one in which the star formation is triggered by cloud-cloud collisions, so that OB star clusters appear on the edge of and near the center of merged clouds. The lower gas masses implied by the calculated dynamical masses for our sample suggest larger values of N, which can only be supported by the more efficient, high mass star formation allowed by cloud-cloud collisions.

Based on our dynamical masses and the works cited above, we conclude that at

least some ULIRGs do not harbor the enormous molecular gas masses calculated from CO emission measurements and that the standard conversion factor from CO to H_2 derived from local giant molecular clouds cannot be used in the dense inner environments of starburst galaxies. Our dynamical masses essentially place upper limits on the amount of molecular gas likely to be at the centers of ULIRGs. We further predict that the star formation efficiencies are higher than those derived from the standard conversion values and that the dominant source of star formation in ULIRGs is likely to be cloud-cloud collisions. Further, we expect that ULIRGs do not have prohibitively high extinctions at near-infrared wavelengths and anticipate that much of their structure and starburst information is well diagnosed with H and K_s-band observations.

Chapter 5

SUMMARY AND CONCLUSIONS

We have explored the dynamical properties of two very different subclasses of galaxies, lenticulars and ultraluminous infrared galaxies, in an attempt to better understand the history and evolution of galaxies in various environments. Both sets of objects are considered to be transitions between the two main types of normal galaxies, spiral and elliptical, and investigating their properties and processes can lead to a better overall understanding of galaxy evolution.

Using I- and H-band photometry and rotation curves derived from stellar absorption line spectroscopy, we have constructed a Tully-Fisher type relation, luminosity versus maximum circular velocity, for 10 S0s in the Coma Cluster and 8 S0s in the Virgo Cluster. We combine these results with similar measurements of 13 S0 galaxies in the Coma cluster by Hinz, Rix, & Bernstein (2001). We find a scatter around the H-band relation of $0.97^{+0.51}_{-0.30}$ mag for Coma S0s, $1.33^{+1.28}_{-0.52}$ mag for Virgo S0s, and $1.09^{+0.43}_{-0.30}$ mag for the combined sample. These intrinsic scatter values are larger than the value of ~ 0.7 mag found for a sample of field S0s by Neistein et al. (1999). The S0 galaxies have significantly larger scatter than the TFR for late-type spirals in these bands, ~ 0.3-0.5 mag. The scatter for the S0 galaxies is also larger than generally predicted by numerical simulations of galaxy formation (e.g., Steinmetz & Navarro 1999).

At a given circular velocity there is at most a small offset of between the absolute H-band magnitudes of late-type spirals and the S0s. Because of their older stellar populations, S0s should have a larger value for their stellar $(M/L)_*$. From this, we would expect the S0s to have a lower luminosity at a given circular velocity compared to late-type spirals. The small offset in our data suggests that S0s and spirals at a

given luminosity have similar total (stellar and dark) masses within $\sim 2R_{exp}$. Together with $(M/L)_{*,S0} > (M/L)_{*,Sc}$ this result implies that S0 galaxies have a higher stellar mass fraction than late-type spirals. Our observations do not support the suggestion (e.g., Mathieu et al. 2002) that a large (~ 1.8 mag) offset from the late-type TFR should be expected if star formation had been suddenly switched off a few Gyr ago, so that the S0 galaxies contain just the old stellar population of a normal spiral galaxy. Two possible explanations for the difference in results are that the Mathieu et al. (2002) S0s were specifically chosen to contain small bulges, so that their S0s are the "prime candidates" to have formed from gas-stripped spirals, or that the small sample size (6) of the Mathieu et al. (2002) study prohibited a complete analysis of the S0 relation.

The large scatter in the Coma and Virgo Cluster S0 TFR in comparison to the known late-type spiral relation, together with the small zero-point offset, seems at odds with the idea that S0s are simply former spirals whose star formation has been truncated by tidal stripping. It indicates that S0s are the results of minor mergers and other interactive processes such as slow encounters with other galaxies, multiple encounters, starvation, strangulation, harassment, or some combination of all of these. In this view of S0 galaxies, the class is heterogeneous and produced by several different evolutionary scenarios even within a particular cluster environment.

We have also explored the dynamics and stellar content of a sample of ten ultra-luminous infrared galaxies (ULIRGs) using near-infrared imaging and spectroscopy. Velocity dispersions for the galaxies were calculated from the CO absorption band-heads present at 2.3μm. Exponential disk and effective bulge scale-lengths for each ULIRG were derived using two-dimensional model fits to H-band imaging. These results were used in conjunction with a series of spherical and disk-like density profile models to determine total dynamical masses for the galaxies.

The dynamical masses for the ULIRGs are in the range $\sim 2 \times 10^9 - 4 \times 10^{10}\,\mathrm{M}_\odot$ for the innermost 1 kpc. We compare these masses to estimates of molecular gas mass

derived from interferometric millimeter wavelength observations of CO (e.g., Bryant & Scoville 1999). The molecular gas masses are usually calculated assuming a standard conversion between CO luminosity and the amount of H_2, based on ratios found for giant molecular clouds in the Milky Way. This conversion has come under some criticism from both theoretical (Maloney & Black 1988) and observational (Shier, Rieke, & Rieke 1996) points of view, and it has been suggested that using such a conversion in the extreme environments of the nuclei of starburst galaxies overestimates the amount of molecular hydrogen present. In agreement with these criticisms, we find that for over half of the ULIRGs in our sample, the molecular gas masses exceed or fill the entire dynamical mass budget, an unreasonable result considering the stellar luminosity that is observed. We conclude that, at least for some ULIRGs, the standard conversion is an inappropriate tool for deriving molecular gas masses.

These results have wide implications for the efficiency of star formation in ULIRGs and for the physical mechanisms responsible for such star formation. Decreased amounts of molecular gas, as implied by our dynamical masses, allow an increase in the power of the global Schmidt law, suggesting that the efficiency and rate of star formation in ULIRGs is higher than predicted by millimeter observations alone (Kennicutt 1998). Such large star formation rates are thought to have been created by efficient cloud-cloud collisions in the inner regions of the ULIRGs, dependent on the square of the density in the area (Scoville, Sanders, & Clemens 1986), rather than by gravitational instabilities in nuclear disks or other dynamical or tidal disturbances (Taniguchi & Ohyama 1998). We also conclude that the huge amounts of extinction implied by large molecular gas masses may not be present and that near-infrared observations are often adequate probes of the dynamics and starburst activity associated with ULIRGs.

References

[1] Aaronson, M. & Mould, J. 1978, BAAS, 10, 664

[2] Aaronson, M., Huchra, J., & Mould, J. 1979, ApJ, 229, 1

[3] Aaronson, M., Bothun, G., Mould, J., Huchra, J., Schommer, R. A., & Cornell, M. E. 1986, ApJ, 302, 536

[4] Alonso-Herrero, A., Engelbracht, C. W., Rieke, M. J., Rieke, G. H., & Quillen, A. C. 2001, ApJ, 546, 952

[5] Bamford, S. P. 2002, astro-ph/0210227, MSci Thesis, University of Durham

[6] Barnes, J. E. & Hernquist, L. E. 1991, ApJ, 370, L65

[7] Bekki, K., Shioya, Y., & Couch, W. J. 2002, ApJ, 577, 651

[8] Bernstein, G. M., Guhathakurta, P., Raychaudhury, S., Giovanelli, R., Haynes, M. P., Herter, T., & Vogt, N. P. 1994, AJ, 107, 1962

[9] Binggeli, B., Sandage, A., & Tammann, G. A. 1985, AJ, 90, 1681

[10] Binney, J. & Tremaine, S. 1987, Galactic Dynamics (Princeton: Princeton Univ. Press)

[11] Bouche, N. & Schneider, S. E. 2000, ASP Conference Series 218, Mapping the Hidden Universe: The Universe behind the Milky Way - The Universe in H I, p. 111

[12] Bryant, P. M. & Scoville, N. Z. 1999, AJ, 117, 2632

[13] Charlot, S. & Bruzual, A. G. 1991, ApJ, 367, 126

[14] Courteau, S., Faber, S. M., Dressler, A., & Willick, J. A. 1993, ApJ, 412, L51

[15] Courteau, S. & Rix, H.-W. 1999, ApJ, 513, 561

[16] Djorgovski, S. & Davis, M. 1987, ApJ, 313, 59

[17] Doi, M., Fukugita, M., Okamura, S., & Tarusawa, K. 1995, ApJS, 97, 77

[18] Downes, D. & Solomon, P. D. 1998, ApJ, 507, 615

[19] Dressler, A. & Sandage, A. 1983, ApJ, 265, 664

[20] Dressler, A., Lynden-Bell, D., Burstein, D., Davies, R. L., Faber, S. M., Terlevich, R., & Wegner, G. 1987, ApJ, 313, 42

[21] Dressler, A., & Faber, S. M. 1990, ApJ, 354, L45

[22] Ebeling, H., Edge, A. C., Bohringer, H., Allen, S. W., Crawford, C. S., Fabian, A. C., Voges, W., & Huchra, J. P. 1998, MNRAS, 301, 881

[23] Engelbracht, C. W., Rieke, M. J., Rieke, G. H., Kelly, D. M., & Achtermann, J. M. 1998, ApJ, 505, 639

[24] Fabricant, D., Cheimets, P., Caldwell, N., & Geary, J. 1998, PASP, 110, 79

[25] Franx, M., Illingworth, G. & Heckman, T. 1989, ApJ, 344, 613

[26] Gavazzi, G., Boselli, A., Scodeggio, M., Pierini, D., & Belsole, E. 1999, MNRAS, 304, 595

[27] Gavazzi, G., Franzetti, P., Scodeggio, M., Boselli, A., & Pierini, D. 2000, A&A, 361, 863

[28] Gavazzi, G., Boselli, A., Donati, A., Franzetti, P., & Scodeggio, M. 2003, A&A, 400, 451

[29] Genzel, R., Tacconi, L. J., Rigopoulou, D., Lutz, D., & Tecza, M. 2001, ApJ, 563, 527

[30] Giovanelli, R., Haynes, M. P., Herter, T., Vogt, N. P., Wegner, G., Salzer, J. J., DaCosta, L. N., & Freudling, W. 1997, AJ, 113, 22

[31] Hernquist, L. 1990, ApJ, 356, 359

[32] Hernquist, L. 1992, ApJ, 400, 460

[33] Hernquist, L. 1993, ApJ, 409, 548

[34] Hinz, J. L., Rix, H.-W., & Bernstein, G. M. 2001, AJ, 121, 683

[35] Iodice, E., Arnaboldi, M., Bournaud, F., Combes, F., Sparke, L. S., van Driel, W., & Capaccioli, M. 2003, ApJ, 585, 730

[36] Kennicutt, R. C., Jr. 1998, ApJ, 498, 541

[37] Kleinmann, S. G. & Hall, D. N. B. 1986, ApJS, 62, 501

[38] Kodama, T. & Smail, I. 2001, MNRAS, 326, 637

[39] Landolt, A. U. 1992, AJ, 104, 340

[40] Larson, R. B., Tinsley, B. M., & Caldwell, C. N. 1980, ApJ, 237, 692

[41] Lisenfeld, U., Isaak, K. G., & Hills, R. 2000, MNRAS, 312, 433

[42] Malhotra, S., Spergel, D., Rhoads, J., & Li, J. 1996, ApJ, 473, 687

[43] Maloney, P. & Black, J. H. 1988, ApJ, 325, 389

[44] Mathewson, D. S., Ford, V. L., & Buchhorn, M. 1992, ApJS, 81, 413

[45] Mathieu, A., Merrifield, M. R., & Kuijken, K. 2002, MNRAS, 330, 251

[46] McCarthy, D. W., Jr., Ge, J., Hinz, J. L., Finn, R. A., & de Jong, R. S. 2001, PASP, 113, 353

[47] Moore, B., Lake, G., Quinn, T., & Stadel, J. 1999, MNRAS, 304, 465

[48] Moss, C. & Whittle, M. 2000, MNRAS, 317, 667

[49] Neistein, E., Maoz, D., Rix, H.-W., & Tonry, J. L. 1999, AJ, 117, 2666

[50] Pierce, M. J. & Tully, R. B. 1988, ApJ, 330, 579

[51] Pierce, M. J. & Tully, R. B. 1992, ApJ, 387, 47

[52] Puxley, P. J. & Brand, P. W. J. L. 1999, ApJ, 514, 675

[53] Rix, H.-W. & White, S. D. M. 1992, MNRAS, 254, 38

[54] Rix, H.-W. & Zaritsky, D. 1995, ApJ, 447, 82

[55] Rix, H., Guhathakurta, P., Colless, M., & Ing, K. 1997, MNRAS, 285, 779

[56] Roberts, M. S., Hogg, D. E., Bregman, J. N., Forman, W. R., & Jones, C. 1991, ApJS, 75, 751

[57] Sakai, S. et al. 2000, ApJ, 529, 698

[58] Sanders, D. B., Scoville, N. Z., & Soifer, B. T. 1991, ApJ, 370, 158

[59] Sanders, D. B., Soifer, B. T., Elias, J. H., Madore, B. F., Matthews, K., Neugebauer, G., & Scoville, N. Z. 1988, ApJ, 325, 74

[60] Sargent, W. L. W., Schechter, P. L., Boksenberg, A., & Shortridge, K. 1977, ApJ, 212, 326

[61] Schmidt, G. D., Weymann, R. J., & Foltz, C. B. 1989, PASP, 101, 713

[62] Schmidt, M. 1959, ApJ, 129, 243

[63] Schlegel, D.J. 1995, Ph.D. Thesis, University of California at Berkeley

[64] Schommer, R. A., Bothun, G. D., Williams, T. B., & Mould, J. R. 1993, AJ, 105, 97

[65] Schweizer, F. 1986, Science, 231, 193

[66] Scoville, N. Z. & Good, J. C. 1989, ApJ, 339, 149

[67] Scoville, N. Z., Sargent, A. I., Sanders, D. B., & Soifer, B. T. 1991, ApJ, 366, L5

[68] Scoville, N. Z. et al. 2000, AJ, 119, 991

[69] Scoville, N. Z., Sanders, D. B., & Clemens, D. P. 1986, ApJ, 310, L77

[70] Shier, L. M. 1995, Ph.D. Thesis, University of Arizona

[71] Shier, L. M., Rieke, M. J., & Rieke, G. H. 1994, ApJ, 433, L9

[72] Shier, L. M., Rieke, M. J., & Rieke, G. H. 1996, ApJ, 470, 222

[73] Simkin, S. 1974, A&A, 31, 129

[74] Solomon, P. M., Downes, D., Radford, S. J. E., & Barrett, J. W. 1997, ApJ, 478, 144

[75] Steinmetz, M. & Navarro, J. F. 1999, ApJ, 513, 555

[76] Tacconi, L. J., Genzel, R., Lutz, D., Rigopoulou, D., Baker, A. J., Iserlohe, C., & Tecza, M. 2002, ApJ, 580, 73

[77] Taniguchi, Y. & Ohyama, Y. 1998, ApJ, 509, L89

[78] Taniguchi, Y., & Wada, K. 1996, ApJ, 469, 581

[79] Tonry, J. & Davis, M. 1979, AJ, 84, 1511

[80] Toomre, A. & Toomre, J. 1972, ApJ, 178, 623

[81] Tremaine, S., Richstone, D. O., Byun, Y., Dressler, A., Faber, S. M., Grillmair, C., Kormendy, J., & Lauer, T. R. 1994, AJ, 107, 634

[82] Tully, R. B. & Fisher, J. R. 1977, A&A, 243, 71

[83] van Driel, W. & van Woerden, H. 1991, A&A, 243, 71

[84] Williams, D. M., Thompson, C. L., Rieke, G. H., & Montgomery, E. F. 1993, Proc. SPIE, 1946, 482

[85] Worthey, G. 1994, ApJS, 95, 107

[86] Yamaoka, H., Kato, T., Filippenko, A. V., van Dyk, S. D., Yamamoto, M., Balam, D., Hornoch, K., & Plsek, M. 1998, IAU Circ. 6859, 1

[87] Zabludoff, A., Geller, M. J., Huchra, J. P., & Vogeley, M. S. 1993, AJ, 106, 1273